SUBSTRATE CHARACTERIZATION OF PUTATIVE ANCESTRAL XYLOGLUCAN
ENDOTRANSGLYCOSYLASE/HYDROLASES

by
Dilara Tüzün

Submitted to Graduate School of Natural and Applied Sciences
in Partial Fulfillment of the Requirements
for the Degree of Master of Science in
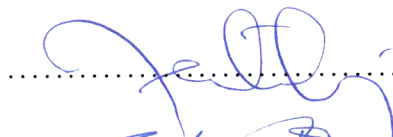Biotechnology

Yeditepe University
2016

SUBSTRATE CHARACTERIZATION OF PUTATIVE ANCESTRAL XYLOGLUCAN
ENDOTRANSGLYCOSYLASE/HYDROLASES

APPROVED BY:

Assist. Prof. Dr. Andrew John Harvey   ....

(Thesis Supervisor)

Assoc. Prof. Dr. Fatma Neşe Kök   ....

Assist. Prof. Dr. Bahar Soğutmaz Özdemir   ....

DATE OF APPROVAL: ..../..../....

ACKNOWLEDGEMENTS

ABSTRACT

SUBSTRATE CHARACTERIZATION OF PUTATIVE ANCESTRAL XYLOGLUCAN ENDOTRANSGLYCOSYLASE/HYDROLASES

Plant cell walls are composites of various carbohydrates, glycoproteins, and structural proteins. Xyloglucan is a non-cellulosic β-linked polysaccharide which is very abundant in the cell walls of dicots and is in short supply of monocots. Xyloglucan endotransglycosylase/hydrolases (XTHs) catalyze matrix polysaccharide rearrangement, cleaving and ligating glycosidic bonds of xyloglucan chains. A sub-group of the XTH superfamily, the EG16 group, have recently been shown to be strict hydrolases, lacking the transferase ability, but are able to act on a range of different polysaccharides. Therefore, XTHs are involved in processes such as wall loosening and strengthening.

Characterization of XTH enzymes can help us to understand about various cell wall modifications. Until today, only a few studies have been done to enlighten these cell wall modifications. In this study, the aim was to examine various member of the XTH superfamily, specifically GhEG16 from *Gossypium hirsutum*, HvEG16 from *Hordeum vulgare*, AtXTH3 from *Arabidopsis thaliana*, and TaXTH9 from *Triticum aestivum,* in detail. Heterologous expression and purification were attempted for all enzymes. Finally, substrate characterization and kinetic studies were performed. Heterologous expression of active GhEG16 and HvEG16 enzymes could not be achieved, however the two true XTH enzymes were successfully expressed. Interestingly, AtXTH3 was shown to have a higher affinity for barley-β-glucan than tamarind seed xyloglucan as a substrate donor, the first time that such a ratio has been detected. Also of note, TaXTH9 has a higher affinity for hydroxyethyl-cellulose donor substrate rather than tamarind seed xyloglucan.

Enlightening the substrate specificities and roles of these XTHs may lead to their development in agricultural and industrial areas such as food, cosmetics, paper and bioethanol production.

ÖZET

ATASAL KSİLOGLUKAN ENDOTRANSGLİKOZİLAZ/HİDROLAZLARIN SUBSTRAT KARAKTERİZASYONU

Bitki hücre duvarı polisakkarit, glikoprotein ve yapısal proteinlerden oluşur. β zincirlerinden oluşan ksiloglukan, dikot hücre duvarında en bol bulunan, aynı zamanda monokot hücre duvarında da az miktarda bulunan selülozik olmayan polisakkarittir. Ksiloglukaz transglükozilaz/hidrolaz enzimi ksiloglukanın temel zincirini katalizler ve ksiloglukaz zincirinde bulunan glikoz bağlarının kırılıp tekrar bağlanmasında görev alır. Ayrıca bazı Ksiloglukaz transglükozilaz/hidrolaz enzimleri hidrolaz aktivitesi gösterir. Böylece, hücre duvarının gevşemesi ve güçlenmesinde büyük etkisi vardır.

Ksiloglukaz transglükozilaz/hidrolaz enzimini karakterize etme hücre duvarındaki modifikasyonları daha iyi anlamamıza yardımcı olur. Bugüne kadar hücre duvarı modifikasyonlarını daha iyi anlamamızı sağlayan çok az çalışma yapılmıştır. Bu projede, *Gossypium hirsutum* GhEG16, *Hordeum vulgare* HvEG16, *Arabidopsis thaliana* AtXTH3, ve *Triticum aestivum* TaXTH9 enzimlerinin ayrıntılı bir şekilde incelemesinin yapılması amaçlanmıştır. Her enzimin heterolog üretimi ve saflaştırılması yapılmıştır. Sonrasında substrat karakterizasyonu ve kinetik çalışmaları yapılmıştır. Çalışmalar sonrasında, GhEG16 ve HvEG16enzimlerinin heterolog ekspresyonları başarıyla gerçekleştirilememiş. Ayrıca TaXTH9 enziminin hint hurması tohumu yerine hidroksietil selüloz donor polisakkaritine daha fazla eğiliminin olduğu ve AtXTH3 enziminin hint hurması tohumu yerine arpa- β-glukan donor polisakkaritine daha fazla eğiliminin olduğu gözlemlenmiştir.

XTH enziminin substrat özgüllüğü ve rollerinin aydınlatılması gıda, kozmetik, kağıt üretimi ve biyoethanol üretimi gibi endüstriyel alanların gelişmesine yardımcı olacaktır.

TABLE OF CONTENTS

LIST OF FIGURES

LIST OF TABLES

LIST OF SYMBOLS/ABBREVIATIONS

AOX1	Alcohol oxidase 1
Ara$f$	Arabinofuranosyl
BA	1,3:1,4-β-glucotetraose A
BB	1,3:1,4-β-glucotetraose B
BBG	Barley β-glucan
BC	1,3:1,4-β-glucotetraose C
BMGY	Buffered Glycerol Complex Medium
BMMY	Buffered Methanol Complex Medium
BSA	Bovine Serum Albumin
CAZy	Carbohydrate-Active enZymes
CESA	Cellulose synthase
CMC	Carboxy-methyl cellulose
Csl	Cellulose Synthase-Like
CT	1,4-β-cellotetraose
ddH$_2$O	Double Distilled Water
DTT	Dithiothreitol
EDTA	Ethylenediaminetetraacetic acid
GalA	Galacturonic acid
GlcA	Glucuronic acid
GM	Galactosyl mannotriose
GTs	Glycosyltransferases
HEC	Hydoxyl-ethyl cellulose

HG	Homogalacturonan
HPLC	High Performance Liquid Chromatography
IPTG	Isopropyl-β-D-thiogalactopyranosid
LB	Luria-Bertani
LT	Laminaritetraose
MeGlcA	Methyl-glucuronic acid
MLGs	Mixed-linked β-glucans
MXE	Mixed-linked glucan: xyloglucan endotransglucosylase
Ni-NTA	Nichel- Nitrilotriacetic Acid
PBS	Phosphate-buffered saline
PMSF	Phenylmethylsulfonyl Fluoride
SOC	Super Optimal Broth With Added Glucose
TAE	Tris-Acetate EDTA
TBS	Tris Buffered Saline
TBS- T	Tris Buffered Saline- Tween 20
TCA	Trichloroacetic acid
TEMED	Tetramethylethylenediamine
TXG	Tamarind seed xyloglucan
UDP-glucose	Diphospho-α-glucose
UV-Vis	Ultraviolet–visible
YPDS	Yeast Extract Peptone Dextrose Sorbitol
XTH	Xyloglucan endotransglycosylase/hydrolase
XGOs	Xyloglucan oligosaccharides
XT	1,4-β-D-xylotetraose

XyG   Xyloglucan

X7   Xyloglucan heptasaccharides

1. INTRODUCTION

1.1. PLANT CELL WALL

Terrestrial ecosystems comprise of several plant species that vary from each other according to their body plans, habitats, and adapted physiologies. A common feature of land plants is cell wall that consists of plenty of carbohydrates [1]. Plant cell wall is a complex, diverse, and dynamic structure. It has a key role in plant growth, cell differentiation, resistance to pathogen threats, intercellular communication, and water movement. Cell wall shows an alteration when cells divide, grow, and differentiate. The thickness of cell walls changes between 0.1–1 μm. Although the wall is very thin and flexible, it strengthens the plant cells [2]. Plants have ~35 cell types which are distinguished from each other according to the different size, position, and wall characteristics. For this reason, cell wall structure has diversified according to growth phase, cell type and cell position [3].

The cell wall is an essential structure for cells to supply their water requirement. Plant cells stick together, and they divide without migration. Therefore, enlargement occurs in the cell wall. The growing cells are under tensile wall stress [4]. When the wall polymers resist turgor pressure, load-bearing linkages between cellulose microfibrils become loose and start to stretch. As a result, cell wall extension occurs. Plant cells expand 10- to 100- fold in volume. Also, there are some exceptions that xylem vessel elements expand more than 10,000- fold in volume. During cell wall extension, new polymers are integrated into the wall to make the wall thicker and stronger. Disruption of stress-bearing linkages results in wall stress relaxation, and then cells are induced to uptake of water needed for cell growth [5].

Plant cell wall is an essential source for the productivity of soil, human health, and industrial products. Because plant cell wall is the most abundant organic carbon in nature, it is a necessary source for the carbon flow process. Cell wall, as an organic carbon source, enriches soil structure and fertility. Also, the cell wall is used as a high-fiber diet which has many contributions for human health. Finally, cell wall has been used as a natural or in the form of extracted polysaccharides in the production of industrial products. The cell wall is used in the form of paper, textile, fibers, and wood as a fuel. Also, extracted cell wall

polysaccharides have been modified for the production of various products such as plastics, films, and adhesives [6].

1.2. PLANT CELL WALL STRUCTURE

There is a diversity of plant cell wall structures, but most of them consist of cellulosic and non-cellulosic matrix polysaccharides that are embedded into load bearing network. Cell wall also consists of structural proteins, glycoproteins, and phenolic polymers such as lignin and ferulic acid [5]. A plant cell is composed of two types of the wall which are primary and secondary cell wall. Primary cell wall has a thin structure and is located in the extracellular matrix of the plasma membrane of young and growing cells. It develops during cell growth and differentiation. Secondary cell wall has a thicker structure and comes into existence after cell enlargement. Because secondary cell wall mostly comprises of lignin, it provides mechanical strength, structural reinforcement, and develop resistance to the pathogens [6].

The primary cell wall of both dicots and monocots is made up of cellulose, non-cellulosic polysaccharides, structural proteins, and phenolics, but the amount of these compounds vary in dicots and monocots. The primary cell wall of dicots consists of 15-30% of cellulose, 20-25% of xyloglucan, 5% of xylan, 5-10% of mannan and glucomannans, 20-35% of pectins, 10% of structural proteins, and a minor amount of phenolics such as lignin and ferulic acid [7]. The primary wall of monocotyledons is composed of the high level of glucuronoarabinoxylans and mixed-linked-β-glucans, but low level of pectic polysaccharides, glucomannans, and xyloglucans. Grass as a monocot consists of 20-30% of cellulose, 1-5% of xyloglucan, 20-40% of xylan, 10-30% of mixed-linked-β glucan, 5% of pectins, 1% of structural proteins, and 1-5% of phenolics [8]. Phenolic compounds are mostly found in the secondary cell wall of woody gymnosperms. They have various functions in the cell wall. They are used as defense compounds against herbivores and pathogens. Also, they have a role in mechanical support, in attracting pollinators and fruit dispersers, in absorbing harmful ultraviolet radiation, or in reducing the growth of nearby competing plants [6].

There is a diversity of matrix polysaccharides which are named according to the sugars of their structure. Matrix polysaccharides which made up of sugars are called as *glycan*. If

matrix polysaccharide consists of glucose, it is named as *glucan*. If matrix polysaccharide consist of xylose, it is called as *xylan*. If matrix polysaccharide made up of galactose, it is named as *galactan*. When there are substitutions of polysaccharide chain, last part of its name develops according to the backbone of the polysaccharide. For instance, when xylose is substituted to the glucan backbone, it is called as *xyloglucan*. If glucuronic acid and arabinose are attached to xylan backbone, it is named as *glucuronoarabinoxylan*. There are some exceptions that name of a polysaccharide does not indicate substitutions. For instance, the backbone of *glucomannan* is made up of glucose and mannose sugars [6].
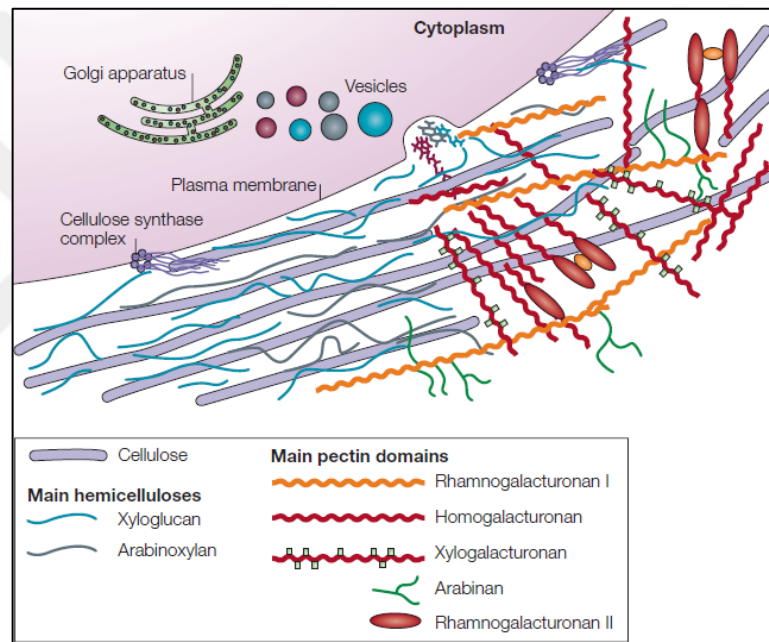
Figure 1.1. Structure of primary cell wall [2].

The most abundant component found in the cell wall is cellulose. Cellulose is composed of 1,4- *β*-linked glucan chains, and the glucan chains form a crystalline microfibrils via hydrogen bonds [5]. In primary cell wall of dicots, cellulosic crystalline microfibrils are enmeshed in a hydrated matrix that consists of two major polysaccharides which are hemicelluloses and pectins [9]. Hemicelluloses are hydrogen-bonded to the cellulose and sometimes they are entrapped between the microfibrils. Hemicellulose xyloglucan binds to cellulose and connect the adjacent cellulose microfibrils together [10]. This load bearing structure provides strength and flexibility.

The composition of cell wall polysaccharides varies in different plant species. In primary cell wall of dicots and non-commelinoid monocots, the main non-cellulosic polysaccharides are xyloglucan and pectic polysaccharides. In primary cell wall of grasses, the main non-cellulosic polysaccharides are xylans. The cell wall of wheat endosperm mostly consists of arabinoxylan which constitutes the 70% w:w of the cell wall. Other polysaccharides found in wheat cell wall are 20-29% w:w of mixed-linked-β-glucans, 2-7% w:w of glucomannans, and 2-4% w:w of cellulose [11]. The cell wall of grown barley coleoptile mostly consists of cellulose which constitutes the 35-40 mol % of the cell wall. Other polysaccharides are 25-30 mol % of arabinoxylan, 6-10 mol % of xyloglucan, 10 mol % of pectic polysaccharides, and 1 mol % of mixed-linked-β glucans [12]. The cell wall of *Arabidopsis thaliana* leaves mostly consist of pectic polysaccharides which constitute 40% of the cell wall. Other polysaccharides are 20% of xyloglucan, 14% of cellulose, and 4% of glucuronoarabinoxylan [13].

1.3. CELLULOSE

Cellulose is the most abundant polysaccharide in plants. Cellulose is mostly found in vascular plants, but it is also found in lower plants such as algae, bacteria, Oomycetes, and tunicates [14]. Cellulose is made up of parallel and linear *β*-1,4-linked glucose chains. Glucans can range from hundreds to thousands in primary cell walls, and up to 15,000 in secondary cell walls. It is synthesized at the cytoplasmic side of the plasma membrane [15]. There are hydrogen bonds within a glucose chain and between neighboring glucose chains. Hydrogen bonds and van der Waals forces result in aggregation of glucose chains together and formation of a crystallized cellulose [16]. Crystallization makes cellulose insoluble. Also, crystallized cellulose form a cellulose microfibril that are lengthen transversely to the axis of elongation. Cellulose microfibrils provide cell wall rigidity [17]. Cellulose microfibrils are mostly crystalline, and glucans in crystalline domains are highly ordered. There are also a minor amount of non-crystalline regions. In non-crystalline regions, hydrogen bonds are broken, and the ordered arrangement is lost. The glucose chains are not parallel and linear due to the twists and torsions [18]. From 40% to 95% of the cellulose is comprised of crystalline regions, and the rest is non-crystalline region [19]. Each cellulose microfibrils contain 18-24 chains. Diameters of cellulose microfibrils vary from species to

species. In higher plants, microfibrils with 3 nm in width can assemble into cellulose microfibrils with 5-10 nm in the primary cell wall and 30-50 nm in secondary cell wall [16].
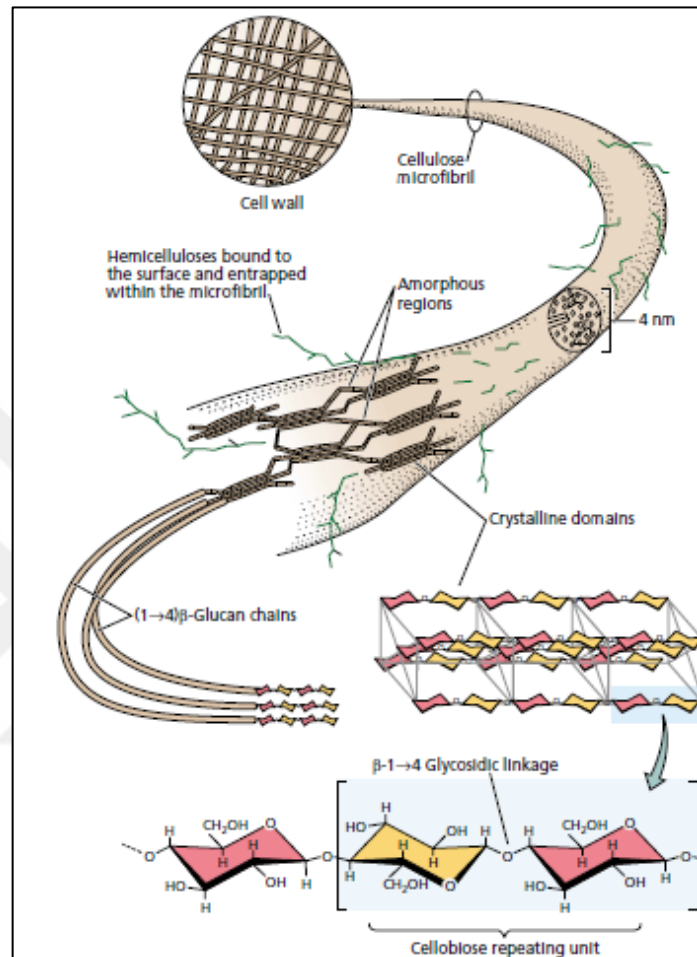
Figure 1.2. Structural model of a cellulose microfibril [6].

Plant cellulose synthase (CESA) proteins catalyze the polymerization and crystallization of glucan chains at the plasma membrane. CESA enzymes transfer glucose residue from cytosolic uridine diphospho-α-glucose (UDP-glucose) to the growing glucan chain that coalesces into cellulose microfibrils. Catalytic subunit of the CESA enzymes is tightly linked together with the growing end of glucans [17]. In *Arabidopsis thaliana*, there are ten number of *CESA* genes, but three different genes are enough to form a cellulose-synthesizing complex [20]. In *Arabidopsis*, mutations may occur in the genes that encode cellulose synthase, so cellulose synthesis is decreased [21]. A different set of genes is co-expressed in cell walls. For example, *CESA1*, *CESA3* and *CESA6* are responsible for cellulose synthesis

in primary cell wall [22], whereas *CESA4*, *CESA7* and *CESA8* are responsible for synthesis in secondary cell wall [23].

CESA enzymes are occupied in protein complexes which are called as particle rosettes in plasma membranes. Only a part of the rosette structure is exposed to the plasma membrane, whereas most of the part is introduced in a cytoplasm of the cell [24]. In the first step of rosette structure formation, three different homodimers are gathered together to form a linear array with six particles. Each homodimer is comprised of three different CESA enzymes. In the second step, the linear arrays are arranged in a rosette with a six-fold symmetry. These processes occur in the endoplasmic reticulum and Golgi apparatus. Then, the rosette complex is transported to the plasma membrane to start the cellulose microfibril synthesis [25]. Also, there are two stages of the cellulose crystallization process. Firstly, glucan sheets are formed in linear arrays by van der Waals forces. Then, six separate glucan chain sheets are gathered together to from cellulose microfibrils [26].

Although it is proved that rosette complex and cellulose synthesis is related, in some systems such as cotton fibers rosette structure is not detected. For this reason, there is a possibility that there can be different kind of cellulose which maybe synthesized by various enzyme complexes rather than rosettes. Also, cellulose is mostly synthesized at the plasma membrane, but there are some exceptional cases such as cell plate formation, in which cellulose is made in the tubulo-vesicular membrane [27].

CESA family belongs to a much larger family of glycosyltransferases that is called as *Cellulose Synthase-Like (Csl)* family which are subdivided into nine families, CslA through CslH and CslJ [28]. Proteins from the CslA, CslC, CslF, and CslH families are involved in the synthesis of β-linked glucan backbones of non-cellulosic polysaccharides [29]. CslA is responsible for the mannan backbone synthesis. *CslB* and *CslG* are synthesized only in eudicots. *CslH, CslF,* and *CslJ* are specially synthesized in Poaceae. *CslC* synthesizes the xyloglucan backbone [30]. *CslD* gene is suggested to be involved in the synthesis of a non-crystalline form of cellulose. *CslJ* gene is only present in grasses of barley, wheat, sorghum, and maize. *CslF*, *CslH*, and *CslJ* genes from rice are also responsible for the synthesis of mixed-linked β-glucans in transgenic *Arabidopsis* [31]. The functions of the other Csl families are unknown [32].
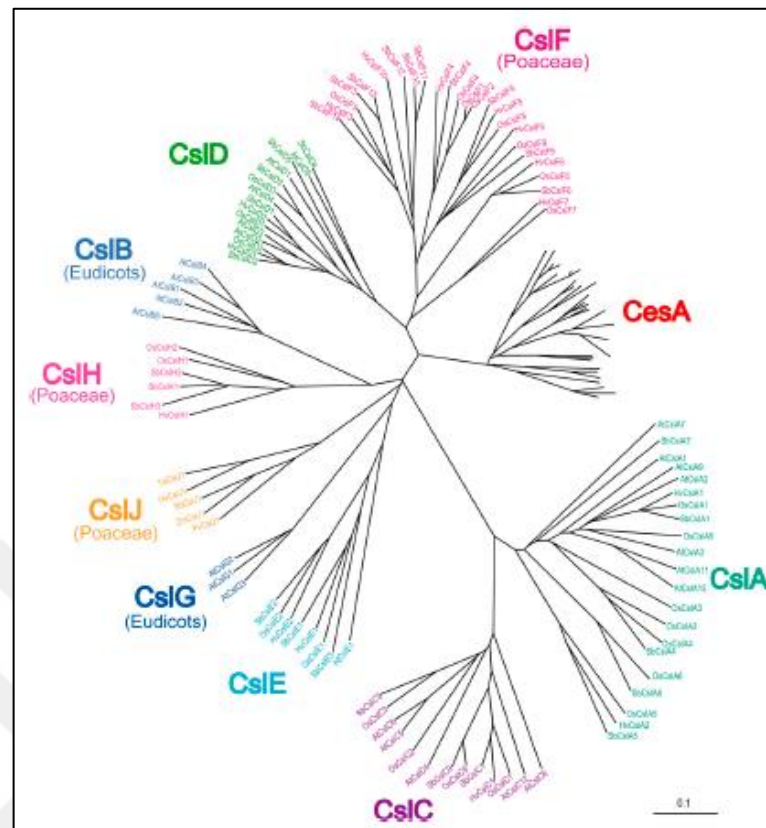
Figure 1.3. Phylogenetic tree of cellulose synthase (CESA) and cellulose synthase-like (CSL) genes in higher plants [33].

1.4. XYLOGLUCAN

Xyloglucan (XyG) is the most abundant hemicellulose in primary cell walls of dicots and non-graminaceous monocots. XyGs comprise up to 25% of primary cell walls of flowering plants, whereas they comprise a minor amount in the primary cell wall of non-graminaceous monocots. For example, they constitute only 2% of primary cell walls of celery species and 2-5% of grasses and cereals. Xyloglucan backbone is made up of β-(1,4)-linked glucan residues, and three out of four glucose residues are linked with α-xylosyl residues at O-6 position [34]. There are also other substitutions of mono-, di-, or trisaccharides on xylosyl residues which generates different types of xyloglucan motifs. β-(1,2)-linked galactosyl residues can be attached to xylosyl residues, and β-(1,2)-linked fucosyl residues can be attached to galactosyl residues. Also, O-acetyl substituents can be attached to galactosyl residues at O-2 position [35]. In tomato (*Lycopersicon esculentum*) and galactosyl,

substituents are attached to O-acetyl residue at the O-6 position [36]. In *Arabidopsis thaliana*, galactosyl substituents are attached to the O-acetyl residue at the O-6 position [37].

Cellulose and hemicellulose xyloglucan together comprise about two-thirds of the dry wall mass, so the network between cellulose and xyloglucan is essential for primary cell wall. It is suggested that a minimum number (12–16) of glucose units in the backbone are required for the adsorption of xyloglucan to cellulose [38]. The branching residues of xyloglucan affect the connection to cellulose. In the previous works, it is suggested that β-(1,2)-linked fucosyl residues increase the adsorption level of xyloglucan to cellulose while β-(1,2)-linked galactosyl residues have a reducing effect on adsorption affinity. Lima et al. showed that both fucosylated and non-fucosylated xyloglucan have same binding capacity if they have the similar molecular weight, but the main fact of binding capacity is molecular weight of xyloglucan. XyGs with low molecular weight, mainly of storage xyloglucans have a higher adsorption capacity to cellulose than xyloglucan with high molecular weight. Furthermore, the energy of binding to cellulose can change with substituted fucosyl residues [39].

Xyloglucan is one of the matrix polysaccharides and embedded in cellulose microfibrils via hydrogen bonds and van der Waals forces. They form a tension-bearing structure with cellulose. Because xyloglucan tethers the cellulose microfibrils, it has a role in wall rigidity when it cross-links the microfibrils. Also, xyloglucan tethers are the principal tension-bearing molecules, so degradation of these tethers causes a reversible cell wall loosening in elongating tissue [40]. Although xyloglucan is synthesized in the Golgi apparatus, it is transported with secretory vesicles to the plasma membrane, and then interacts with cellulose microfibrils which are synthesized in the outer surface of the plasma membrane [41]. Xyloglucan is hydrogen bonded to cellulose in the apoplastic space [42].

There are some ideas about the interaction between xyloglucan and cellulose microfibrils. It is believed that hemicelluloses can spontaneously bind to the cellulose microfibrils and connect adjacent microfibrils together. Also, it is believed that xyloglucans can remain in between cellulose microfibrils, and the untrapped part of xyloglucans can bind to other cellulose surfaces or non-cellulosic polysaccharides. Thus, cellulose microfibrils can be tethered together. Another idea is that cellulose microfibrils are coated with xyloglucans, and xyloglucans bind to other non-cellulosic polysaccharides [43].

There are different backbone patterns which are termed as a single-letter nomenclature by Fry et al. (1993) [44]. For example, the letter G indicates an unbranched glucosyl residues. X shows the attachment of α-D-xylosyl residue to glucosyl backbone with α-1-6 linkage. Xylosyl residues can carry a β-D-galactosyl residue with β-(1,2) linkage and named as L motif. If an α-L-Fucosyl residue can be linked to galactosyl residues in the L side chain with α-(1,2) linkage, it is named as F motif. The letter S indicates the attachment of an α-L-arabinosyl on an X motif with α-(1,2) linkage. T denotes the substitution of α-L-arabinosyl to arabinose residue in the S side chain with α-(1,3) linkage. J denotes the substitution of β-D-galactosyl residue to is galactosyl in the L side chain with α-(1,2) linkage [45].
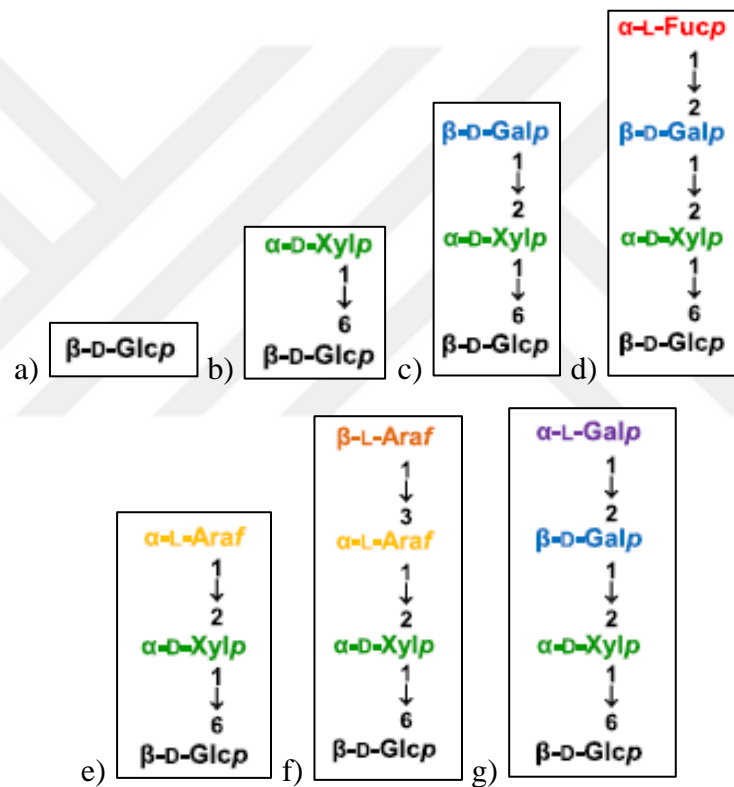
Figure 1.4. Structures of different xyloglucan side chains. a) G motif b) X motif c) L motif d) F motif e) S motif f) T motif g) J motif [46].

The xyloglucan backbone structure varies from species to species. In most of the vascular seed-bearing plants, XXXG- type xyloglucan is observed [47] whereas grasses have XXGG- and XXGGG- type xyloglucan with fewer xylose on the glucan [48]. XXXG-type xyloglucans consist of XXXG, XXFG, XXLG, and XLFG subunits. In *Arabidopsis,* galactosyl residues in XXLG, XXFG, and XLFG can carry acetyl groups . In many flowering and non-flowering plants, the fucosyl residue is linked to β-D-galactosyl residue at the *O*-2

position, while in Equisetum and Selaginella the fucosyl residue linked to an α-L-arabinosyl residue at the *O*-2 position [49]. In the commelinid monocotyledons, predominantly nonfucosylated XXGn-type xyloglucan is observed. They have both XXGn and XXXG core motifs with few XXFG units, and no XLFG. In the Poales, the Poaceae have only XXGn-type xyloglucan without fucosyl residue, but the other families contain either the mixed type xyloglucan with XXXG and XXGn core motifs or only XXXG and XXFG motifs, but no XLFG [50]. Frequently, in XXGG-or XXGGG-type xyloglucan, one or two unbranched glucose have acetyl groups instead of the α-xylosyl residue [35].
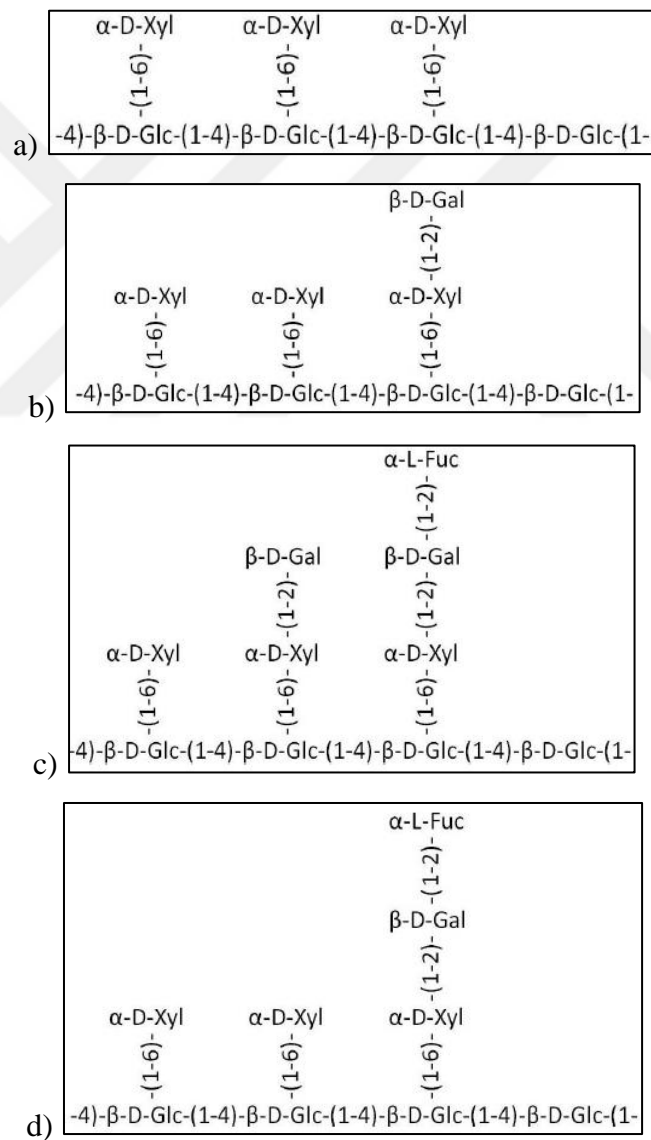
Figure 1.5. Structures of xyloglucan oligosaccharides. a) XXXG, b) XXLG, c) XLFG, d) XXFG.

The glucan backbone of xyloglucan is synthesized by glucan synthase, and the side chains are synthesized by different types of glycosyl transferases . It is suggested that a combination of at least one (1,4)-β-glucansynthase, three (1,6)-α-xylosyltransferases, two (1,2)-β-galactosyltransferases, and one (1,2)-α-fucosyltransferase is required for the generation of XLFG subunit. In *Arabidopsis*, five enzymes are involved in xyloglucan synthesis: glucan synthase to synthesize the glucan backbone, xylosyltransferases named as XXT1, XXT2, and XXT5 to transfer xylose residue onto a specific glucose residues, galactosyltransferases named as MUR3 to attach galactose to the xylosyl residue at C-3 position, fucosyltransferase named as FUT1 to transfer fucose onto galactosyl residue, and acetyltransferase to substitute the acetyl group to galactosyl residue [51]. Also, CSLC family has a role in synthesizing *β-1,4*-glucan [52]. CSLCs are integral membrane proteins in the Golgi apparatus. In *Arabidopsis*, AtCSLC4 is responsible for the synthesis of xyloglucan backbone [53].

1.5. MIXED-LINKED B-GLUCANS

Mixed-linked β-glucans (MLGs) are unbranched linear polysaccharides with a (1;3,1;4)-β-D-glucopyranose (Glcp) backbone. Two or more (1,4)-β-D-glucosyl residues are attached, and a (1,3)-β-D-glucosyl residue comes between these adjacent (1,4)-β-D-glucosyl residues irregularly. The (1;3,1;4)-β-D-glucosyl residues are not arranged in regular repeating sequences. However, they are not arranged at random. Up to 10% of the glucan chain consists of 5 to 20 adjacent (1,4)-β-D-glucosyl residues. Molecular kinks of (1,3)-β-D-glucosyl residues make polysaccharide asymmetric. As a result of the asymmetric structure, polysaccharides become soluble at high degrees of polymerization . The backbone of MLGs is mostly made up of tetrasaccharide β-D-Glcp-(1,4)- β-D-Glcp-(1,4)- β-D-Glcp-(1,3)-Glcp and trisaccharide β-D-Glcp-(1,4)- β-D-Glcp-(1,3)-Glcp residues. The ratio of (1,4)-β-D-glucosyl residue to (1,3)-β-D-glucosyl residue changes between species, but generally it differs from 2.2:1 to 2.6:1 [54]. (1,4)-β-linkages have a role in wall strengthening, and (1,3)-β-linkages provide flexibility and water solubility [55].

Enzymes have been detected that are capable of MLG transferase activity and have been labelled as mixed-linkage glucan:xyloglucan endotransglucosylase (MXE). MXEs can catalyze the formation of covalent linkages between mixed-linked β–glucan polysaccharide and xyloglucan oligosaccharides. MXE activity is detected in some embryophytes, but most

importantly it has been recently observed in *Equisetum* (*E. arvense*, *E. fluviatile*, *E. scirpoides*, *E. sylvaticum* and *E. trachyodon*) [56]. Because MLGs in *Equisetum* can be found in aged tissues, MXE activity increases in old, tough *Equisetum* tissues. For this reason, it is suggested that MXEs have a role in wall strengthening.

MLGs are present in Poales, including grasses and cereals, *Equisetum*, and some lichens, such as Icelandic moss. MLGs have not been detected in many algae and fungi. MLGs found in the vegetative tissues of Poales and *Equisetum* act as a hemicellulose because β-D-glucosyl backbone binds to cellulose with hydrogen bonds and tethers the adjacent cellulose microfibrils [57]. In Poales, MLG is found in endosperm and rapidly expanding vegetative tissues. It is often hydrolyzed to glucose after germination and after the completion of the cell. For this reason, MLG in Poales may act as a carbohydrate storage [58]. There is a difference of MLG backbone between Poales, *Equisetum*, and lichens. The ratio of (1,3)-β-D-glucan : (1,4)-β-D-glucan is higher than 24 in lichens [59], 1.5-4.5 in Poales, and lower than 0.25 in *Equisetum* [57] . The location where MLGs are synthesized has still been discussed. There is a suggestion that MLGs are synthesized in Golgi, but they have not been detected inside the cell yet [60]. On the other hand, Carpita and McCann (2010) suggested that mixed-linked β-glucans are synthesized in Golgi of developing maize coleoptiles [61].

1.6. XYLAN

Xylans are hemicelluloses comprised of (1,4)-*β*-D-linked-xylose backbone with arabinose, glucuronic acid, and 4-*O*-methyl-glucuronic acid substitutions at the 0-2 or 0-3 position, or substituted at both 0-2 and O-3 positions. Di-substitution at 0-2 and O-3 positions are mostly detected in barley [62]. They are mostly located in secondary cell walls, but they are also found in the primary cell wall of cereal grains and other grass species. Xylans constitute about 5% of the polysaccharide of dicots, where as ~30% of the polysaccharide of primary grass walls. They are one of the main polysaccharides of the secondary cell wall. Xylans are classified as arabinoxylan and glucuronoarabinoxylan. The composition of backbones varies between species [63]. When backbone of *β*-1,4-linked-xylose is substituted with single α-1,2- or α-1,3-L-arabinofuranosyl (Ara*f*) residue, it is named as arabinoxylan. In some grass species, ferulic acid is appended at O-5 of Ara*f* residues. In cereal species, xylan which is mostly found is arabinoxylan . Arabinoxylan constitutes the 60-70% of endosperm cell wall

of many cereal species, but it constitutes only about 20% of oats and barley cell walls. Ara*f* residues make polysaccharide more soluble because residues prevent intermolecular clustering and aggregation [64]. If *β*-1,4-linked-xylose backbone is substituted with single α-1,2-D-glucuronic acid (GlcA) and 4-*O*-methyl- glucuronic acid (MeGlcA) residues, it is named as glucuronoarabinoxylan. Glucuronoarabinoxylan is found in walls of the pericarp seed coat tissues [65].

In *Arabidopsis*, there are many glycosyltransferases (GTs) that are responsible for the xylan synthesis, including multiple members of GT43 and GT47 families. 4 number of GT43 genes (*IRX9*, *IRX9L*, *IRX14*, and *IRX14L*) are involved in elongation of xylan chain cooperatively. 2 number of GT47 genes (*IRX10* and *IRX10L*) are also involved in elongation of xylan backbone. It is still unknown that why two different family members are involved in xylan synthesis. It is suggested that the IRX9, IRX14 and IRX10 phenotypes can be functionally changeable with overexpression of IRX9L, IRX14L and IRX10L. It is suggested that IRX9L, IRX14 and IRX10L have a role in synthesizing xylan in the primary cell wall, whereas IRX9, IRX14L and IRX10 predominantly synthesize the secondary wall xylan [66].

1.7. MANNAN

Mannans are polysaccharides consist of *β*-1,4-mannose backbone or a combination of *β*-1,4-linked glucose and mannose residues. They are mostly found in green algae and terrestrial plants. Mannans are found as pure mannan, glucomannan, galactomannan, and galactoglucomannan. The pure mannan only consists of mannose backbone. Glucomannan is made up of backbone with glucose and mannose residues. If α-1,6-galactosyl residues are linked to mannan backbone, it is called as galactomannan. When α-1,6-galactosyl residues are appended to glucomannan backbone, it is called as galactoglucomannan. Galactosyl residues increase the solubility and interaction with other polysaccharides [67].

Mannans are found in primary cell walls and secondary cell walls of plants. Galactoglucomannans are the main polysaccharides of secondary cell walls of coniferous plants. Wood part of coniferous consists of high amount of mannans. Galactoglucomannans are very abundant in xylem elements of gymnosperms, especially softwoods. Glucomannans

are mostly present in monocotyledonous plants. Also, mannans are very abundant in angiosperm seeds, such as coffee and palm seeds as storage polysaccharides. In *Arabidopsis thaliana*, mannans are found in secondary cell walls of xylem elements. Galactomannans are abundant in storage tissues, primarily endosperm of leguminous seeds [68]. In tomato seed endosperm, mannan polysaccharides provide rigidity, and also control radicle protrusion [69].

1.8. PECTIN

Pectins are a family that consist of structurally most complex polysaccharides and are rich in galacturonic acid residues. 70% of pectins are made up of galacturonic acid which is substituted at 0-1 and 0-4 positions. Pectins are abundant in growing cells of higher plants and gymnosperms. They are also localized in soft parts of plants such as middle lamella, xylem, and fiber cells of the woody tissue. Pectins are found in approximately 35% of primary cell walls in dicots and non-commelinoid monocots. There is a minor amount of pectins; 2-10% in primary cell walls of grasses and other commelinoid monocots. In woody tissues, up to 5% of walls are comprised of pectic polysaccharides [70]. Pectins are synthesized in Golgi and transported to the wall via Golgi vesicles [71].

Homogalacturonan (HG) is the major pectic polysaccharide which comprises approximately 65% of pectic polysaccharides. HG is made up of approximately 100 amount of α-1,4-linked galacturonic acid (GalA) residues [72]. HG is methyl esterified at the C-6 carboxyl and may be *O*-acetylated at *O*-2 or *O*-3. There are other pectic polysaccharides; Rhamnogalacturonan II, xylogalacturonan, apiogalacturonan, and rhamnogalacturonan I which are formed by substitution of HGs. They are involved in many processes of primary cell walls and secondary cell walls, such as plant growth, defense mechanism, signaling, and cell-cell adhesion [73]. Pectins are also used as an industrial product such as a gelling and stabilizing agent in the food and cosmetic industries, and as a dietary food.

1.9. XYLOGLUCAN ENDOTRANSGLYCOSYLASE/HYDROLASE (XTH) ENZYMES

The structure of land plants develops depend on the cell wall strength, flexibility, and porosity. The cell wall changes throughout the processes of cell division, growth, and differentiation, so cells are adapted to changing functional requirements and to cell wall stresses which are induced by environments and pathogens. The cell wall is also very essential for the cell-cell communication, and it is permeable to water, nutrients, and growth regulators [74]. During cell elongation and loosening, modifications are necessary for cell wall. During cell wall extension process which is caused by turgor pressure, the wall polysaccharides maintain cellulose microfibrils spacing and wall thickness. Cell wall loosening occur to prevent the cell expansion uncontrollably by the modifications on xyloglucan cross-links of the xyloglucan-cellulose network [75]. The network between xyloglucan and cellulose is very essential for the primary cell wall strength and extensibility of dicotyledons. Therefore, the enzymes that control the loosening of the cellulose-xyloglucan network and modify the xyloglucan cross-links are very important for cell growth [76].

Xyloglucan endotransglycosylase/hydrolases (XTHs) catalyze the covalent linkages between different xyloglucanchains, and between xyloglucan and other non-cellulosic polysaccharides. XTHs generally have two main catalytic activities: xyloglucan endo-transglycosylase activity or both xyloglucan endotransglycosylase and xyloglucan endohydrolase activities. Xyloglucan endohydrolases hydrolyse the (1,4)-β-glucosyl linkages of the xyloglucan backbone, whereas xyloglucan endotransglycosylases cleave the (1,4)-β-glucan backbone, and then transfer the nonreducing fragment of the original xyloglucan substrate onto another xyloglucan molecule or xyloglucan oligosaccharide. Recently, a subclade of the XTH phylogenetic tree was determined to contain enzymes that are strict hydrolases with no transferase activity and have been labelled as Endo-β-glucanases of Family 16 (EG16). EG16 enzymes have been shown to hydrolyse not only xyloglucan, but also on barleyβ-glucan, Icelandic moss lichenan, and the cellulose analogues HEC and CMC [77].

Cleavage of the xyloglucan backbone by endohydrolase activity might be part of the process of cell wall loosening, but lack of wall synthesis and reinforcement results in a reduction of

tensile strength of cell wall. Therefore, endotransglycosylase activity which cleaves xyloglucan, and then transfers to a new substrate is essential for maintenance of stable cell wall structure. XTHs may also integrate newly synthesized xyloglucan into the cell wall to make it thicker. The energy required for formation of new glycosidic linkages is supplied largely from the cleavage of glycosidic linkages of the original xyloglucan backbone. As a result of XTH activity, the molecular mass of xyloglucan increases or decreases according to the cleavage position [78].

XTH genes are expressed and may be upregulated with various developmental, environmental, and hormonal issues. It has been supposed that XTHs carry out various functions, including cell wall loosening, the cross-linking of different xyloglucan molecules to strengthen the cell wall and covalent cross-linking with other non-cellulosic polysaccharides. XTH activity is highest in expanding regions of the plant. Therefore, a decrease of the cell wall extensibility is coupled to decreases of XTH activity in the roots of maize plants [79]. Growth hormones, including gibberellic acid, auxin, and brassinolide upregulate *XTH* genes [80]. It has been observed that XTH activity increases during fruit ripening so that XTHs may be responsible for cell wall degradation during fruit ripening. XTH activity on degradation increases if nascent xyloglucan substrate is secreted, and xyloglucan polymer is assembled. If new xyloglucan is not secreted, XTH rearranges or degrades the previously deposited xyloglucan [81]. The secretion of new xyloglucan and rearrangement of deposited xyloglucans maintain or increases wall strengthening [82]. Xyloglucan can act as a storage polysaccharides in nasturtium seeds. XTHs function in xyloglucan reserve mobility during germination [83]. Furthermore, it is suggested that XTHs also have a role in organogenesis, gravitropic responses, and secondary wall deposition [84].

XTHs are part of large gene families, and the features of each member can vary in tissue-, time-, and stimulus-dependent conditions. *XTH* genes are the subfamily of GH16 in Carbohydrate-Active enZymes (CAZy) classification system which based on protein sequence and structure similarities. Glycoside hydrolases (GHs) comprise the approximately 47% of the enzymes in CAZy. Therefore GHs are the most important enzyme family for biotechnological and biomedical applications. GHs are grouped into clans GH-A to GH-N that are similar in 3D-structure and catalytic domains but differ in amino acid sequences. Enzyme mechanisms and protein fold are mostly analyzed and classified rather than enzyme

specificity. In CAZy classification there are 300 protein families responsible for the build and breakdown of carbohydrates [85]. There are approximately 22 families that contain enzymes which are responsible for post-synthetically modifying the cell wall [86]. The classes of CAZy vary in the catalytic and carbohydrate-binding domain of proteins and consist of glycoside hydrolases, glycosyltranferases, polysaccharide lyases, carbohydrate esterases, and carbohydrate binding modules [87].

XTHs are apoplastic enzymes, so their optimum pH values are generally between 5 and 6. The catalytic sites of XTHs are highly conserved in DEIDFEFLG or DEIDIEFLG motifs where the conserved glutamic acids are the catalytic residues. Another common sequence motif of XTHs is signal peptide sequences which are located in the first exon to secrete the XTHs into the apoplast. Also, XTHs contain N-linked glycosylation site/s. The most common site is located 5-15 residues away from C-terminus of the conserved active site. Removal of N-linked glycosylation by enzymatic treatment leads to a rapid reduction of transglycosylase activity [88].
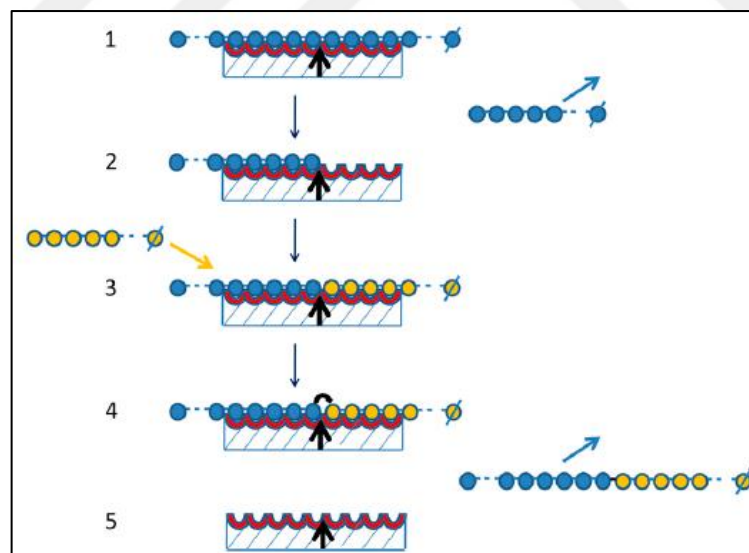
Figure 1.6. Mechanism of endotransglycosylase activity. Step 1, the enzyme binds to the donor polysaccharide (blue) and cleave the (1,4)-β-linked glucan backbone by amino acid residues at the catalytic center (black arrow). Step 2, the reducing terminal part of cleaved donor substrate moves away from the enzyme surface, while nonreducing part of the substrate remains covalently linked to the enzyme. Step 3, the acceptor substrate (orange)

is bound to the cleaved donor substrate. The nonreducing end residue of acceptor substrate come side by side with the reducing end residue of the cleaved donor substrate. Step 4, donor substrate is transferred to the acceptor substrate. Step 5, The polysaccharide product moves away from the enzyme [89].

XTHs cleave the (1,4)- β-linked glucan backbone and transfer the reducing end of the cleaved donor substrate to the nonreducing end of acceptor substrate. Fincher et al. 2006, revealed that XTH from barley covalently link the donor polysaccharides tamarind xyloglucan (TXG), hydroxyethyl cellulose (HEC), and (1,3;1,4)-β-glucans (BBG) to the different acceptor substrates [90]. In general, ^{3}H-labelled acceptors are used to detect the XTH activity. When XTH enzyme works on donor polysaccharide and radioactively labeled acceptor substrate, the labeled hybrid product with high molecular weight forms which is distinguished from donor and acceptor substrates. Also, fluorescently labeled acceptors with pyridylamino, sulphorhodamine, or fluorescein are used in a high-throughput screen for XTH activity [91].

XTH genes are divided into four major groups according to their amino acid sequences; Group I, Group II, Group III, and Ancestral Clade. Group I and Group II members mediate transglycosylase activity, whereas Group III members catalyze the hydrolase activity. For this reason, XTH genes might be classified into two groups according to their acceptor substrate specificity, but special biochemical characteristics and mechanism of action have not been detected in these groups. The EG16 clade can be seen in Figure 1.7 as and unhighlighted clade that is fully separate, with four sequences shown here as HvXTH10 (HvEG16), TaXTH10, OsXTH31, and Cotton (GhEG16). It is likely that the EG16 group represents the true ancestral origin of the XTHs before they acquired the transferase ability [77].
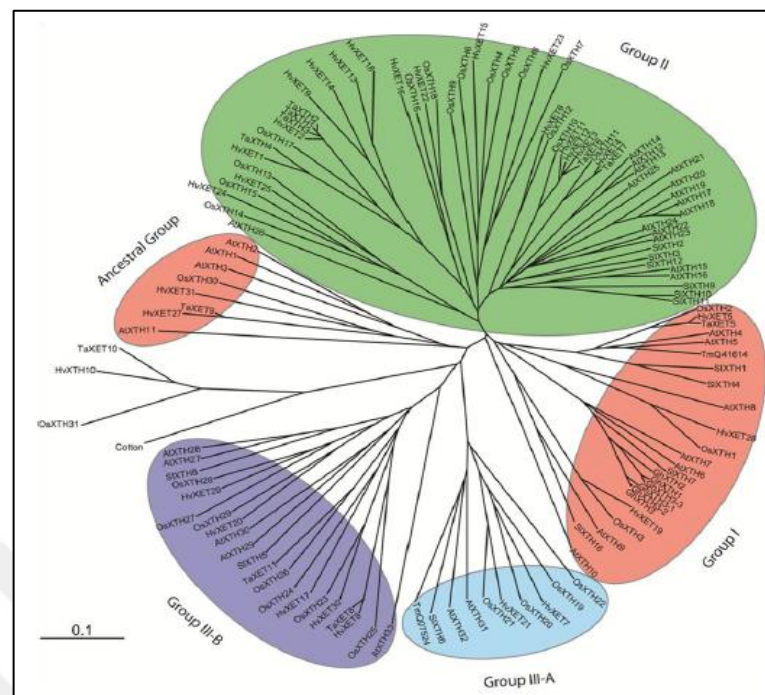
Figure 1.7. Phylogenetic tree of *XTH* genes based on amino acid sequences [92].

There are large multi-gene families which encode the XTH enzyme, including 33 genes in *Arabidopsis*, 41 in poplar, at least 29 in rice, 25 in tomato, at least 38 in barley, more than 58 in wheat, and at least 9 in the early-diverging spore-plant Selaginella. Studies show that XTH enzymes are located in different organs. It is indicated that mostly roots of young seedlings have XTH expression [93]. *Arabidopsis thaliana XTH* genes, *AtXTH14* and *AtXTH26* are expressed in the root differentiation zone, near the root/shoot junction, and in root hairs [94]. Also, *AtXTH5, AtXTH9, AtXTH15, AtXTH17*, *AtXTH18*, *AtXTH19*, *AtXTH20, AtXTH21, AtXTH28*, and *AtXTH31* are highly expressed in roots, however the expression regions may differ [95]. Some of *Arabidopsis thaliana* genes, *AtXTH1, AtXTH29, AtXTH30,* and *AtXTH33*, are highly expressed in flower organs [96]. *Oryza sativa* genes, *OsXTH22*, *OsXTH24*, and *OsXTH28* are predominantly expressed in the elongation regions of leaves [97]. In celery (*Apium graveolens*), *XTH1* was detected in the phloem, whereas it was not detected in xylem and parenchyma [98]. In Royal Gala apple, *MdXTH1*, *MdXTH9*, and *MdXTH5* genes have the greatest expression in flower, root, and leaf tissues. Kiwifruit (*Actinidia deliciosa)* gene, *AdXTH4,* is mostly found in leaf and root tissues, whereas *AdXTH10* transcript is predominant in flowers [99]. In chickpea (*Cicer arietinum)*, *CaXTH1* is expressed in apical epicotyls and lesser in roots [100]. In different poplar species,

PttXTH16A gene was upregulated in the mature stem, where it was expressed both in the phloem/cambium the xylem fractions containing primarily secondary wall-forming cells. The gene also was expressed in root tips and young roots, in developing leaves, and in the apical bud (at low levels) [101].

1.10. POLYSACCHARIDES AND OLIGOSACCHARIDES SUBSTRATES

There are distinctive polysaccharide and oligosaccharide substrates which vary according to their structures. BBG is made of β-1,3- and β-1,4-linked D-glucosyl residues. The structure of HEC is different than normal cellulose. Some of –OH groups of glucose are –OCH$_2$CH$_2$. For this reason, it is soluble while normal cellulose is insoluble. TXG is composed of main chain of β-D-(1.4) linked glucosyl units. α-1,6-xylosyl can be attached to glucosyl backbone, and β-1,2-galactosyl units can be attached to xylosyl residues.
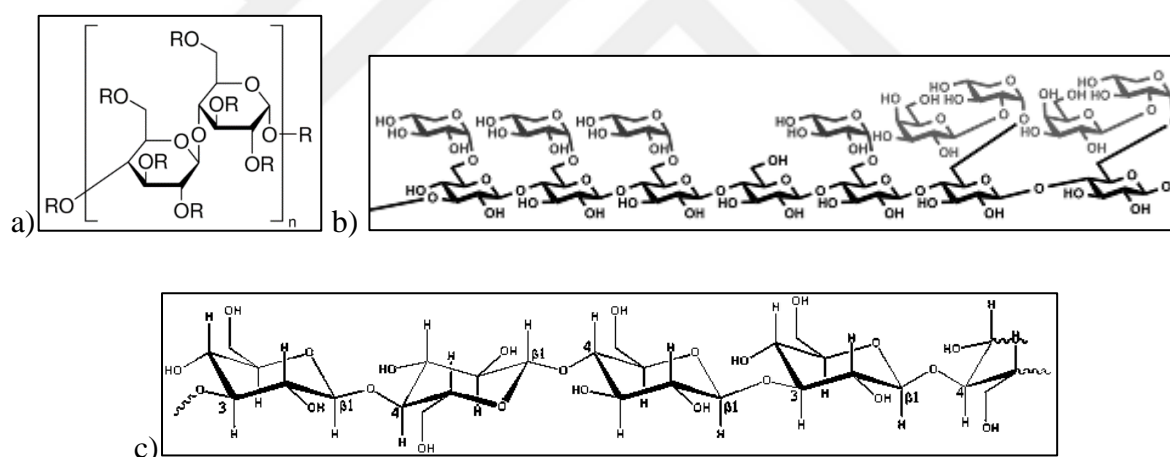
Figure 1.8. Representations of polysaccharide donors. a) HEC, b) TXG, c) BBG

The structure of oligosaccharides differs from each other according to their glucose backbones and side chains. The backbone of Xyloglucan oligosaccharides (XGO) consists of β-D-glucosyl residues connected by β-1-4 linkages. Also, α-D-xylosyl, β-D-galactosyl, and α-L-fucosyl residues can be attached to glucosyl backbone as mentioned above. 1,3:1,4-β-glucotetraose A (BA), 1,3:1,4-β-glucotetraose B (BB), and BC are made of four glucosyl residues linked together, but there are differences. BA is composed of glucosyl residues linked by β-1,3-, β-1,4-, β-1,4- linkages. BB is composed of glucosyl residues linked by β-

1,4-, β-1,4-, β-1,3- linkages. 1,3:1,4-β-glucotetraose C (BC) is composed of β-1,4-, β-1,3- and β-1,4- linkages. 1,4-β-D-xylotetraose (XT) is a xylan which is made of four xylopyranosyl residues linked by β-1,4-linkages. Laminaritetraose (LT) consists of four glucosyl residues linked by β-1,3-linkages. Galactosyl mannotriose (GM) consists of three β-1,4-linked mannose backbone which is substituted with α-1,6-linked galactose residues. 1,4-β-cellotetraose (CT) is made of of four glucosyl residues linked by β-1,4-linkage. Xyloglucan heptasaccharides (X7) consist of four β-(1,4)-linked glucosyl residues which are substituted with three β-(1,6)-linked xylosyl residues.

1)
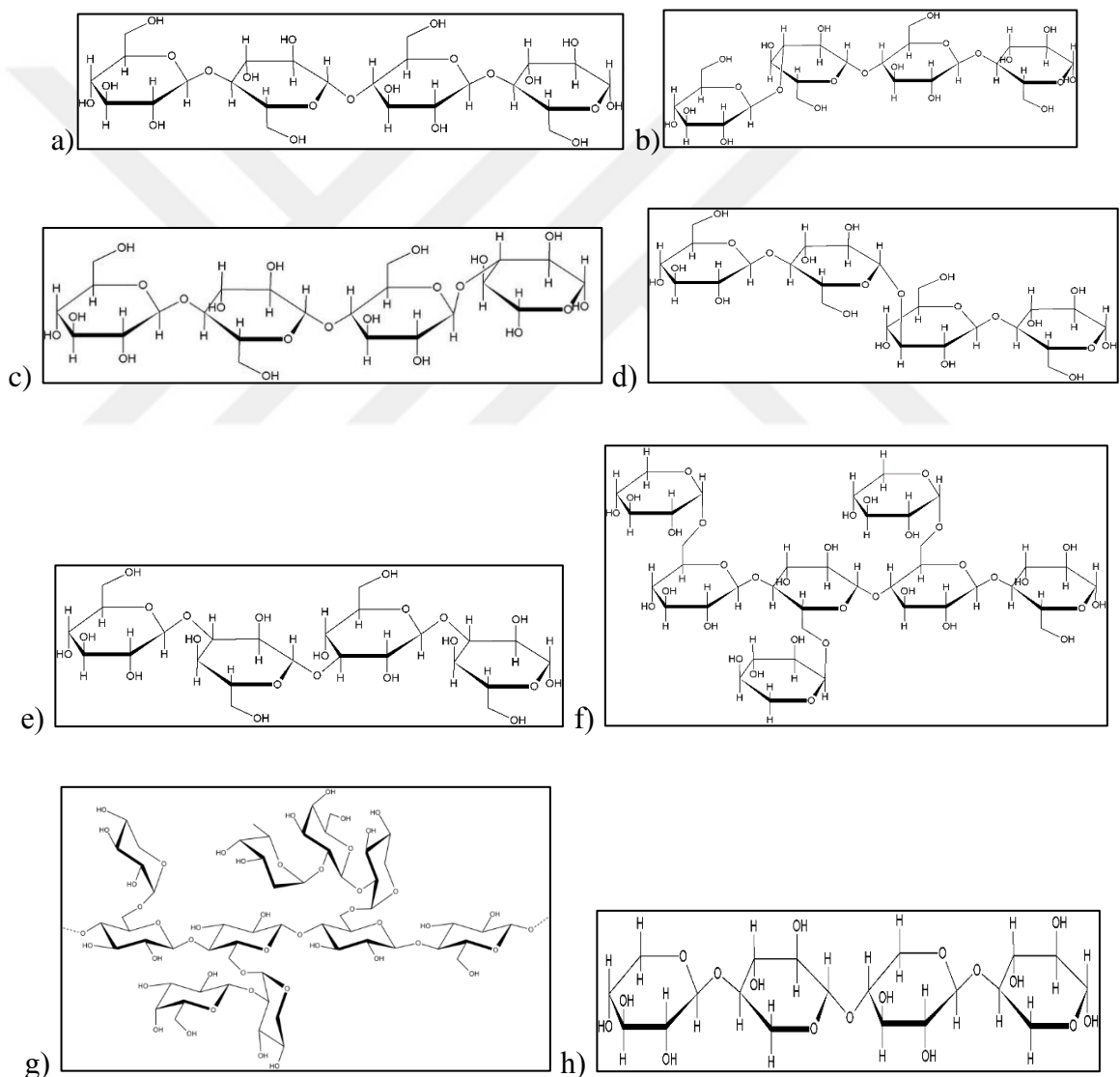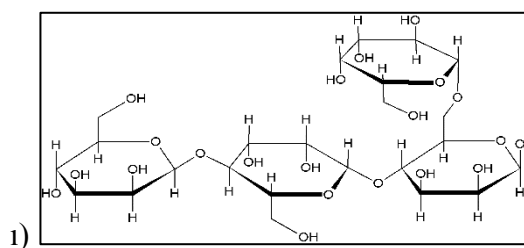
Figure 1.9. Representations of oligosaccharide acceptors. a) CT, b) BA, c) BB, d) BC, e) LT, f) X7, g) XGO, h) XT, ı) GM

1.11. HETEROLOGOUS EXPRESSION AND THE *PICHIA PASTORIS* SYSTEM

The growth in the use of recombinant proteins has increased greatly in recent years. Heterologous synthesis of recombinant proteins are commonly used in plant-based products such as food, textile, fiber, medicine, detergent, and wood [102]. Heterologous expression is easy to study, and it is a cost-effective system [103]. Prokaryotic and eukaryotic systems are the two general categories of expression systems. The system required for the successful expression is very dependent on the characteristic of the protein of interest.

Over the past three decades, *Escherichia coli* has been used as a host cell for the protein expression. Since *E.coli* is a prokaryote, it may not fold foreign proteins correctly and cannot perform other post-translational modifications [104]. Therefore, it has been problematic for *E.coli* to produce the proteins that contain a high level of disulfide connectivity or proteins that require other types of post-translational modifications such as N-linked glycosylation. In past years, *Pichia pastoris* has been commonly used as a host cell to produce heterologous eukaryotic proteins which cannot be expressed in *E.coli* at the correct level of post-translational maturation [105]. Also, compared to mammalian cells, yeasts can grow rapidly on simple media. *P. pastoris* can perform post-translational modifications such as correct folding, disulfide bond formation, *O* and *N*-linked glycosylation and processing of signal sequences [106]. Since *Pichia pastoris* has the ability for the *N*-linked glycosylation, it is a preferable system for the heterologous XTH production [107].

P. pastoris expression system is suitable for the large scale production using bioreactors where high-density cultures can be obtained. If the inexpensive growth medium is used,

expression in *P. pastoris* can be highly efficient and cost-effective expression system [108]. Furthermore, *P.pastoris* system can ease the genetic manipulations such as gene targeting, high-frequency DNA transformation, cloning by functional complementation, and high levels of protein expression at the intra- or extracellular level [109].

P. pastoris is a methylotrophic yeast that can utilize methanol as the sole carbon source and energy source. There are various promoters, including *AOX1*, *GAP*, *FLD1*, *PEX8*, and *YPT1*. A plasmid with an inducible AOX1 (Alcohol oxidase 1) promoter is preferred for *P.pastoris* expression. AOX1 promoter tightly regulates and controls the transcription of the foreign protein by a repression/derepression mechanism. AOX1 promoter controls the expression of *AOX1* and *AOX2* genes which are related with the metabolism of methanol. *AOX2* gene has 10–20 times less activity than the *AOX1* gene [110]. AOX1 promoter is repressed by glucose and glycerol, but it is induced in the presence of methanol. Nevertheless, using highly amount of methanol can be cytotoxic which can cause a reduction in culture viability and protein expression. In addition, methanol is mainly obtained from petrochemical sources which may be not proper for the production of food products [111]. The initial reactions of methanol utilization pathway occur in peroxisomes, and the rest of the metabolic steps arise in the cytoplasm [112]. The enzymes responsible for the heterologous protein production in *P. pastoris* are present when there is methanol in the media during cell growth [113].

Pichia pastoris SMD1168 and GS115 strains both contain *AOX1* gene which is responsible for the approximately 85% of methanol utilization pathway by the alcohol oxidase enzyme. For this reason, SMD1168 and GS115 strains are commonly used for the heterologous protein expression [114]. These strains have wild-type methanol utilization phenotype which is called as Mut[+]. SMD1168 strain is inadequate in the vacuole peptidase A (*pep4*) which has a key role in activating carboxypeptidase Y and protease B1 [115]. The KM71 strain contains *AOX2* gene and consumes methanol slowly. This strain has phenotype which is called as methanol utilization slow (Mut[S]). The strains with Mut[+] phenotype requires large amount of methanol which can be dangerous because of its flammability in large scale fermentation process. The strains with Mut[S] can be chosen for the expression to decrease the level of methanol requirement [114].

AOX1 enzyme has a weak affinity for oxygen, so *P. pastoris* substitutes for this deficiency by up-regulating the AOX1 promoter to increase the expression of *AOX1* gene. There are

many advantages of AOX1 promoter. Although a single copy of foreign protein is integrated into the *P. pastoris*, AOX1 promoter can manage to express the protein at high levels. Also, AOX1 promoter can be switched off at a high level of glucose and glycerol carbon sources [109].

The foreign proteins can be produced in yeast either intracellularly or extracellularly. It is better to express the heterologous proteins extracellularly to avoid the first steps of purification which are cell lysis and clarification. Because the secreted native protein level in *P.pastoris* is very low, it is easy to purify the foreign protein from the fermentation fluid by simple removal of whole cells by centrifugation or filtration. Secretion signals can be attached to the protein of interest, and lead to secretion of protein out of the cell. The most commonly used secretion signal is *Saccharomyces cerevisiae* α-factor prepro-peptide [112].

XTH enzymes have a key role in cell wall strengthening and loosening. Previous studies have shown that XTHs can use different polysaccharides of the plant cell wall as a substrate besides xyloglucan. We analyzed four different XTH enzymes which are obtained from various plant species, including AtXTH3 from *Arabidopsis thaliana*, TaXTH9 from *Triticum aestivum*, GhEG16 from *Gossypium hirsutum*, and HvEG16 from *Hordeum vulgare*. We aim to obtain purified AtXTH3, TaXTH9, HvEG16, and GhEG16 enzymes and detect their ability to use various donor and acceptor polysaccharide substrates. Activity assays and kinetic studies of these enzymes are carried out with cellulosic and non-cellulosic polysaccharides and oligosaccharides. The gathered data will help us to understand the role of these enzymes in cell wall modification. After the functions of these XTHs are elucidated, this will assist us in understanding the contribution of different wall components to food quality and texture, dietary fiber, paper and pulping, and ruminant digestibility. Also, new opportunities can arise to manipulate crops and other plants directly, and thereby to enhance the quality and processing efficiencies of plant-based products.

2. MATERIALS

2.1. POLYSACCHARIDE DONORS

Polysaccharides were supplied from Megazyme International Ireland, except hydroxyethyl-cellulose (HEC). HEC was supplied from Sigma-Aldrich, USA. They were used as donor substrates to detect enzyme activities.

Table 2.1. List of polysaccharide donors. Donor abbreviations and catalog numbers are described.

Donor Substrates	Donor Substrate Abbreviations	Cat no.
Hydroxy-ethyl cellulose	HEC	54290
Tamarind seed xyloglucan	TXG	P-XYGLN
Barley β-glucan	BBG	P-BGBM

2.2. OLIGOSACCHARIDE ACCEPTORS

Oligosaccharides were supplied from Megazyme International Ireland and used in enzyme activity assays as acceptor substrates.

Table 2.2. List of oligosaccharide acceptors. Acceptor abbreviations and catalog numbers are described.

Acceptor Substrates	Acceptor Substrate Abbreviations	Cat No.
1,4-β-cellotetraose	CT	O-CTE
1,3:1,4-β-glucotetraose A	BA	O-BGTETA
1,3:1,4-β-glucotetraose B	BB	O-BGTETB

1,3:1,4-β-glucotetraose C	BC	O-BGTETC
Laminaritetraose	LT	O-LAM4
Xyloglucan heptasaccharides	X7	O-X3G4
Xyloglucan oligosaccharides	XGOs	O-XGHON
1,4-β-D-xylotetraose	XT	O-XTE
Galactosyl mannotriose	GM	O-GM3

2.3. EQUIPMENT AND MATERIALS

AKTA Primeplus Chromatography System, His-Trap™ FF 5 ml Column, HiPrep™ 26/10 Desalting Column, and Superdex 75 16/100 Size Exclusion Column were supplied from GE Healthcare Life Sciences, UK. BioSep-SEC 4000 Column was supplied from Phenomenex, USA. T100™ Thermal Cycler, Trans-Blot Turbo™ Transfer System, ChemiDoc™ XRS+ System, and Gene Pulser were supplied from Bio-rad, USA. 1100 Series High Performance Liquid Chromatography (HPLC) system was supplied by Agilent Technologies, USA. NanoDrop 2000c Ultraviolet–visible (UV-Vis) Spectrophotometer and Forma™ 900 Series -86°C Upright Ultra-Low Temperature Freezer were supplied from Thermo Fisher Scientific, USA. Mighty Small II for 8x9Cm Gels were supplied from Hoefer, USA. New Brunswick 44/44R Incubator Shaker, 5424 Microcentrifuge, and Micropipettes were supplied from Eppendorf Innova, USA. SUB Aqua 12 Plus and SUB Aqua 26 Plus were supplied from Grant, UK. Minisart® SRP15 Syringe Filters were supplied from Sartorius, Germany. Dialysis Tubing Cellulose Membrane, Whatman Cellulose Filter Paper, and UV Transilluminator were supplied from Sigma-Aldrich, USA. Ultrospec 3000 UV/Visible Spectrophotometer was supplied from Pharmacia Biotech, UK. MS-H280-Pro Circular-top LED Digital Hotplate Stirrers were supplied from Scilogex, USA. Elite 300 Plus Power Supply was supplied from Wealtec, USA. Power Source 300V Electrophoresis Power Supply, Heater/Refrigerated Circulator, and Rocking Platform Shaker were supplied from VWR, USA. Arium Pro Ultrapure Water System and Microsart® e.jet Vacuum Laboratory

Pump were supplied from Sartorius, Germany. Avanti J-E High Speed Centrifuge was supplied from Beckman Coulter, USA. Drying and Heating Chamber was supplied from Binder, Germany. Minifors 2 Bioreactor was supplied from INFORS HT, Switzerland. WUC Digital Ultrasonic Cleaner was supplied from WiseClean, Germany. Nichel- Nitrilotriacetic Acid (Ni-NTA) Spin Columns were supplied from Qiagen, USA. Petri dish, 1.5 and 2 ml Centrifuge Tubes, 0.2 ml PCR Tubes, and Inoculation Loops were supplied from ISOLAB, Germany. 200 μl and 1000 μl Pipette Tips were supplied from CAPP, Denmark. 0.5-10 μl pipette tips were supplied from Axygen Scientific, USA. Pechiney Plastic Packaging was supplied from Parafilm "M", USA.

2.4. CHEMICALS

pPicZα-C Expression Vector, EasySelect *Pichia pastoris* Expression Kit Manual, 1 kb plus DNA ladder, 50 bp DNA ladder, EasySelect Pichia Expression Kit, T4 DNA Ligase, NotI, 10X Green Restriction Buffer, 6X DNA Loading Dye, PageRuler Prestained Protein Ladder, *Pichia* EasyComp Transformation Kit, SMD1168H *Pichia pastoris* Yeast Strain, Zeocin, Pierce BCA Protein Assay Kit, D(+)-Sucrose 99.7%, Potassium Carbonate 99+%, Distilled Water (DNase/RNase free), Nuclease Free Water, Dithiothreitol (DTT) and Kanamycin Sulphate were supplied from Thermo Fisher Scientific, USA. pGEM-T Easy Vector System was supplied from Promega, USA. Amersham^{TM} ECL^{TM} Prime Western Blotting Detection Reagent was supplied from GE Healthcare Life Sciences, UK. DraI, ClaI, XbaI, 10X Standard Taq Reaction Buffer, and Taq DNA Polymerase were supplied from New England BioLabs (NEB), UK. Gel Extraction Kit, NucleoSpin Plasmid, and NucleoSpin Gel and PCR Clean-up Kit were supplied from Macherey-Nagel, Germany. 10X Reaction Buffer was supplied from GeneOn, Germany. Magnesium Chloride ($MgCl_2$) was supplied from Kapa Biosystems, USA. Calcium Chloride ($CaCl_2$) was supplied from Avantor, USA. 2-Propanol, Ammonium di-Hydrogen Phosphate, Methanol, Bromophenol blue, Sodium Dodecyl Sulphate, Sodium Hydroxide Solution 40 %, D(+)- Glucose, Formic Acid 98-100%, Tetramethylethylenediamine (TEMED), Glycine, Phenylmethylsulfonyl Fluoride (PMSF), and Sodium Carbonate anhydrous were suplied from PanReac AppliChem, Spain. 50X Tris-Acetate EDTA (TAE) Buffer, iQ SYBR Green Supermix, Transblot Turbo transfer pack Midi format 0.2 um nitrocellulose, and Gene Pulser Cuvette were supplied from Bio-rad, USA. Acetic acid 100%, Acetone ≥ 99.5%, Acrylamide 30%,

Agarose, Ammonium Phosphate Monobasic, Ammonium Sulphate, Bradford Reagent, Chloramphenicol, Ethidium Bromide, Ethanol Absolute, Formaldehyde Solution, D-sorbitol, Glass Beads Acid Washed, Glycerol approx 87%, Imidazole, Phenol:Chloroform 5:1, Potassium Phosphate Monobasic, Potassium Phosphate Dibasic, Silver Nitrate, Sodium Acetate, Sodium Chloride, Sodium Sulphate, Sodium Phosphate Monobasic Dihydrate, Yeast Nitrogen Base, Agar, Ammonium Acetate, Tween 20, Yeast Extract, Hydroxyethyl Cellulose, Bovine Serum Albumin (BSA), Potassium Chloride $\geq 99.0\%$, and Lyticase from arthrobacter were supplied from Sigma-Aldrich, USA. Trizma base was supplied from Fisher Scientific, USA. Isopropyl-β-D-thiogalactopyranosid (IPTG) was supplied from Peqlab, Germany. Maximo Taq DNA Polymerase was supplied from GeneOn, Germany. Peptone from casein, Trichloroacetic acid (TCA), and Peptone from meat were supplied from Merck Millipore, USA. Rb pAb to 6x His-tag was supplied from Abcam, UK. Tris Buffered Saline (TBS): powder was supplied from Santa Cruz Biotechnology, USA. TALON Superflow Metal Affinity Resin was supplied from Takara Bio, USA.

3. METHODS

3.1. ENZYME SELECTION

The different codon optimized genes of ancestral group were chosen from GenScript, USA for the heterologous expression. - AtXTH3 from *Arabidopsis thaliana*, and TaXTH9 from *Triticum aestivum* are expected to have xyloglucan endotransglycosylase activity, whereas GhEG16 from *Gossypium hirsutum*, and HvEG16 from *Hordeum vulgare* likely have hydrolytic activity.

3.2. PRODUCTION AND PURIFICATION OF AtXTH3, AND TaXTH9 ENZYMES

3.2.1. Plasmid Isolation

For the heterologous expression in *Pichia pastoris*, the pPicZα-C/*AtXTH3*, and pPicZα-C/ *TaXTH9* plasmids were isolated from *E.coli* DH5α cells. At first, the transformant DH5α cells were grown in 10 ml of low salt Luria-Bertani (LB) broth plus 10 μl of zeocin (final concentration: 100 μg/μl) as described in Invitrogen EasySelect *Pichia pastoris* Expression Kit Manual. Before the plasmid isolation, glycerol stock of transformed bacterial cells were prepared. 820 μl of overnight culture was added to 180 μl of 87% glycerol and then stored at -80 °C freezer for further studies. Then, pPicZα-C/*AtXTH3* and pPicZα-C/ *TaXTH9* plasmids were isolated from the rest of the culture with Macherey-Nagel NucleoSpin Plasmid Kit. The nanodrop measurement was carried out using NanoDrop 2000c UV-Vis Spectrophotometer for the quantitative assessment of DNA concentration.

3.2.2. Preparation of *Pichia pastoris* Competent Cells

Competent cells were prepared as described in EasySelect *Pichia pastoris* Expression Kit Manual. The *Pichia pastoris* strain was grown in Yeast Extract Peptone Dextrose Sorbitol (YPDS) Agar at 30 °C. One of the grown colonies was picked, and cultured in YPD broth until OD_{600} reached 4-6 in a 30 °C shaking incubator. After centrifugation at 500 g for 5 min

at room temperature, the pellet was resuspended with 9 ml ice cold BEDS solution (10 mM bicine-NaOH, pH 8.3, 3% (v/v) ethylene glycol, 5% (v/v) (dimethyl sulfoxide) DMSO, and 1 M sorbitol) supplemented with 1 ml 1.0 M DTT. The cell suspension was incubated at 100 rpm for 5 min in 30 °C shaking incubator. Then, the cell culture was centrifuged at 500 x g for 5 min, and cells were resuspended in 2 ml BEDS solution without DTT. Competent cells were aliquoted into 1.5 ml sterile microcentrifuge tubes, and placed in -80 °C freezer for the following transformation process.

3.2.3. Transformation into Competent *P. pastoris* Cells

pPicZα-C/*AtXTH3* and pPicZα-C/*TaXTH9* plasmids were digested before the transformation. At first, 10 μg of each plasmid was linearized with DraI restriction endonuclease according to manufacturer's instructions. 1% agarose gel electrophoresis was carried out to detect whether the plasmids were digested or not. Then, Phenol Extraction/EtOH Precipitation was performed to remove proteins from DNA sample according to manufacturer's instructions. The digested plasmids were transformed into competent *Pichia pastoris* SMD1168H cells as described by Lin-Cereghino et al., 2005 [116]. The digested plasmids were mixed with the competent *P. pastoris* cells in centrifuge tubes, and the mixture was transferred into electroporation tubes. Bio-Rad Gene Pulser was used as a modular electroporation system and arranged to 1.5 kV, 200 Ω, and 25 μF values. After electroporation was carried out, electroporation solution was added into each tube. The mixtures were incubated at 30 °C, 150 rpm shaking incubator for 2 hours. The transformant cells were spread onto the YPDS+zeocin plates. Screening of colony that synthesizes the most active enzyme was carried out as described in Invitrogen EasySelect *Pichia pastoris* Expression Kit Manual.

3.2.4. Selection of Colony Which Synthesize the Most Active Enzyme

12 colonies for each gene were subcultured on YPDS+zeocin plates at 30 °C for three days. Cells were grown in 10 ml Buffered Glycerol Complex Medium (BMGY) media until OD$_{600}$ reached 4-6 in 30 °C, 200 rpm shaking incubator. After centrifugation, cells were resuspended in 10 ml Buffered MethanolComplex Medium (BMMY) media at 22 °C, 175

rpm shaker incubator, and 1% methanol induction was carried out at every 24 hours for five days. Then, centrifugation of cells was performed at 22 °C, 3220 x g, 10 min, and the supernatant was removed for the next assay.

TCA & acetone precipitation was carried out to precipitate the proteins from solutions according to manufacturer's instructions. 900 μl of sample and 100 μl of ice-cold 100% TCA (final concentration is 10%) were mixed, vortexed, and then incubated on ice for 1 hour. Centrifugation was carried out at 4 °C, 12000 x g for 10 min to precipitate proteins. After centrifugation, the pellet was resuspended in 800 μl of -20 °C pure acetone. Proteins were incubated at -20 °C overnight to get rid of excess TCA. Then, proteins were centrifuged at 4 °C, 6500 x g for 10 minutes. The pellet was resuspended with fresh -20 °C pure acetone, vortexed, and incubated at -20 °C for 30 minutes. Proteins were precipitated, and the washing step was repeated. Acetone was discarded, and protein pellet was dried on ice completely. The pellet was dissolved in ultra pure water.

Proteins were mixed with 2X Laemmli buffer and incubated at 95 °C for 7 minutes for denaturation. Proteins were separated using 12% polyacrylamide gel-based on their molecular weight. Proteins were stained with Coomassie Brilliant dye for 30 minutes and destained with distilled water until background became clear. The intensity of protein bands was visualized. Then, proteins were separated on another 12% polyacrylamide gel for the western blotting. After electrophoresis, protein bands were transferred from gel to Transfer Pack 0.2 μm nitrocellulose membrane using Bio-Rad Transblot Turbo system. The membrane was blocked with 3% skimmed dry milk powder in Tris Buffered Saline- Tween 20 (TBS-T) solution overnight. The membrane was incubated with Abcam Anti-6X His antibody for 1 hour. After incubation, the membrane was washed with TBS-T twice for 5 minutes. Then, membrane was washed with Phosphate-buffered saline (PBS) solution for 10 minutes. Proteins were visualized with highly sensitive chemiluminescent detection reagents; Luminol enhancer, and Peroxidase solution by using ChemiDoc™ XRS+ System with Image Lab™ Software to detect the target protein.

3.2.5. Enzyme Activity Assay

Enzyme activity produced by each colony was investigated to detect the most active enzyme producing colony. The different donor, and acceptor substrates which was given in Table 2.1, and Table 2.2 used for the activity analysis. 2 µl of protein supernatant was mixed with 10 µl of 0.4% TXG donor substrate, and 1 µl of 50 mM sulforhodomine tagged XGO acceptor substrate. The reaction mixture was incubated at 30 °C for 24 hours. Then, 6 µl of 90% formic acid was added to stop the enzymic reaction.

The activities were analyzed with HPLC technique. 11 µl of ultra pure water was added to the reaction tube, so the total volume was reached to 30 µl. Half of the volume was injected into the BioSep-SEC 4000 column, 75x7.80 mm. Polysaccharides and oligosaccharides were separated at 0.5 ml/min flow rate. Data was analyzed with ChemStation software, and the most active colony for each enzyme was detected to continue with it for large scale production.

3.2.6. Large Scale Production and Protein Purification

Colony that was producing most active enzyme used in large scale production. TaXTH9 enzyme production was carried out once in 3 lt of BMMY, whereas AtXTH3 enzyme production was carried out several times in various BMMY medium between 1.5 lt and 2.5 lt. The selected colony was removed from the petri dish using inoculation loop, and grown in 10 ml BMGY media overnight at 30 °C, 200 rpm shaking incubator. Next day, 3.9 ml of overnight culture was added to 500 ml BMMY media, and incubated at 22 °C, 175 rpm shaker incubator for five days. At the same time, 1% methanol induction was carried out at every 24 hours for five days. At the end of the production, centrifugation was performed at 22 °C, 3220 x g for 10 min to precipitate the cells. The supernatant was filtered using 0.2 µm RC filters. Ammonium sulfate precipitation was carried out at 4 °C until salt saturation was reached to 90%. Proteins were precipitated at 4 °C, 12,000 x g for 15 minutes, and the supernatant was discarded. Pellets were resuspended in 20 mM pH 7.4 sodium phosphate buffer. Dialysis was carried out to get rid of ammonium sulfate in the protein solution. The protein solution was spilled into the cellulose membrane, and then the cellulose membrane was incubated in 14.4 lt sodium phosphate buffer at 4 °C for three hours. After sodium

phosphate buffer was refreshed twice, cellulose membrane incubated overnight in sodium phosphate buffer at 4 °C.

6X-His tagged proteins were purified using HisTrap FF column with AKTAprime plus system according to manufacturer's instructions. Binding buffer with low imidazole concentration was used to bind 6X-His tagged proteins to resins charged with nickel ions. Then, elution buffer with high imidazole concentration was used to elute proteins from the column. The buffer was exchanged from elution buffer to 0.1 M ammonium acetate buffer pH 6.0 using HiPrep 20/10 DeSalting column. Finally, proteins were passed over Superdex 75 16/100 size exclusion column for size-based separation. 0.1 M pH 6.0 ammonium acetate buffer was used as a mobile phase. The purified proteins were concentrated using Millipore Centrifugal Units and stored at 4 °C.

3.2.7. Bradford Protein Assay

AtXTH3 and TaXTH9 protein concentrations were calculated using Bradford assay. 10 μl of BSA standards at different concentrations; 0.1 mg/ml BSA, 0.2 mg/ml BSA, 0.4 mg/ml BSA, 0.6 mg/ml BSA, 0.8 mg/ml BSA, 1 mg/ml BSA, and 10 μl of each purified protein were mixed with 190 μl of Bradford Reagent separately in 96-well plate. They were incubated at room temperature for 5 min in the dark, and then measurement was done at 595 nm wavelength with a spectrophotometer. The calibration curve was plotted with the concentrations of BSA standards, and then protein concentrations were calculated according to the calibration curve.

3.2.8. Western Blot, SDS-PAGE, and Dot Blot Analysis

The purified AtXTH3 and TaXTH9 proteins were separated on 12% polyacrylamide gel according to their molecular weights, and then target proteins were detected by western blot analysis as described before. Then, proteins were separated on second 12% polyacrylamide gel to visualize the protein band intensities by silver nitrate staining which is able to detect less than one ng of protein. Proteins were incubated with solutions for fixation, sensitization, silver impregnation and finally image development. At first, proteins were incubated with 50 ml of 0.8 mM sodium thiosulphate solution for 1 minute and washed with double distilled

water (ddH$_2$O) twice for 1 minute. Then, proteins were impregnated with 50 ml of 12 mM silver nitrate solution for 40 min in the dark, and then proteins were washed with ddH$_2$O for 10-15 second. Finally, proteins were incubated in 50 ml developer solution; 3% potassium carbonate plus 50 μl formalin, and 25 μl of 10% sodium thiosulphate per liter. Because protein bands were not visualized clearly after 15 minutes, the incubation step was repeated. 50 ml of stop solution; 4% (w/v) Trizma base, and 2% (v/v) acetic acid were added to stop the reaction. After washing step with ddH$_2$O, proteins were visualized using ChemiDoc™ XRS+ System with Image Lab™ Software.

Dot blot analysis was performed to identify the target protein activity in protein solutions by detection of luminescence. Enzyme reaction with TXG donor and XGO acceptor was set up for 24 hours. Ammonium acetate buffer was used as a control. The reaction mixture was dropped onto Whatman Cellulose Filter Paper, and then the paper was dried. Washing step of Whatman paper was performed with water for overnight. Luminescence of proteins was visualized using UV Transilluminator.

3.2.9. Activity Analysis

AtXTH3, and TaXTH9 activities on different substrate couples at different time intervals were tested and analyzed with HPLC technique. Different combinations of 9 sulforhodamine tagged acceptors, and three different donor substrates which were described in Table 2.1, and Table 2.2 chosen for tests. Enzyme activity was indicated as picokatals/mg enzyme. Then, relative percentage activity of each substrate couples to TXG-XGO couple were calculated.

3.2.10. Enzyme Kinetic Analysis

Different reactions were set up to detect the optimum TXG donor, and X7 acceptor substrate concentrations for AtXTH3, and TaXTH9 enzyme activities. Enzyme activity with different TXG concentrations; 0.05%, 0.1%, 0.15%, 0.2%, 0.3%, 0.4%, 0.6%, and 0.8% was analyzed, and then optimum TXG concentration was detected. Then, reactions were set up with optimum TXG, and different X7 concentrations; 1 μM, 5 μM, 10 μM, 30 μM, 50 μM, 70 μM, 100 μM, 150 μM, 200 μM, 250 μM, 300 μM, 350 μM, 400 μM, 500 μM, 600 μM,

700 μM, 800 μM, and 1000 μM to identify the optimum X7 concentration. Lineweaver-Burk and Michaelis-Menten graphs were plotted according to the enzyme reaction rate, and substrate concentration. Finally, V_{max} (μM/time), K_m (μM), and K_{cat} (1/time) values were measured.

3.2.11 Cell Lysis, and Protein Extraction

Pichia pastoris cells were lysed to check whether *AtXTH3* was expressed intracellularly, or not. The pellet of AtXTH3 enzyme was resuspended with supernatant in 50 ml falcon after vortex. 1 ml of culture was removed, and centrifuged at 3220 x g, 4 °C for 10 min. The cell pellet was resuspended in 100 μl of Breaking Buffer, and then 100 μl of acid-washed glass beads were added. Cells were vortexed for 10 seconds and then incubated on ice for 30 seconds. Lysation step was repeated for eight times. Cells were precipitated by centrifugation at 4 °C, 15.000 x g for 10 min. Supernatant was removed, and proteins were detected by SDS-PAGE and Western Blot techniques.

3.2.12. DNA Sequencing

Sequencing of pPicZα-C/*AtXTH3* and pPicZα-C/*TaXTH9* plasmids were carried out by Macrogen, Korea. Glycerol stocks of pPicZα-C/*AtXTH3* and pPicZα-C/*TaXTH9* transformant DH5α cells were cultured in 20 ml low salt LB medium plus 20 μl Zeocin at 37 °C, 180 rpm overnight. Plasmids were isolated as described in Invitrogen EasySelect *Pichia pastoris* Expression Kit Manual, and then nanodrop measurement was carried out to determine plasmid DNA concentrations. Then, plasmid digestion was performed using the mixture of 10X NEBuffer 4, 700 ng of pPicZα-C plasmid, 10 mg/ml of 100X BSA, 5.000 U/ml ClaI and 20.0000 U/ml XbaI enzymes, and nuclease-free water at 37 °C for an hour. The reaction mixture was run on 1% agarose gel electrophoresis to determine whether plasmids were digested, or not. After detection of insert and plasmid at expected size, plasmids were sent to the Macrogen for sequencing process.

3.3. PRODUCTION AND PURIFICATION OF GhEG16, AND HvEG16 ENZYMES

3.3.1. Transformation of pET-28/*GhEG16*, and pET-28/*HvEG16* Plasmids into Competent DH5α Cells

Transformation of pET-28/*GhEG16*, and pET-28/*HvEG16* plasmids into competent DH5α cells were carried out as described by Fregel et al., 2008 [116]. Competent DH5α cells were taken out of -80 °C, and thawed on ice. Five μl ligated vector was mixed with 50 μl competent cell in a 2 ml eppendorf tube. The mixture was incubated on ice for 20 min. Then, heat shock was applied by incubation in 42 °C water bath for 45 sec. Tubes were placed on ice for 2 min. 950 μl Super Optimal Broth with added glucose (SOC) media was added, and cells were incubated at 37 °C shaking incubator for 1,5 hour. After centrifugation at 8000 x g for 3 min, 850 μl of supernatant was discarded, and then pellet was resuspended. Resuspended pellet was spread on 20 ml of LB agar plate with 40 μl of kanamycin, and incubated at 37 °C overnight. 10 number of transformant colonies were picked for plasmid isolation.

3.3.2. Plasmid Isolation, and Double Digestion

Selected colonies were grown in 10 ml LB medium plus 20 μl kanamycin at 37 °C, 180 rpm overnight. After plasmids were isolated using Macherey-Nagel NucleoSpin Plasmid Kit, they were digested with restriction enzymes. Double digestion of pET-28/*GhEG16* was carried out with BamHI+NotI restriction endonucleases, whereas digestion of pET-28/*HvEG16* was carried out with ECORI+NotI restriction endonucleases. Digested plasmids were incubated at 37 °C water bath with NotI for 35 min, with BamHI for 15 min, and with ECORI for 20 min. Then, plasmids were placed in 80 °C heater for 5 min to stop the digestion reaction. Plasmids with the gene of interest were visualized using agarose gel electrophoresis. GhEG16-5 and HvEG16-7 colonies consisted of the gene of interest, so further studies were carried out with these colonies.

3.3.3. Preparation of Competent Bl21DE3 Star, and Bl21 Codon Plus DE3 RIPL Cells

Competent Bl21DE3 Star and Bl21 Codon Plus DE3 RIPL cells were prepared as described in manufacturer's instructions. 5 ml of LB media was inoculated with Bl21DE3 Star strain, and 5 ml of LB plus chloramphenicol media was inoculated with Bl21 Codon Plus DE3 RIPL strain at 37 °C, 180 rpm overnight. Next day, cells were subcultured until OD_{600} reached 0.4. Cells were precipitated at 2000 x g, 4 °C for 5 min. The pellet was resuspended with ice-cold 100 mM $MgCl_2$. Cells were harvested by centrifugation at 1000 x g, 4 °C for 5 min, and the pellet was resuspended with ice-cold 100 mM $CaCl_2$. After incubation for 20 min, cells were precipitated, the pellet was resuspended in 2 ml of 85 mM $CaCl_2$ plus 15% v:v glycerol. Finally, cells were snap frozen in liquid nitrogen, and stored at -80 °C freezer.

3.3.4. Transformation into Competent Bl21DE3 Star, and Bl21 Codon Plus DE3 RIPL Cells

Transformation of pET-28/*GhEG16-5* and pET-28/*HvEG16-7* plasmids were carried out as described by Fregel et al., 2008 [116]. The transformant Bl21DE3 Star cells were plated on a petri consisted of LB plus kanamycin, whereas Bl21 Codon Plus DE3 RIPL cells were plated onto 20 μl of LB, 40 μl of kanamycin plus 10 μl of chloramphenicol. The cells were incubated at 37 °C overnight. The grown Bl21DE3 Star colonies were cultured in LB media with kanamycin, and Bl21 Codon Plus DE3 RIPL colonies were cultured in LB media with kanamycin and chloramphenicol at 37 °C overnight. Finally, glycerol stocks were prepared, and placed in -80 °C freezer.

3.3.5. Small Scale Production, and Protein Purification

Small scale production of GhEG16 and HvEG16 enzymes were carried out in different conditions depend on IPTG concentrations, incubation times, incubation temperatures, and type of broth. At first, IPTG concentration was constant, but incubation time and temperature were variable. Transformant glycerol stocks were taken out of -80 °C and extracted using a loop to inoculate 5 ml of LB media with 10 μl of kanamycin, and 2.5 μl of chloramphenicol. The mixture was incubated at 37 °C shaker-incubator overnight. 100 μl of subculture was

mixed with 10 ml of LB, 20 µl of kanamycin, and five µl of chloramphenicol until OD_{600} reached 0.8. Then, 1 M IPTG was added to the cell cultures, and different incubation times and temperatures were performed such as 22 °C for 5 hours, 30 °C for 3 hours, and 16 °C overnight.

At the second trial, Terrific broth was chosen instead of LB broth. Also, incubation time and temperature were constant, but IPTG concentration was variable. 0.5 M IPTG, 1 M IPTG, 2 M IPTG, and 5 M IPTG were added to the cell cultures at 37 °C shaker-incubator for 5 hours. Cultures were centrifuged at 3220 x g, 4 °C for 15 min. Supernatant was discarded, and the pellet was stored at -20 °C. The next day, pellets were resuspended with 20 mM sodium phosphate ($NaPO_4$), 100 mM sodium chloride (NaCl), 0.1 M PMSF, and 20 mM lysozyme. Cells were disrupted using probe sonicator. Cells were exposed to sonic for 10 seconds and then placed on ice for 20 seconds. Sonication was repeated for five times. Then, disrupted cells were precipitated by centrifugation at 4 °C, 16000 x g for 30 min. Supernatant was discarded, and then concentrated to 1 ml, and finally stored at 4 °C.

The concentration of proteins was measured by performing Bradford Assay as described before. Because low amount of concentration was detected, TCA Acetone Precipitation was carried out to concentrate the proteins. Western Blotting and coomassie dye staining were performed to visualize the proteins. Finally, Somogyi-Nelson Method was applied for detection of reducing sugars of proteins. At first, Nelson's reagent A solution, Nelson's reagent B solution, Nelson's reagent C solution- 25:1 reagent A: reagent B and Nelson's color reagent- arsenomolybdate reagent were prepared. 50 µl of protein samples were mixed with 150 µl of 50 mM sodium acetate ($C_2H_3NaO_2$), and 100 µl of 0.4% TXG donor substrate, and then incubated at RT for 22 hours. An equal volume of Nelson's reagent C was added, and vortexed. The mixture was boiled in 95 °C water bath for 10 min and then cooled on ice for few seconds. After proteins were taken to room temperature, an equal volume of color reagent was added, vortexed, and centrifuged at 9000 x g, 22 °C for 3 min. Finally, the absorbance of proteins was measured at 540 nm using a spectrophotometer.

4. RESULTS

4.1. PRODUCTION AND PURIFICATION OF TaXTH9 ENZYME

4.1.1. Transformation into *Pichia pastoris*, and Positive Colony Selection

Transformation of pPicZα-C/*TaXTH9* into competent *P. pastoris* cells were carried out. 12 of transformant colonies were picked randomly, and TaXTH9 enzyme production was started in 10 ml BMMY medium. *P. pastoris* cells were induced by addition of 1% v:v methanol at each 24 hours for five days. Enzyme activity assay, SDS-PAGE analysis, and western blotting were performed to detect the colony which expressed the most active TaXTH9 enzyme (Figure 4.1).

Figure 4.1. pPicZα-C/*TaXTH9* transformant *P. pastoris* colonies that were grown in YPDS agar+zeocin plate.

Selected colonies were separated on a 12% polyacrylamide gel according to their molecular weights (Figure 4.2). It was aimed to visualize TaXTH9 enzyme which has 33.2 kDa molecular weight. As a result of coomassie dye staining, several protein bands were detected for each colony. As a result of western blot analysis, TaXTH9 enzyme was visualized at 55 kDa size in each colony, except colony 1, and 6.
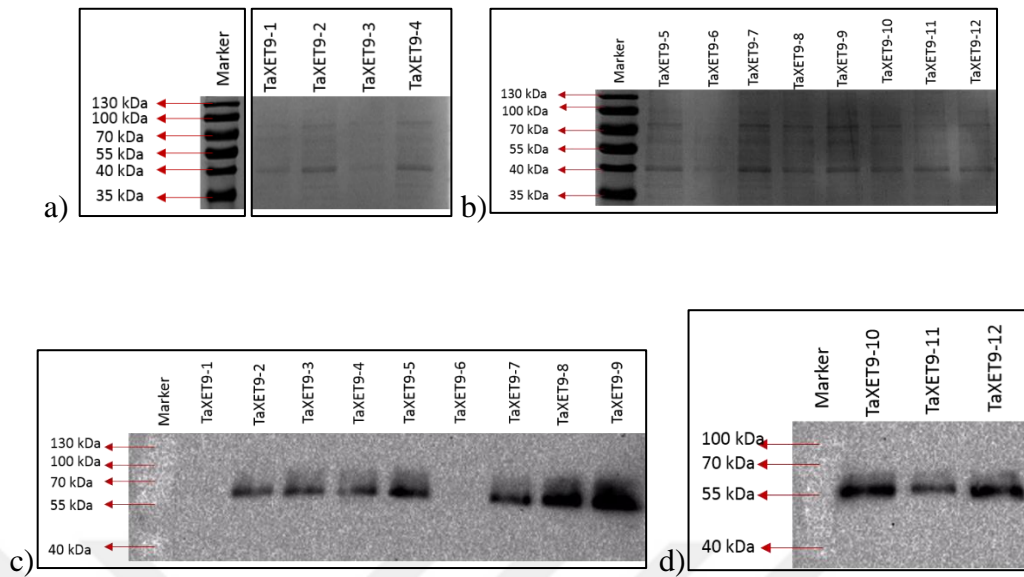
Figure 4.2. Detection of the heterologously expressed TaXTH9 enzyme in selected colonies using polyacrylamide gel electrophoresis. a) Coomassie dye staining of colonies between 1 and 4. b) Coomassie dye staining of colonies between 5 and 12. c) Western blot analysis of colonies between 1 and 9 using 6X-His tag antibody. d) Western blot analysis of colonies between 10 and 12 using 6X-His tag antibody. The size of the marker was indicated on the gel figures.

4.1.2. Expression of TaXTH9 Enzyme in *Pichia pastoris*

Transformant *P. pastoris* cells were grown in 3 lt of BMMY media and induced by addition of 1% v:v methanol at each 24 hours for five days. Before the addition of methanol, 1 ml of culture was removed, and absorbance measurement was carried out at 600 nm to observe the cell growth for five days. After the second day, the growth rate was decreased with increasing methanol concentration. (Figure 4.3.).
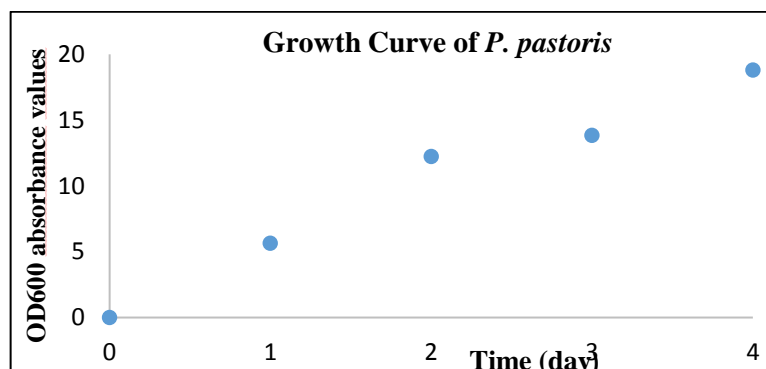
Figure 4.3. Growth curve of TaXTH9 transformant *P. pastoris* cells during methanol induction for five days. *P. pastoris* culture was diluted to 1/10 before the measurement.

4.1.3. Purification of TaXTH9 Enzyme Using Affinity and Size Exclusion Chromatography Techniques

6X-His tagged TaXTH9 colony 12 enzyme was purified using GE Healthcare HisTrap FF column which was precharged with nickel ions (Figure 4.4). At first, a huge protein peak was observed until 93 min. These proteins were not bound to the column. Then, the peak of TaXTH9 enzyme was detected. Totally, 13 fractions were obtained, but the collected fractions were started from 2nd to 7th according to the UV observed.
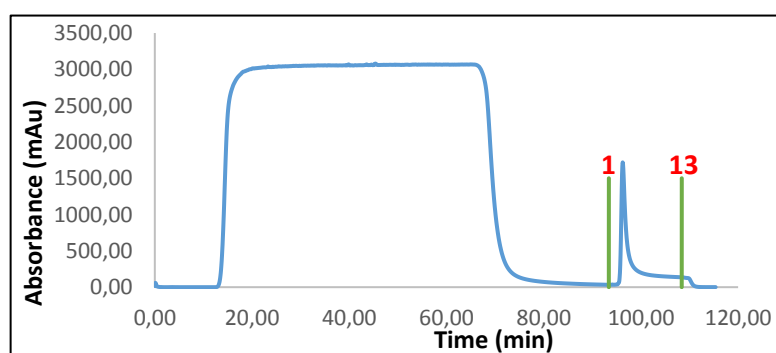
Figure 4.4. GE Healthcare HisTrap FF column chromatogram of purified TaXTH9 enzyme. The volume of each fraction was 3 ml. The fraction numbers were indicated on the graph as red color.

Heterologously expressed TaXTH9 enzyme was purified using Superdex 75 16/100 size exclusion column. When the absorbance (mAu) - time (min) chromatogram was analyzed, two peaks were noticed (Figure 4.5). The first peak was belong to f44-61, and the second peak which was the larger one belong to f62-120. When the absorbance levels were compared, it was determined that protein concentration of the second peak was higher.
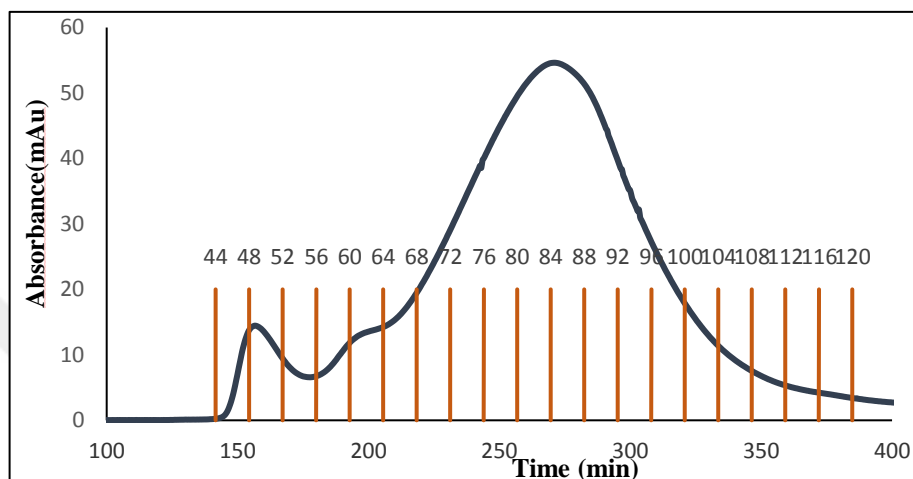
Figure 4.5. The GE Healthcare Superdex 75 16/100 size exclusion column chromatogram of purified TaXTH9 enzyme. The volume of each fraction was 3 ml. The fraction numbers were indicated on the graph as red color.

4.1.4. Detection of TaXTH9 Enzyme Using SDS-PAGE, Western Blot, and Dot Blot Techniques

TaXTH9 enzyme fractions were gathered in groups of threes and then concentrated to 1.5 ml approximately. The concentrated protein fractions were visualized by silver nitrate staining and western blotting. Furthermore, dot blot assay was performed to detect the enzyme activity of each group of fractions. Although, the size of the TaXTH9 protein was 33.2 kDa, size of the visualized protein bands were about 40 kDa-55 kDa (Figure 4.6). At the SDS-PAGE results, protein bands were detected only in f44-68. Protein bands belong to f44-70, and f53-59 were smear, but band belongs to f62-68 was clear. As a result of western blot analysis, protein bands were observed only in f44-77. Band of f71-77 was very slight. Band of f62-68 was clear than f44-50, and f53-59. According to the dot blot result, the luminescence of f44-95 was brighter than control.
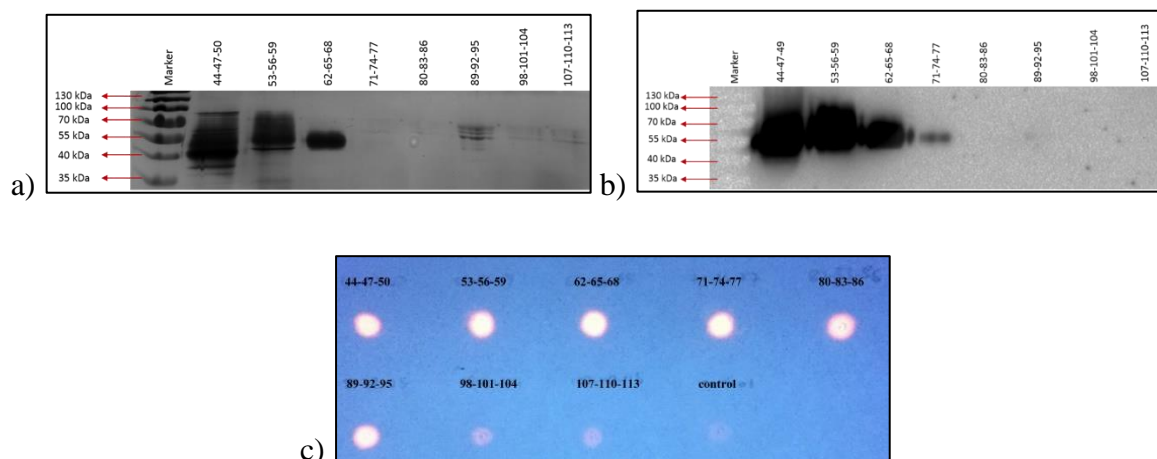
Figure 4.6. Analysis of purified TaXTH9 enzyme by GE Healthcare HiPrep 26/60 Sephacryl S-200 HR column a) Silver nitrate staining of f44-113, b) Western blot analysis of f44-113 using anti-6X His antibody c) Dot blot assay of f44-11. The size of the marker was indicated on the gel figures.

4.1.5. Bradford Assay, and Enzyme Activity Analysis

Bradford assay was performed to detect the protein concentration of f44-61 and f62-68 according to the BSA standard curve (Figure 4.7). Considering the Bradford assay result, the protein concentration of f44-61 was approximately six times more than f62-68 (Table 4.1).
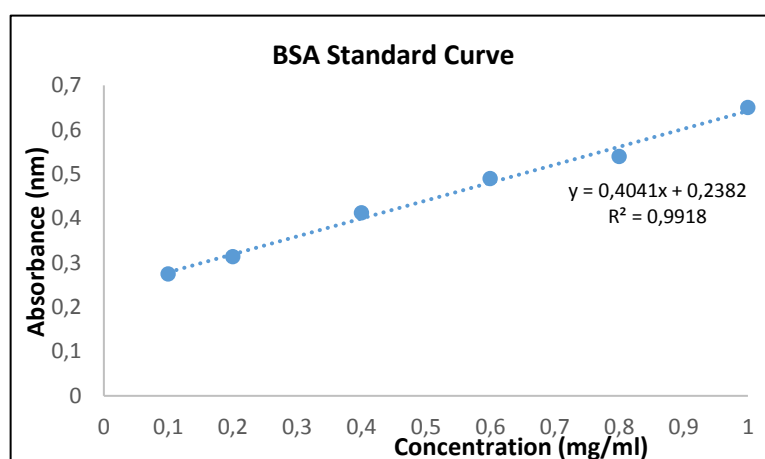
Figure 4.7. Standard Curve of BSA standards. Protein concentration was determined according to the standard curve.

Table 4.1. Bradford assay of purified TaXTH9 enzyme fractions.

Fraction range	Protein Concentration (mg/ml)
44-61	2.14 mg/ml
62-68	0.33 mg/ml

Diluted protein fractions were incubated with TXG donor, and XGO acceptor substrates for 1 hour to identify the enzyme activity. Although f44-61 was diluted ten times more than f62-68, enzyme activity (picokatals/mg) of f44-61 was higher due to the abundance of 6X-His tagged TaXTH9 proteins (Table 4.2). For the further TaXTH9 enzyme activity assays, f44-61 were chosen, while enzyme kinetic studies were carried out with f62-68.

Table 4.2. The enzyme activity of f44-61 and f62-68 in picokatals/mg unit. Dilution factor, incubation time, and fluorescence were also given below.

Fraction range	Donor-Acceptor Couple	Dilution Factor	Incubation Time	Fluorescence (Lu)	Picokatals/mg protein
44-61	TXG-XGO	1/200	1 hour	446	116.567
62-68	TXG-XGO	1/20	1 hour	1007	49.944

Activity analysis of different polysaccharide donor and oligosaccharide acceptor couples performed with fractions between 44 and 61 at different time intervals, and dilution factors. The hybrid donor-acceptor product was analyzed with fluorescence detector of HPLC system. The graph of fluorescence (Lu)-time (min) was plotted to observe the increase of hybrid donor-acceptor product (Figure 4.8). As a result, each of the hybrid donor-acceptor product was increased linearly at specific time intervals.
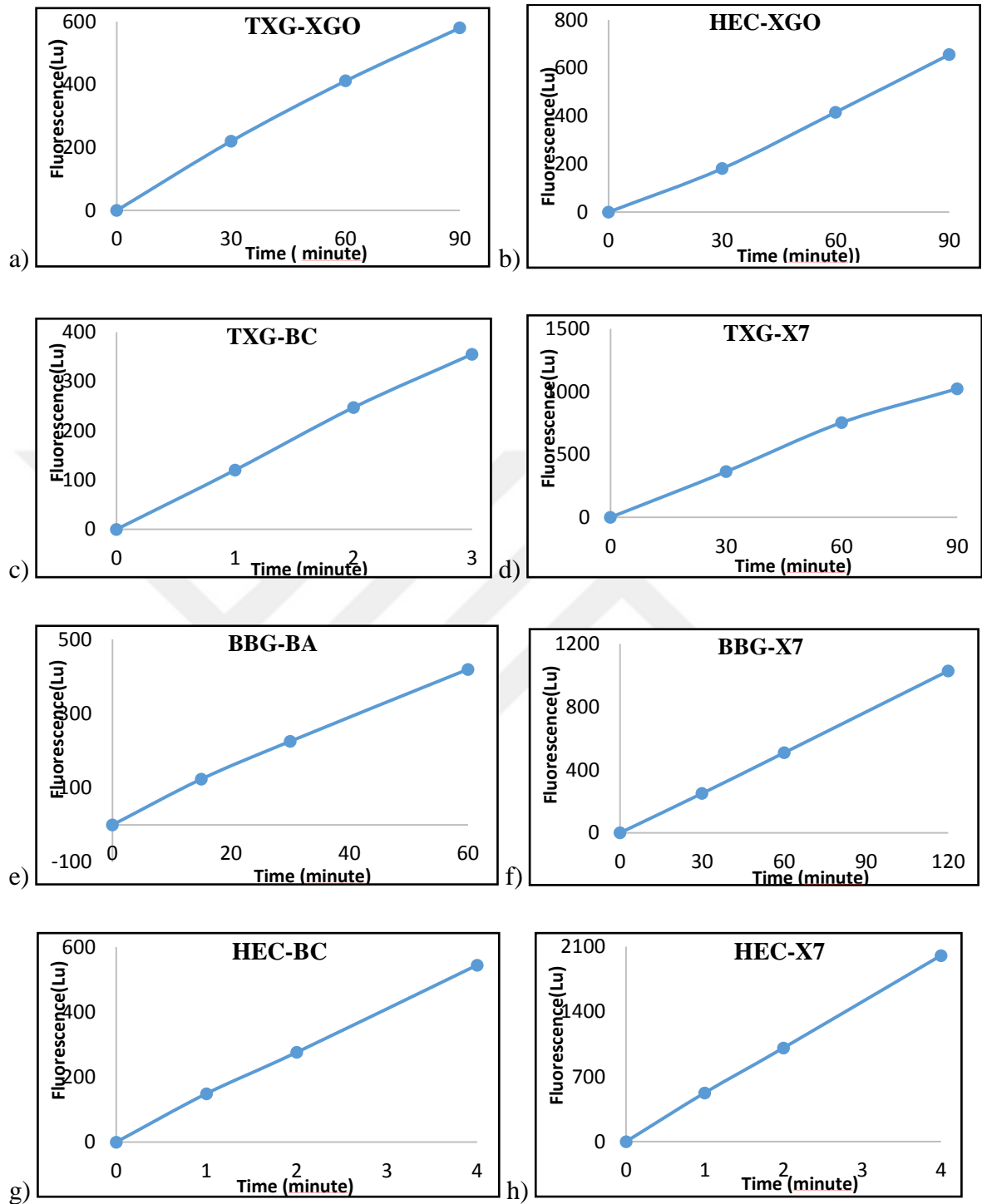
Figure 4.8. The fluorescence (Lu)-time (min) graph of TaXTH9 enzyme by using different substrate couples at different time intervals, and dilution factors. a) The enzyme activity graph of TXG-XGO substrate couple at 0,30,60,90 min. b) The enzyme activity graph of HEC-XGO substrate couple at 0,30,60,90 min c) The enzyme activity graph of TXG-BC substrate couple at 0,1,2,4 hour d) The enzyme activity graph of TXG-X7 substrate couple

at 0,30,60,90 min e) The enzyme activity graph of BBG-BA substrate couple at 0,20,40,60 min f) The enzyme activity graph of BBG-X7 substrate couple at 0,30,60,90,120 min g) The enzyme activity graph of HEC-BC substrate couple at 0,1,2,3,4 hour h) The enzyme activity graph of HEC-X7 substrate couple at 0,1,2,3,4 hour

After fluorescence belongs to different substrate couples were analyzed, specific enzyme activities were indicated as picokatal/mg enzyme unit (Table 4.3). Relative activity percentages of substrate couples were calculated according to TXG-XGO substrate couple. TaXTH9 enzyme exhibited the highest activity with HEC-XGO couple as 141,5 %. Also, TXG-X7 activity was higher than TXG-XGO couple.

Table 4.3. Enzyme activity of TaXTH9 with different substrate couples. The specific activities of each substrate couples were estimated to TXG-XGO percentage.

Donor-acceptor couple	Specific Activity (Picokatal/mg enzyme)	Relative Activity (%) to TXG-XGO
TXG-XGO	118.13	100
TXG-X7	137.34	116.26
TXG-CT	4.01	3.40
TXG-BB	44.62	37.77
TXG-XT	4.93	4.17
TXG-BA	3.03	2.57
TXG-BC	3.64	3.08
TXG-LT	0.64	0.54
TXG-GM	0.64	0.54
HEC-XGO	167.26	141.59
HEC-X7	80.94	68.52
HEC-CT	39.07	33.07
HEC-BB	94.91	80.34
HEC-XT	36.95	31.28
HEC-BA	17.56	15.12

HEC-BC	25.61	7.19
HEC-GM	5.30	9.74
HEC-LT	3.95	7.99
BBG-XGO	17.87	15.12
BBG-X7	23.62	19.99
BBG-CT	11.51	9,74
BBG-BB	9.44	7.99
BBG-XT	8.50	7.19
BBG-BA	5.34	4.52
BBG-BC	4.54	3.85
BBG-GM	1.59	1.34
BBG-LT	1.73	1.46
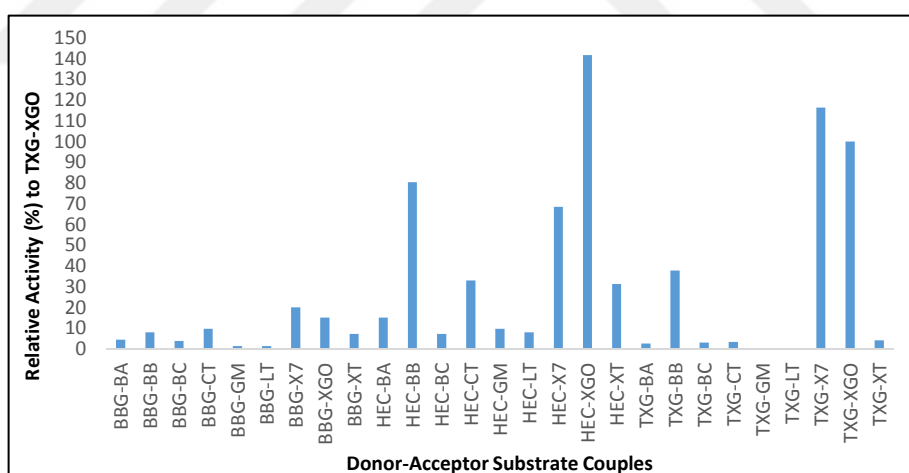
Figure 4.9. Demonstration of relative specific enzyme activity of each substrate couple according to the table 4.3. TXG-XGO was taken as the basis for the evaluating relative activities.

TaXTH9 enzyme activity at picokatal/mg unit with HEC donor and different acceptor substrates were indicated in Table 4.3. Relative activity percentages of substrate couples were calculated according to HEC-XGO substrate couple. As a result, enzyme activity with HEC-BB was the closest one to HEC-XGO (Table 4.4).

Table 4.4. Enzyme activity of TaXTH9 with different substrate couples. HEC-XGO was taken as the basis for the evaluating relative activities.

Donor-acceptor couple	Relative Activity (%) to HEC-XGO
HEC-XGO	100
HEC-X7	48.39
HEC-CT	23.36
HEC-BB	56.74
HEC-XT	22.09
HEC-BA	10.49
HEC-BC	15.31
HEC-GM	3.16
HEC-LT	2.36
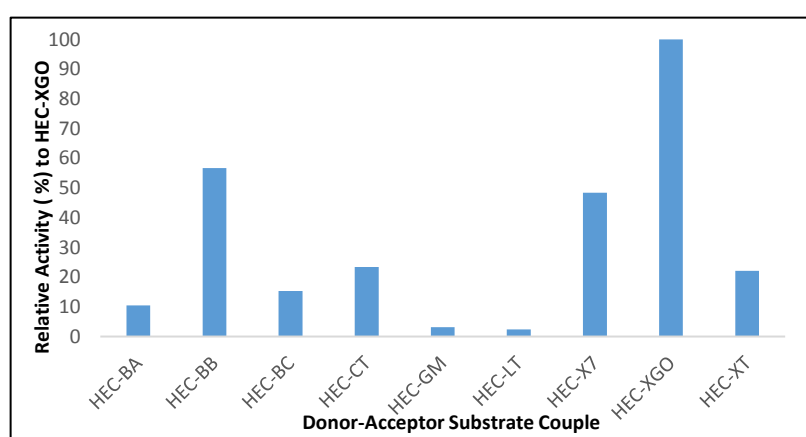
Figure 4.10. Demonstration of relative specific enzyme activity of different substrate couples according to the table 4.4.

4.1.6. Enzyme Kinetic Studies

TXG-X7 and HEC-X7 substrate couples were chosen for the kinetic studies. At first, optimum TXG, and HEC donor substrate concentrations were determined with 50 μM X7 acceptor substrate. Optimum TXG and HEC substrate concentration were detected as 0.4 % (Figure 4.10). Then, optimum X7 substrate concentration with each donor at 0.4% was detected. According to the Michaelis-Menten graph, the curve was reached to plateau phase at 23 μM final X7 concentration (figure 4.12).
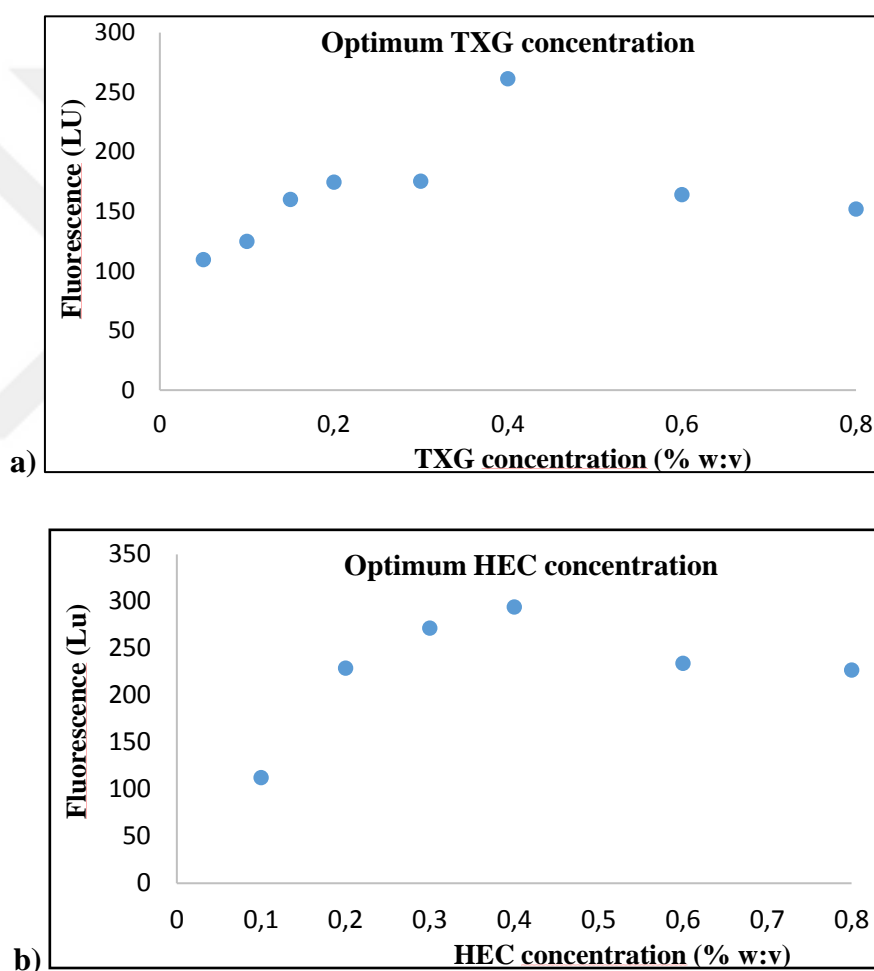
Figure 4.11. Detection of optimum donor concentrations for TaXTH9 enzyme activity. a) Enzyme activity with different TXG donor substrate concentrations. b) Enzyme activity with different HEC donor substrate concentrations.
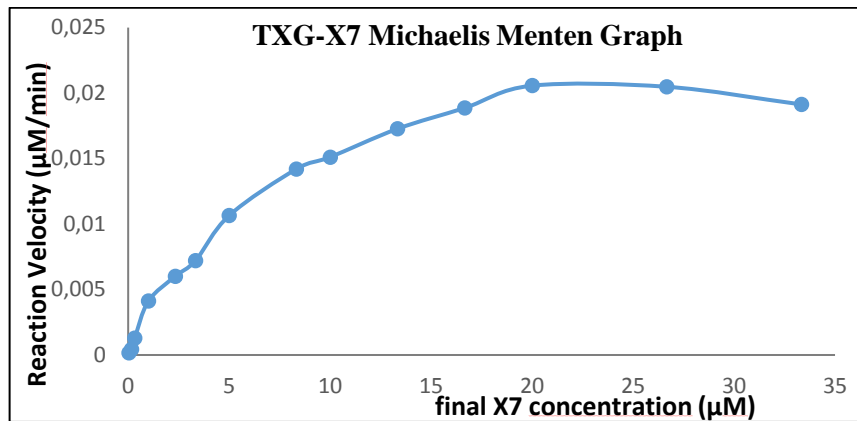
Figure 4.12. Michaelis-Menten graph of TaXTH9 enzyme with 0.4% TXG and various X7 concentrations.

Kinetic calculations of TaXTH9 enzyme were carried out according to the TXG-X7, and HEC-X7 Lineweaver-Burk graphs (Figure 4.13). As a result of kinetic studies with the TXG-X7 couple, it was calculated that enzyme had V_{max} value 0,033 µM/min, K_m value 11,65 µM and K_{cat} value 0.019 min^{-1}. As a result of kinetic studies with the HEC-X7 couple, it was calculated that V_{max} value 0.004 µM/min, K_m value 0.484 µM and K_{cat} value 0.002 min^{-1}.
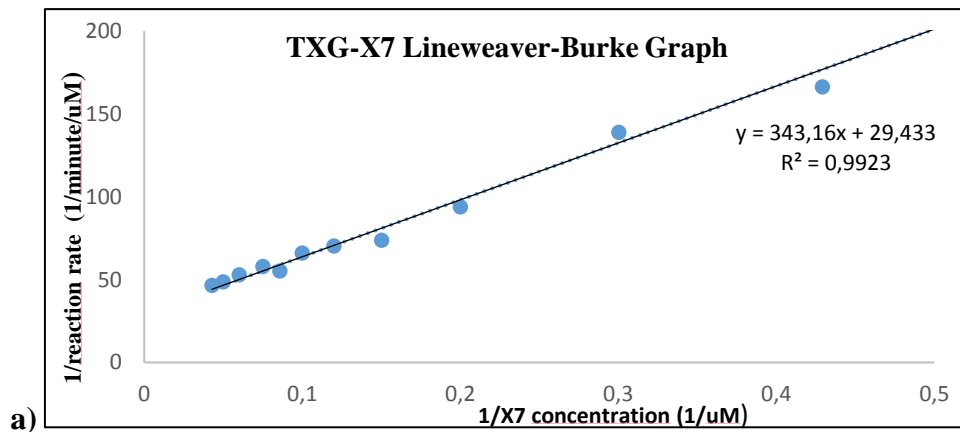
a)
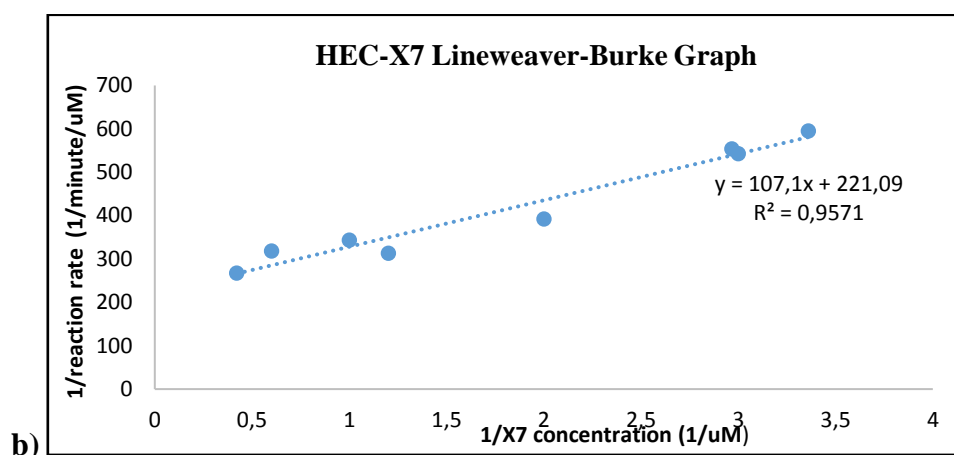
Figure 4.13. Lineweaver-Burke graphs of TaXTH9 enzyme. a) Lineweaver-Burke graph of enzyme with 0.4% TXG and various X7 concentrations b) Lineweaver-Burke graph of enzyme with 0.4% HEC and various X7 concentrations

4.2. PRODUCTION AND PURIFICATION OF AtXTH3 ENZYME

4.2.1. Production of AtXTH3 in 2.5 lt of BMMY Medium in an Erlenmeyer flask

4.2.1.1. Purification of AtXTH3 Using Affinity and Size Exclusion Chromatography Techniques

6X-His tagged AtXTH3 colony eight enzyme was purified using GE Healthcare HisTrap FF column which was precharged with nickel ions (Figure 4.14). At first, a huge protein peak was observed until 200 min. These proteins were not bound to the column. Then, peak of AtXTH3 enzyme was detected. Totally, 13 fractions were obtained, but fractions between 2 and 7 were collected according to the measured absorbance.
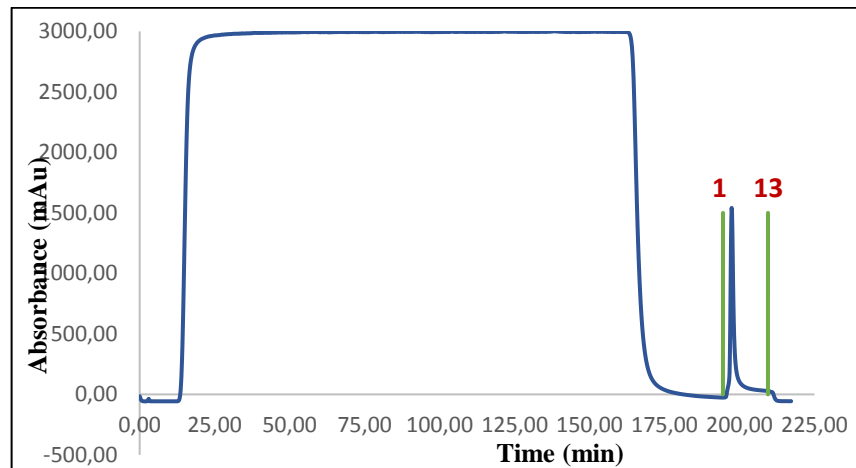
Figure 4.14. GE Healthcare HisTrap FF column chromatogram of purified AtXTH3 enzyme. The volume of each fraction was 3 ml. The fraction numbers were indicated on the graph as red color.

After affinity chromatography technique was performed, AtXTH3 enzyme was purified using size exclusion chromatography. Protein mixture was passed over GE Healthcare Superdex 75 16/100 size exclusion column (Figure 4.15). As a result of separation, two peaks were detected. Absorbance level of the first peak was higher than the second one. Also, the second peak was broader than the first peak. Totally, 96 fractions were obtained, but from the 20th fractions, proteins were collected.
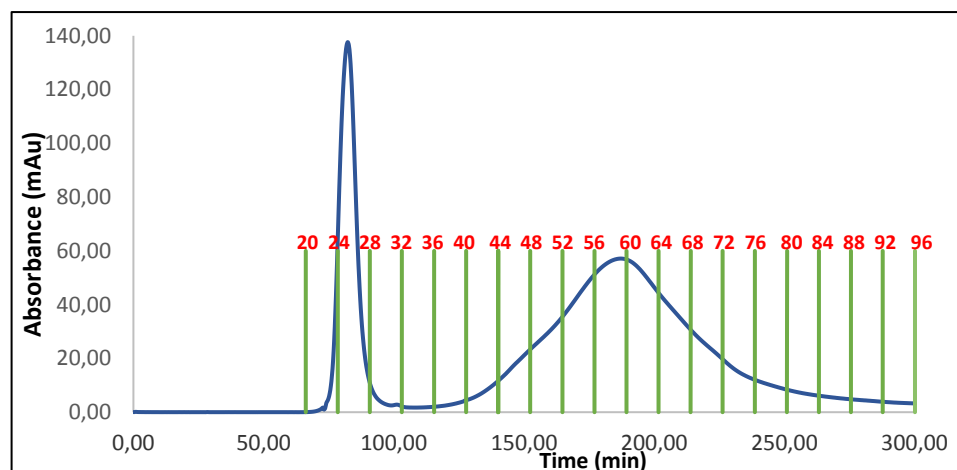
Figure 4.15. The GE Healthcare Superdex 75 16/100 size exclusion column chromatogram of purified AtXTH3 enzyme. The volume of each fraction was 3 ml. The fraction numbers were indicated on the graph as red color.

4.2.1.2. Detection of Protein with SDS-PAGE, Western Blot, and Dot Blot Techniques

Silver nitrate staining was performed to detect the purified AtXTH3 fractions which were gathered in groups of threes and concentrated to 1.5 ml approximately. The expected size of AtXTH3 enzyme was about 33.5 kDa. As a result of SDS-PAGE, the size of visualized AtXTH3 enzyme was about 33.5 kDa. AtXTH3 enzyme bands were detected in f20-34, and f44-64. There were impurities in f23-31, and bands were broader with less distinct edges. Band of f44-46 was very faint. The doublet was indicated in f20-22, and f59-64. Also, proteins were detected in empty wells because of loading high amount of sample. Also, western blotting was performed to detect the 6X His-tagged AtXTH3 with 6X His antibody. The size of visualized AtXTH3 enzyme was about 33.5 kDa. AtXTH3 proteins were detected in f20-34, and f38-64. Protein bands were smear in f23-28, and f41-46. Proteins bands of f47-64 were distinct, but f59-64 had faint bands. Furthermore, dot blot analysis was carried out to detect the enzyme activity. As a result, the luminescence of f25-31, and f41-58 was brighter than control (Figure 4.16).
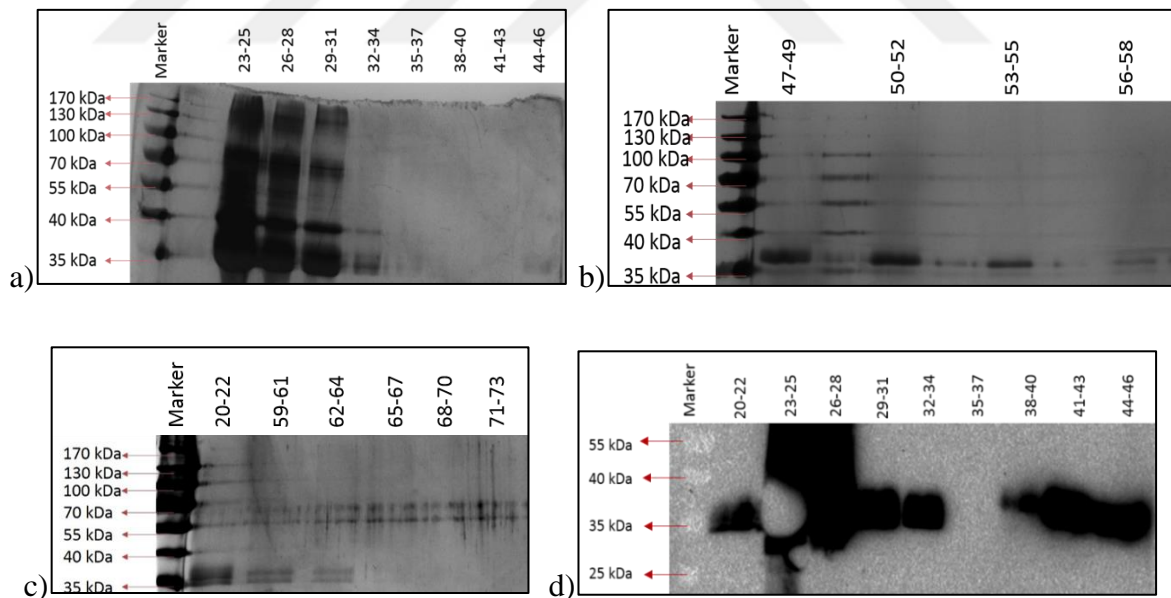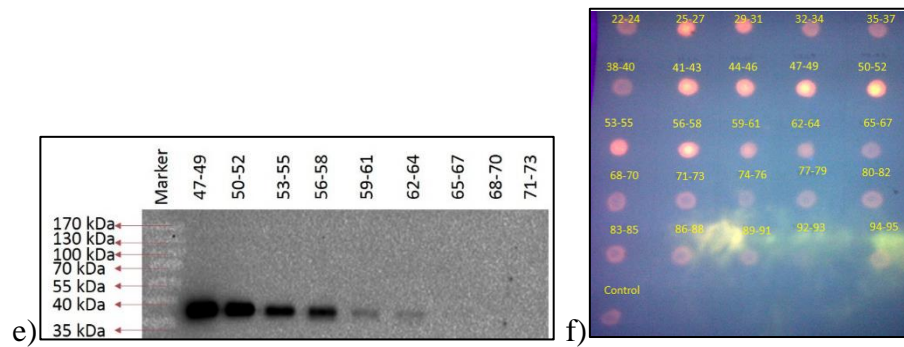
Figure 4.16. Analysis of purified AtXTH3 enzyme by GE Healthcare HiPrep 26/60 Sephacryl S-200 HR column a) SDS-PAGE analysis of f20-46, b) SDS-PAGE analysis of f47-58 c) SDS-PAGE analysis of f20-23 plus f59-73 d) Western blot analysis of f20-46 using anti 6X His antibody d) Western blot analysis of f47-58 using anti 6X His antibody c) Dot blot analysis of f22-95. The volume of each fraction was 3 ml. The size of the marker was indicated on the gel figures.

4.2.1.3. Enzyme Activity Analysis

AtXTH3 activity analysis of f44-61 was carried out with TXG, and HEC donor substrates, and XGO acceptor substrate for 1 hour. Fluorescence of each substrate couple was detected by HPLC detector. It was expected from AtXTH3 to have the highest activity with TXG-XGO couple as a xyloglucan endotransglycosylase enzyme. However, it was analyzed that AtXTH3 had more affinity to bind to BBG polysaccharide rather than TXG polysaccharide. The enzyme was approximately five times more active with BBG-XGO substrate couple (Table 4.5). For the further enzyme activity, and kinetic studies, large-scale production of AtXTH3 was carried out in a bioreactor to produce enzyme with more concentration.

Table 4.5. Fluorescence level of TXG-XGO and BBG-XGO couples detected by HPLC detector. Fraction range, the amount of dilution, incubation time were also given below.

Fraction range	Donor-Acceptor Couple	Amount of Dilution	Incubation Time	Fluorescence
f44-61	TXG-XGO	1/20	1 saat	740.6
f44-61	BBG-XGO	1/20	1 saat	4231

4.2.2. Production of AtXTH3 in 2.5 lt of BMMY Medium in a Bioreactor

4.2.2.1. Expression of AtXTH3 in Pichia pastoris

Large scale production of *AtXTH3* colony eight was carried out while transformant *P. pastoris* cells were grown in 2.5 lt BMMY medium and induced by addition of 1% v:v methanol at each 24 hours for five days. Each day, OD600 values were measured before the methanol addition. According to the results, it was detected that growth rate of *P. pastoris* cells was decreased with increasing methanol concentration after the second day. (Figure 4.17).

Figure 4.17. Growth curve of *AtXTH3* transformant *P. pastoris* cells during methanol induction for five days. *P. pastoris* culture was diluted to 1/10 before the measurement.

4.2.2.2. Purification of AtXTH3 Enzyme Using Chromatography Technique

6X-His tagged AtXTH3 enzyme was purified using GE Healthcare HisTrap FF column (Figure 4.18). At first, a huge protein peak was observed until 110 min. These proteins were not bound to the column. Then, the peak of AtXTH3 enzyme was detected. Totally, 13 fractions were obtained, but fractions between 2 and seven were collected according to the measured absorbance.

Figure 4.18. GE Healthcare HisTrap FF column chromatogram of purified AtXTH3 enzyme. The volume of each fraction was 3 ml. The fraction numbers were indicated on the graph as red color.

4.2.2.3. Detection of Protein with SDS-PAGE Analysis

Fractions between 8 and 37 were separated on 12% polyacrylamide gel-based on their molecular weight, and silver nitrate staining was performed to detect the AtXTH3 enzyme in these fractions (figure 4.19). As a result, protein bands about 33.5 kDa size were observed in f18-27, but there were at least two bands which were in similar density, and thickness that migrate close together. Also, there was a dark line at 55 kDa, and 70 kDA on each gel.
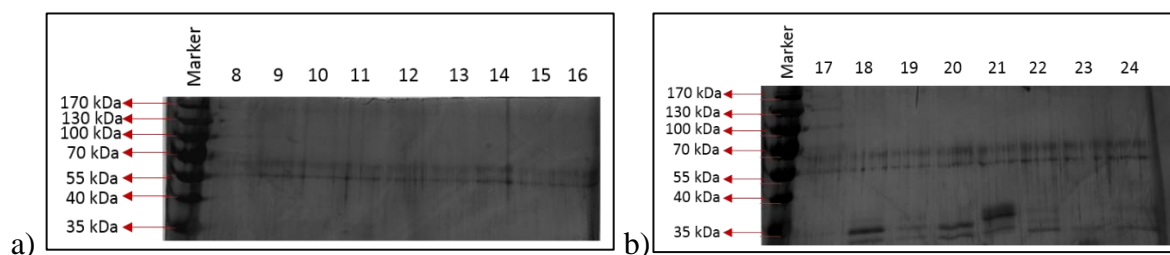
Figure 4.19. Analysis of AtXTH3 fractions which were separated using GE Healthcare HiPrep 26/60 Sephacryl S-200 HR column. a) SDS-PAGE coomassie dye staining of f8-16 b) SDS-PAGE coomassie dye staining of f17-24 c) SDS-PAGE coomassie dye staining of f25-33 d) SDS-PAGE coomassie dye staining of f34-37. The volume of each fraction was 9 ml. The size of the marker, and number of fractions were indicated on the figures.

4.2.2.4. Detection of Protein with Western Blotting, and Dot Blot Analysis

6X-His tag antibody was used to detect 6X-His tagged AtXTH3 enzyme in fractions between 8 and 37 (Figure 4.20). According to the gel images, it was observed that fractions 18, 20, 21, and 25 contained AtXTH3 enzyme. Bands of f18 and f21 were very dark, whereas bands of f19, and f25 were faint. In addition, dot blotting was performed to detect the xyloglucan endotransglycosylase activity in these fractions. As a result, it was observed that luminescence of f17, f18, f19, and f21 were brighter than control.

Figure 4.20. Analysis of AtXTH3 fractions which were separated using GE Healthcare HiPrep 26/60 Sephacryl S-200 HR column. a) Western blot analysis of f8-16 using anti-6X His tag antibody b) Western blot analysis of f17-25 using anti-6X His tag antibody c) Western blot analysis of f26-31 using anti-6X His tag antibody d) Western blot analysis of f32-37 using anti-6X His tag antibody e) Dot blot analysis of f8-37. The volume of each fraction was 9 ml. The size of the marker, and number of fractions were indicated on the figures.

4.2.3. Production of AtXTH3 in 1.5 lt of BMMY Medium in an Erlenmeyer flask

4.2.3.1. Expression of AtXTH3 Enzyme in Pichia pastoris

AtXTH3 colony eight was expressed in competent *P. pastoris* using 2.5 lt BMMY medium. 1% v:v methanol induction was carried out at each 24 hours for five days. Each day, OD600 values were measured before methanol addition. According to the results, it was detected that growth rate of *P. pastoris* cells was decreased with increasing methanol concentration after the second day. (Figure 4.21).
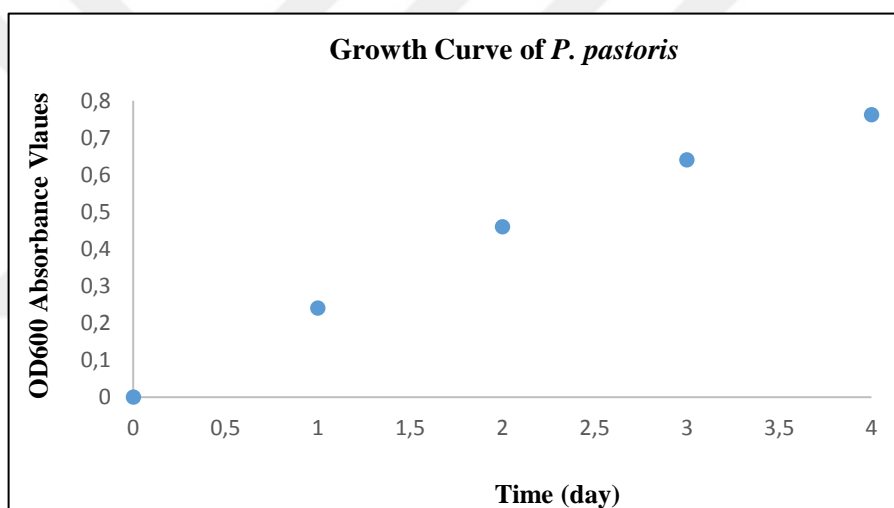
Growth Curve of *P. pastoris*
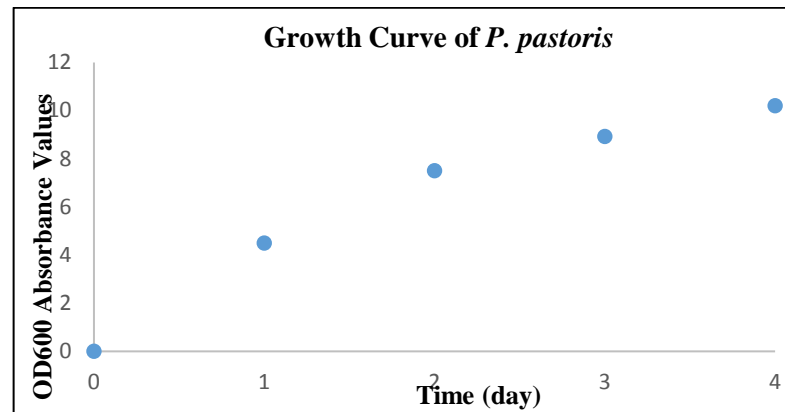
Figure 4.21. Growth curve of *AtXTH3* transformant *P. pastoris* cells during methanol induction for five days. *P. pastoris* culture was diluted to 1/20 before the measurement.

4.2.3.2. Purification of AtXTH3 Enzyme Using Chromatography Technique

6X-His tagged AtXTH3 enzyme was purified using GE Healthcare HisTrap FF column (Figure 4.22). At first, a huge protein peak was observed until 80 min. These proteins were not bound to the column. Then, extra peak was detected between 80 min and 100 min. Then, AtXTH3 enzyme was detected at the third peak. Totally, 13 fractions were obtained, but fractions between 2 and 7 were collected according to the measured absorbance.
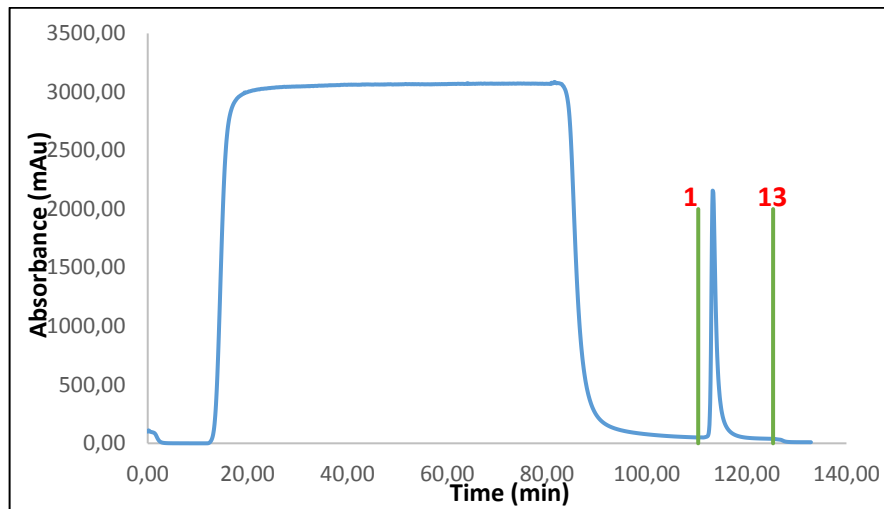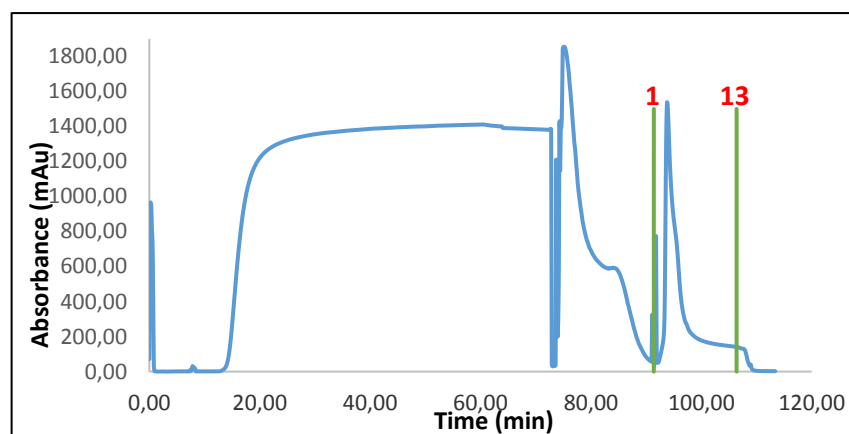

Figure 4.22. GE Healthcare HisTrap FF column chromatogram of purified AtXTH3 enzyme. The volume of each fraction was 3 ml. The fraction numbers were indicated on the graph as red color.

6X-His tagged AtXTH3 enzyme was purified using GE Healthcare Superdex 75 16/100 size exclusion column (Figure 4.23). The absorbance of the peak was very low. Proteins were not detected. Totally, 40 fractions were obtained, but fractions between 9 and 26 were collected for the further studies.
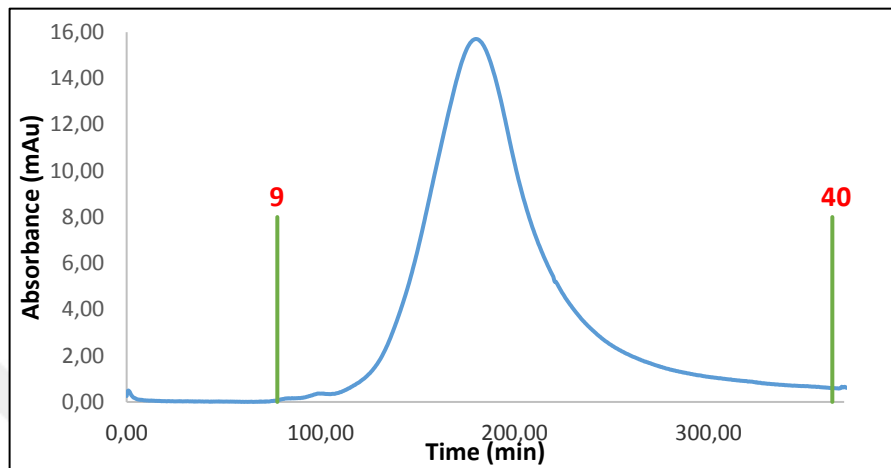
Figure 4.23. The GE Healthcare Superdex 75 16/100 size exclusion column chromatogram of purified AtXTH3 enzyme. The volume of each fraction was 3 ml. The fraction numbers are indicated on the graph as red color.

4.2.3.3. Detection of Protein with Western Blot, and Dot Blot Analysis

6X-His tag antibody was used to detect AtXTH3 enzyme in fractions between 9 and 26 (Figure 4.24). According to the result, AtXTH3 enzyme was not detected. Also, dot blot analysis was performed, but luminescence signal level of fractions and control were not distinguishable.
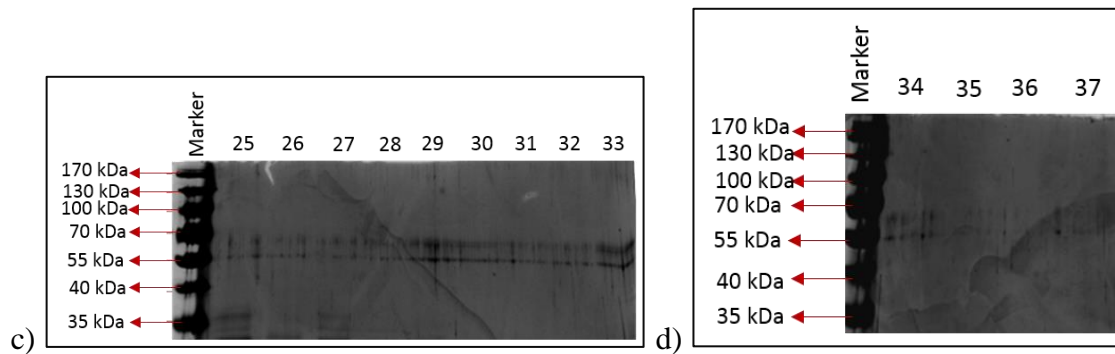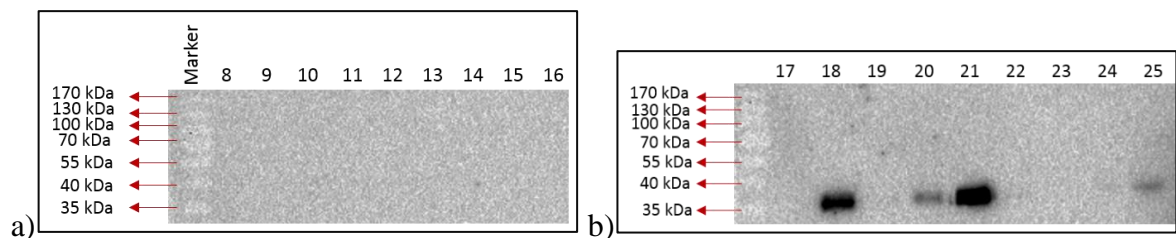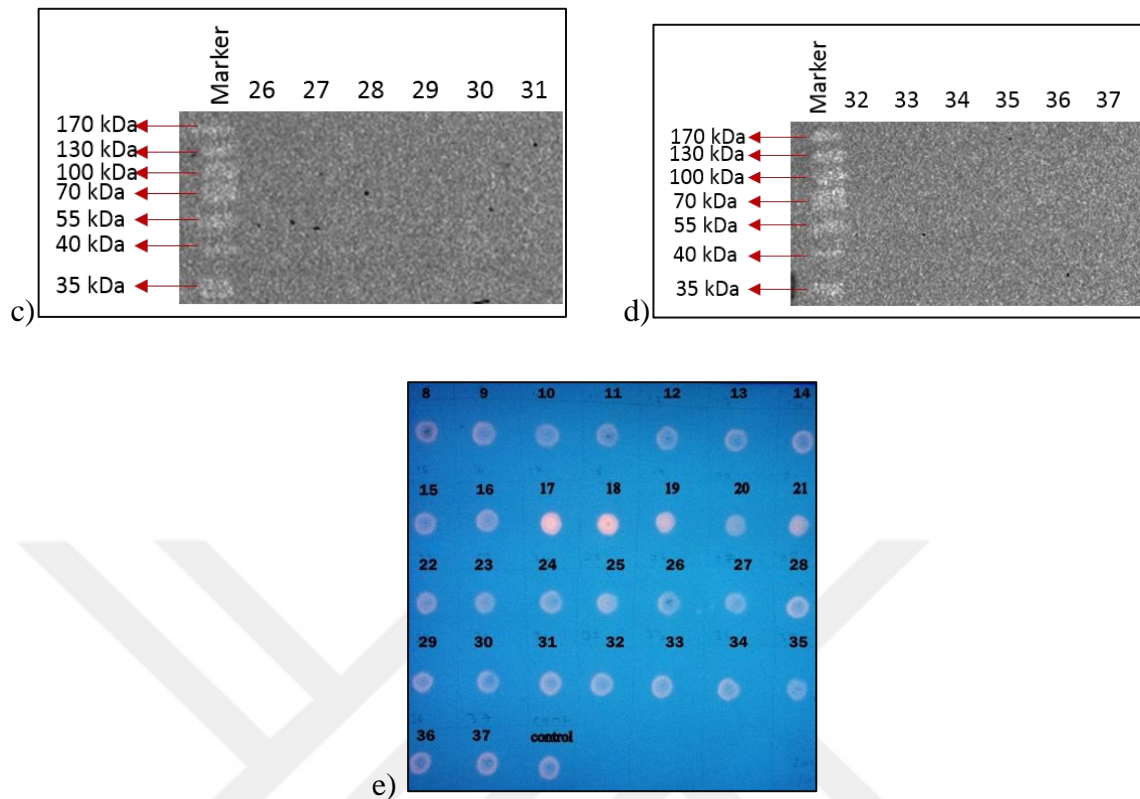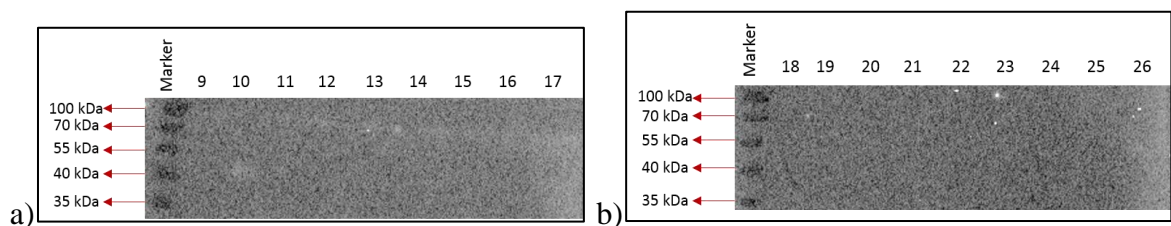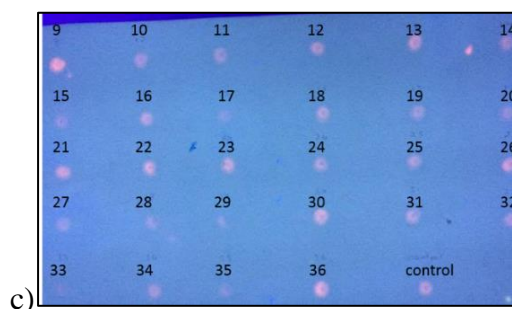
Figure 4.24. Analysis of AtXTH3 fractions which were separated using GE Healthcare HiPrep 26/60 Sephacryl S-200 HR column. a) Western blot analysis of f9-17 using anti-6X His tag antibody b) Western blot analysis of f18-26 using anti-6X His tag antibody c) Dot blot analysis of f9-17. The volume of each fraction was 9 ml. The size of marker, and a number of fractions were indicated on the figures.

4.2.3.4. Enzyme Activity Analysis

2 µl of sample was removed at each step of purification of AtXTH3 enzyme, and incubated with 10 µl of TXG donor, and 1 µl of XGO acceptor substrates for 4 hours to identify the AtXTH3 enzyme activity (Table 4.6). The hybrid donor-acceptor product was analyzed with fluorescence detector of HPLC system. Enzyme activity after ammonium sulfate precipitation and dialysis was very high, but there was a huge decrease after dialysis. When the protein sample was loaded onto GE Healthcare HiPrep 26/60 Sephacryl S-200 HR column, xyloglucan endotransglycosylase activity was lost totally. For this reason, further enzyme activity assays and kinetic studies were not carried out.

Table 4.6. AtXTH3 enzyme activity assay at each step of purification. The volume of sample, incubation time and fluorescence level were indicated.

Method	Volume of Sample	Incubation Time	Fluorescence (Lu)
Methanol Induction	100 ml	4 hour	40
Ammonium Sulphate Precipitation	60 ml	4 hour	3985.5
Dialysis	185 ml	4 hour	2172.1

| Buffer Exchange | 25 ml | 4 hour | 343.1 |
| Purification with Size Exclusion Chromatography | 2 ml | 4 hour | 20 |

4.2.4. Retransformation into *Pichia pastoris*, and Positive Colony Selection

Transformation of pPicZα-C/*AtXTH3* into competent *P. pastoris* cells were carried out (Figure 4.25). 27 of transformant colonies were picked randomly, and AtXTH3 enzyme was expressed in *P. pastoris* cells in 250 ml BMMY medium. *P. pastoris* cells were induced by addition of 1% v:v methanol at each 24 hours for five days. Enzyme activity assay, SDS-PAGE analysis, and western blotting were performed to detect the colony which expressed the most active AtXTH3 enzyme (Figure 4.26).
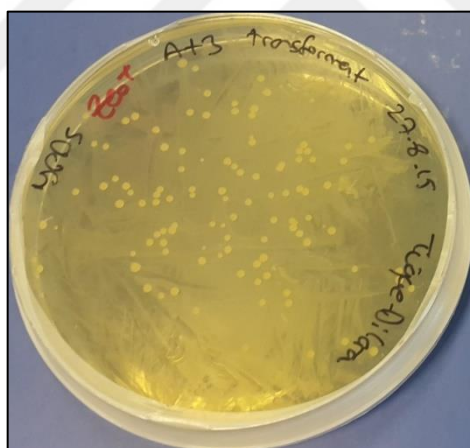
Figure 4.25. pPicZα-C/*AtXTH3* transformant *P. pastoris* colonies that were grown in YPDS agar+zeocin plate.

As a result of coomassie-dye staining, several protein bands were visualized. As a result of western blotting, AtXTH3 enzyme was visualized at 35 kDa size in colonies between 2 and 10, colonies between 19 and 15, and colony 27. Highest intensive bands were observed in colonies 2, 3, 8, and 10. According to the enzyme activity assay, it was detected that AtXTH3 activity of selected colonies were not enough. Because there was a probability of a problem

in extracellular secretion of AtXTH3 enzyme, cell lysation was carried out to control whether AtXTH3 was in intracellular, or not.
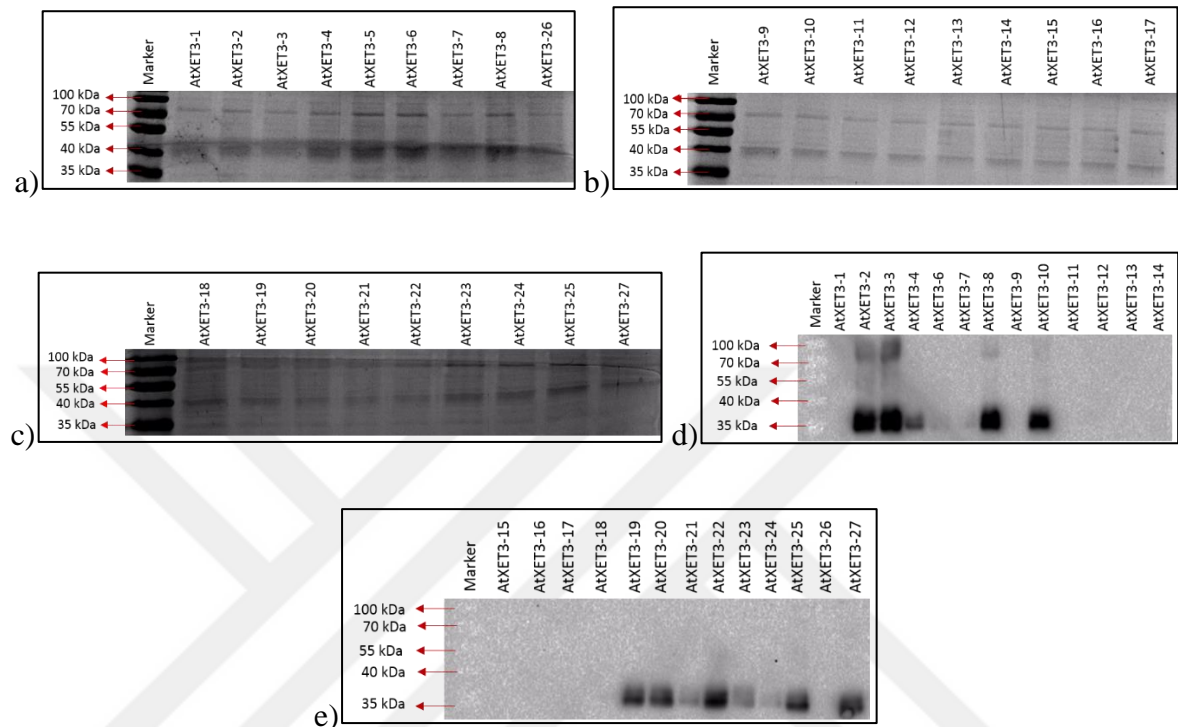
Figure 4.26. Detection of heterologously expressed AtXTH3 enzyme in selected colonies using polyacrylamide gel electrophoresis. a) Coomassie dye staining of colonies between 1 and 8, and colony 26 b) Coomassie dye staining of colonies between 9 and 17. C) Coomassie dye staining of colonies between 18 and 25, and colony 27. d) Western blot analysis of colonies between 1 and 14 using 6X-His tag antibody. e) Western blot analysis of colonies between 15 and 27 using 6X-His tag antibody. The size of the marker was indicated on the gel figures.

4.2.5. Cell Lysis and Protein Extraction

The most active colonies were selected for the cell lysation. After cells were lysed using acid-washed glass beads, proteins were obtained. Then, SDS-PAGE coomassie brilliant blue staining, and western blot analysis were performed to detect AtXTH3 enzyme (Figure 4.27). Protein bands were visualized as a result of each analysis. The detected bands could be a

sign of intracellular AtXTH3 enzyme, so sequencing of pPicZα-C/*AtXTH3* plasmid was carried out. As a result of reading the nucleotide bases in pPicZα-C/*AtXTH3* plasmid, it was determined that there was not any problem such as frameshift mutation in plasmid DNA.
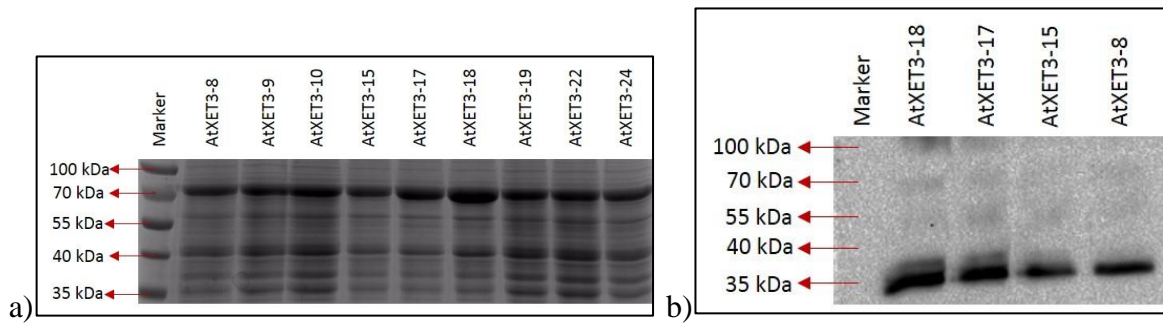
Figure 4.27. Detection of heterologously expressed AtXTH3 enzyme in selected colonies using polyacrylamide gel electrophoresis. a) Coomassie brilliant blue staining of colonies 8, 9, 10, 15, 17, 18, 19, 22, and 24. b) Western blot analysis of colonies 18, 17, 15, and 8 using 6X-His tag antibody. The size of the marker was indicated on the gel figures.

4.3. PRODUCTION AND PURIFICATION OF GhEG16, AND HvEG16 ENZYMES

4.3.1. Plasmid Isolation, and Double Digestion

10 number of pET-28/*GhEG16* and pET-28/*HvEG16* plasmids were isolated from transformant DH5α cells. Double digestion of plasmids was carried out to find out whether plasmids consisted of the gene of interest, or not. pET-28/*GhEG16* was digested with BamHI+NotI restriction endonucleases, whereas pET-28/*HvEG16* was digested with ECORI+NotI restriction endonucleases. As a result of agarose gel electrophoresis, it was visualized that colony 7 consisted of *HvEG16*, and colony 7 consisted of *GhEG16* (Figure 4.28).
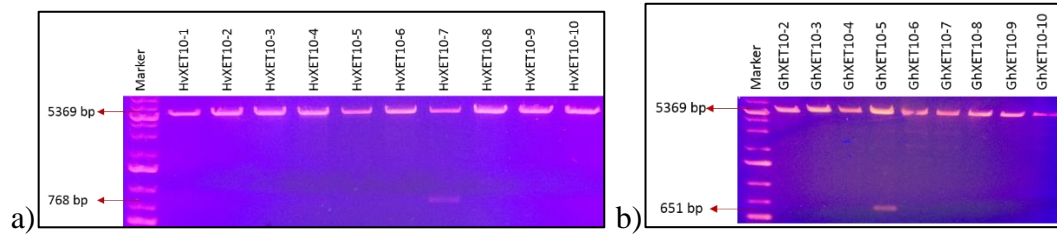
Figure 4.28. Double digestion of pET-28/*GhEG16*, and pET-28/*HvEG16* plasmids. a) Digestion of pET-28/*GhEG16* plasmid with BamHI+NotI restriction endonucleases. b) Digestion of pET-28/*HvEG16* plasmid with ECORI+NotI restriction endonucleases. The size of marker was indicated on gel figures.

4.3.2. Detection of Protein with SDS-PAGE, and Western Blot Analysis

At first trial, GhEG16, and HvEG16 enzymes were expressed in Bl21DE3 Star and Bl21 Codon Plus DE3 RIPL cells at variable growth conditions. 1M IPTG addition was carried out to each sample, but incubation time and temperature was variable. A group of cell was incubated at 16 °C overnight, whereas another group was incubated at 30 °C for 3 hours. Coomassie dye staining was performed to visualize the GhEG16 and HvEG16 enzymes which were separated from intracellular. It was expected to detect GhEG16 enzyme at 26.2 kDa, and HvEG16 at 33.2 kDa. As a result of SDS-PAGE, several bands were visualized for each sample, but there were not any difference between empty plasmids and transformant plasmids, between induced and non-induced, and between 16 °C incubation and 30 °C incubation (Figure 4.29). Western blotting was performed to detect GhEG16 and HvEG16enzymes using 6X His antibody. As a result, only 1 M IPTG induced HvEG16 which was expressed in Bl21 DE3 star cell at 16 °C was detected. The size of the enzyme was about 33.2 kDa, but bands at higher size were also detected.
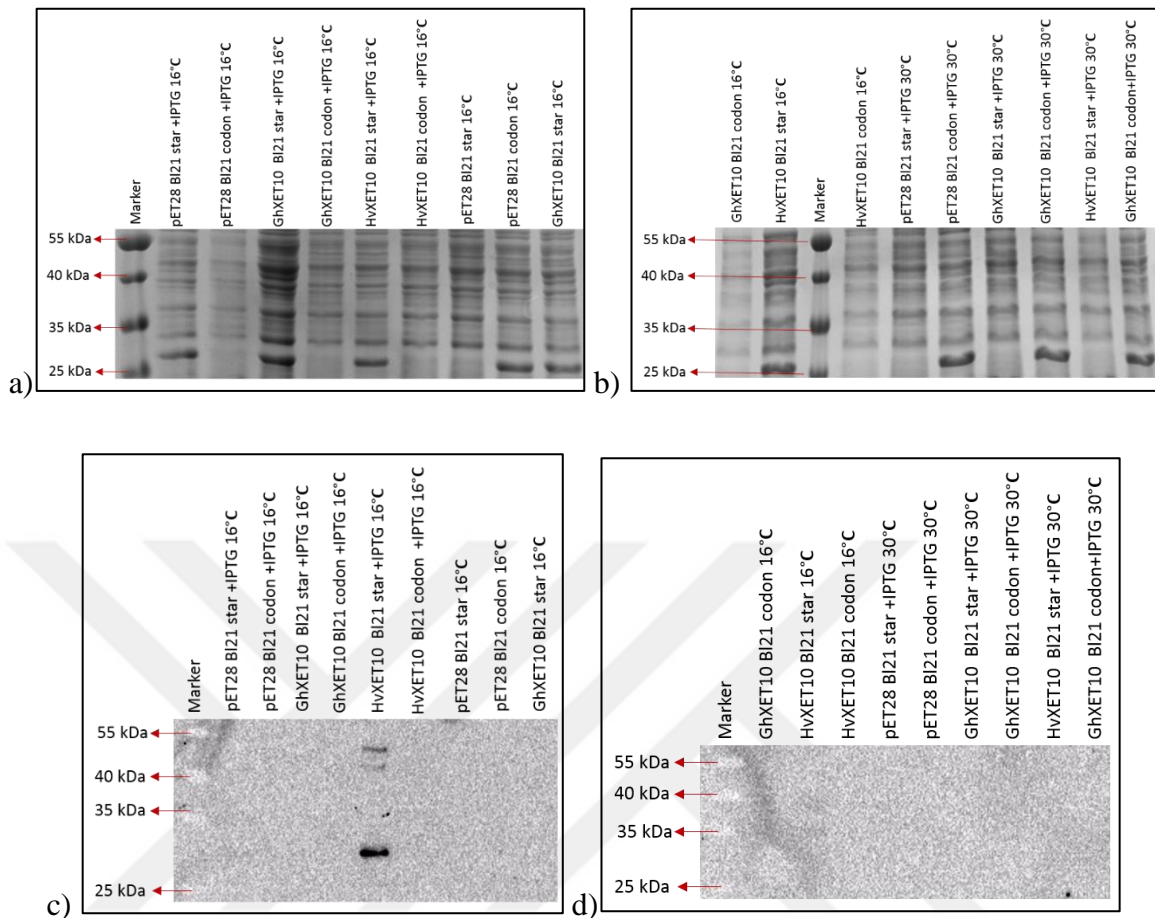
Figure 4.29. Analysis of HvEG16, and GhEG16 enzymes. a) Coomassie dye staining of HvEG16 and GhEG16 enzymes. b) Coomassie dye staining of HvEG16 and GhEG16 enzymes. c) Western blotting of HvEG16 and GhEG16 enzymes using anti-6X His antibody. d) Western blotting of HvEG16 and GhEG16 enzymes using anti-6X His antibody. Name of the samples, and size of the marker was indicated on gel figure.

At the second trial, incubation time and temperatures were constant, but IPTG concentration was variable. 0.5 M, 1 M, 2 M, and 5 M of IPTG was added, and cells were incubated at 37 °C for 5 hours. Coomassie dye staining was performed to detect the proteins (Figure 4.30). As a result, protein bands were very faint, and there were not any difference between each sample. HvEG16 and GhEG16 enzymes were not detected.
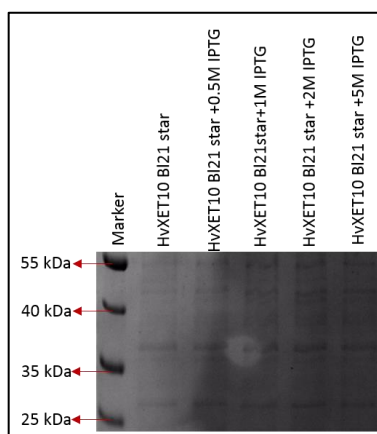
Figure 4.30. Coomassie dye staining of HvEG16 Bl21 star non-induced, HvEG16 Bl21star induced with 0.5M IPTG, HvEG16 Bl21star induced with 1M IPTG, HvEG16 Bl21star induced with 2M IPTG, and HvEG16 Bl21star induced with 5M IPTG. The size of marker was indicated on gel figure.

4.3.3. Somogyi-Nelson Method

Somogyi-Nelson method was used for quantitative determination of reducing sugars which arise by hydrolytic activity of enzymes. The absorbance of samples was measured at 520 nm. As a result, absorbance values were very low (Table 4.7). Hydrolytic activity of HvEG16 and GhEG16 enzymes were not detected.

Table 4.7. Spectrophotometer measurement of HvEG16 and GhEG16 enzymes at 520 nm.

Enzymes	Absorbance
pET28 Bl21 star	0.033
pET28 Bl21 codon plus	0.022
pET28/*GhEG16* Bl21 star	0.023
pET28/*GhEG16* Bl21 codon plus	0.039
pET28/*HvEG16* Bl21 star	0.027

pET28/*HvEG16* Bl21 codon plus	0.029
pET28 Bl21 star +IPTG	0.020
pET28 Bl21 codon plus +IPTG	0.018
pET28/*GhEG16* Bl21 star +IPTG	0.026
pET28/*GhEG16* Bl21 codon plus +IPTG	0.029
pET28/*HvEG16* Bl21 star +IPTG	0.016
pET28/*HvEG16* Bl21 codon plus +IPTG	0.025

5. DISCUSSION

Plant cell wall consists of many polysaccharides and proteins. Xyloglucan (XyG) is the most abundant hemicellulose in primary cell walls of dicots and non-graminaceous monocots. XyG consists of β-(1,4)-linked glucosyl residues which are appended with xylosyl, galactosyl, and fucosyl residues [34]. The network between xyloglucan and cellulose microfibrils is crucial for wall strength. Therefore, xyloglucan endotransglycosylase/hydrolases (XTHs) which modify the xyloglucan cross-links are very essential for wall extension and loosening [76]. XTHs cleave the donor polysaccharide and transfer the reducing end of the original substrate to the nonreducing end of another polysaccharide molecule, or oligosaccharide acceptor substrate. In addition, some XTHs can catalyze the hydrolysis of donor polysaccharides.

The molecular evolution of the XTH gene family has yet to be elucidated. It has been suggested that bacterial licheninases that have a high affinity to hydrolyze β-(1,3);(1,4)-linked glucan chains are closest relatives to XTH enzymes [77]. Enzymes that are involved in the synthesis of xyloglucan, and those that modify xyloglucan and other wall polysaccharides have not been clearly identified. For this reason, XTHs have been examined in detail to clarify the cell wall structure and modifications. In this current study, it was aimed to express At*XTH3* and *TaXTH3* genes in the methylothropic *Pichia pastoris*, and also *GhEG16* and *HvEG16* genes in *E. coli* heterologously in order to make active enzyme and to perform substrate characterization.

SDS-PAGE, western blot, and dot blot analysis were performed to detect the purified enzymes. TaXTH9 enzyme was detected, but the molecular weight of visualized protein bands was higher than expected. The first suspected situation was a problem with the sequence of pPicZα-C/*TaXTH9* plasmid, but it was determined that there was not any problem with the plasmid and insert sequence. Because of the N-glycosylated sites which were situated close to the catalytic site of *TaXTH9* sequence, the protein could have low electrophoretic mobility during the gel electrophoresis. AtXTH3 was only detected after the first large scale production trial out of four trials. There could be a problem during the production step. Maybe, the AOX1 promoter of the expression plasmid *pPicZα-C* was not induced with 1% methanol [110]. Also, protein loss could happen during the purification

steps. Protease contamination of the columns could result in protein loss. If ubiquitin was added to the protein, proteases could degrade the protein by hydrolysis of peptide bonds [117]. Also, AtXTH3 enzyme may not have been secreted to the extracellular matrix. Finally, GhEG16 and HvEG16 enzymes were not detected. There could be a problem with the expression of the genes or purification step. Maybe, proteins were not expressed in BL21 Star DE3 and BL21 Codon Plus DE3 RIPL cells, or intracellular lysis of *E. coli* cells could may have successfully been achieved. Also, *E. coli* cells may not have properly synthesized the GhEG16 and HvEG16, or they may have been incorrectly folded and may have accumulated in inclusion bodies.

Activity assays of TaXTH9 with three donor polysaccharides and nine oligosaccharide substrates was performed at different time intervals. Because of the presence of catalytic site "DEIDFEFLG" of XTH enzyme in TaXTH9 sequence, it was expected to detect the enzyme activity [118]. It was aimed to demonstrate a linearly increasing line of the product among time. Otherwise, the enzyme could be in an increasingly substrate limiting situation, and the exact enzyme activity could not be determined. It was expected to detect the highest enzyme activity with TXG as the donor substrate as has been seen with all other previousiy measured xyloglucan endotransglycosylase enzymes. However, among different trials, it was observed that TaXTH9 had the highest activity on the HEC-XGOs substrate couple. As with most cell walls, the major part of the vegetative cell walls of wheat plants consists of cellulose, TaXTH9 was observed to have the highest affinity to bind and cleave the HEC donor substrate [11]. The enzyme could work well on cellulose under various situations including stress conditions. The second highest enzyme activity was detected on TXG-X7. For the acceptor substrate, TaXTH9 enzyme preferred X7, which has only the xyloglucan heptasaccharide XXXG, rather than XGOs, which consists of a mix of the heptasaccharide XXXG, one or both of the octasaccharides XXLG/XLXG, and the nonasaccharide XLLG. Thus the enzyme was more active with XXXG, rather than with XXXLG/XLXG and XLLG. On the other hand, HEC demonstrated higher activity with XGOs, whereas BBG demonstrated higher activity with X7. Enzyme activity with XGOs and X7 could be related with donor substrates. Maybe, the enzyme has higher affinity to link HEC to X8 and/or X9 instead of X7. Moreover, TaXTH9 had activity with the mixed-linked β-glucans, including BA, BB, and BC. BB demonstrated the highest activity with each donor substrates. The reason could be the affinity of enzyme to bind to the β-1,4-, β-1,4-, β-1,3- linkages instead

of β-1,3-, β-1,4-, β-1,4-, and β-1,4-, β-1,3-, β-1,4- linkages. Besides that, HEC-BB demonstrated very high activity which is close to the TXG-XGO activity. The reason could be the abundance of mixed-linked β-glucans in wheat cell walls, and suggests a role for TaXTH9 in crosslinking cellulose, XyG, and mixed-linked β-glucans. TaXTH9 also showed activity with LT, GM, XT, and CT acceptors. Although arabinoxylan is the most abundant polysaccharide in wheat cell walls, it showed less activity with TXG and BBG donor substrates [11]. XT and CT substrates demonstrated higher activity with HEC instead of TXG and BBG. This could be due to the high affinity of enzyme to link (1,4)-β-D-xylotetraose residues with (1,4)-β-linked glucosyl residues instead of (1,3;1,4)-β-linked glucosyl and substituted (1,4)-β-linked glucosyl residues.

Activity assay of AtXTH3 was performed with TXG, BBG, and XGO substrates. Because of the presence of the conserved XTH catalytic motif "DEIDFEFLG" in the AtXTH3 sequence, it was expected to detect XTH activity [118]. The BBG-XGO substrate couple demonstrated approximately five times more activity than the TXG-XGO couple. XTH had more affinity to bind and cleave BBG instead of TXG. Until these studies, it was unproven that the enzymes of the ancestral clade have XTH activity [77]. However, we might say that the ancestral enzymes may have MXE activity according to the activity results.

Optimum concentrations of TXG, HEC, and X7 substrates were determined for the TaXTH9 kinetic studies. TaXTH9 had the highest activity with 0.4% TXG and 0.4% HEC. Donor concentrations higher than 0.4% cause a significant increase in viscosity which results in a reduction in enzyme activity. According to the Michaelis-Menten graph, it was determined that 23 μM final X7 concentration was optimum for enzyme activity. Kinetic calculations were carried out according to the Lineweaver-Burke graph. The maximum rate, V_{max} of TaXTH9 with TXG-X7 was 0,033 μM/min, and with HEC-X7 was 0.004 μM/min. The V_{max} values were low because TaXTH9 did not convert much substrate to product per unit of time when the enzyme is saturated.

To sum up, production, purification, enzyme characterization, and kinetic studies of TaXTH9 were successful. However, some problems arose during the studies of AtXTH3, GhEG16, and HvEG16 enzymes. After some characterization studies of AtXTH3 enzyme, further studies could not have been achieved due to the contamination of protein. For further studies, ATXTH3 can be stored at -20 °C if the enzyme will not be used immediately for enzyme activity assays. Moreover, different kinds of host cells or *E. coli* strains can be used

for GhEG16 and HvEG16 production. XTHs should be examined in details to understand their cell wall modifications more clearly.

6. CONCLUSION

Xyloglucan endotransglycosylase/hydrolases (XTHs) have a key role in cell wall extension and loosening because they modify the xyloglucan cross-links of the cellulose and xyloglucan network. In this study it was detected that each polysaccharide-acceptor substrate couples demonstrated distinctive enzyme activities and substrate specificities. TaXTH9 had the highest activity on the HEC-XGO substrate couple rather than the expected TXG-XGO. The results for AtXTH3 were surprising and of great interest since it was approximately five times more active on BBG-XGO than on TXG-XGO, the first XTH enzyme to show such activity. The performed activity analyses of TaXTH9 and AtXTH3 enzymes enlightened the specificities of these XTH enzyme. After the functions of XTH enzymes are found out, the cell wall modifications will be elucidated. Then, new transgenic plants may be generated, and new hybrid plants may be developed to sustain agricultural practices in unsuitable environments. Also, many developments can be carried out in different areas such as paper production, food quality and texture, malting and brewing, and bioethanol production.

REFERENCES

1.   B. L. Ridly, M. A. O'Neill and D. Mohnen. Pectins: Structure, Biosynthesis, and Oligogalacturonide-Related Signaling. *Phytochemistry*, 57:929–967, 2001.

2.   D. J. Cosgrove. Growth of the Plant Cell Wall. *Nature Reviews Molecular Cell Biology*, 6:850-861, 2005.

3.   N. C. Carpita, M. Defernez, K. Findlay, B. Wells, D. A. Shoue, G. Catchpole, R. H. Wilson and M. C. McCann. Cell Wall Architecture of the Elongating Maize Coleoptile. *Plant Physiology*, 127: 551-565, 2001.

4.   C. Somerville, S. Bauer, G. Brininstool, M. Facette, T. Hamann, J. Milne, E. Osborne, A. Paredez, S. Persson and T. Raab. Toward a Systems Approach to Understanding Plant Cell Walls. *Science*, 306:2206-2211, 2004.

5.   D. J. Cosgrove. Wall Extensibility: Its Nature, Measurement and Relationship to Plant Cell Growth. *New Phytologist*, 124:1-23, 1993.

6.   L. Taiz and E. Zeiger. *Plant physiology and plant cells*. Plant Physiology, 2002.

7.   B. G. Smith and P. J. Harris. The Polysaccharide Composition of Poales Cell Walls: Poaceae Cell Walls Are Not Unique. *Biochemical Systematics and Ecology*, 27: 33-53, 1999.

8.   J. Vogel. Unique Aspects of the Grass Cell Wall. *Current Opinion in Plant Biology,* 11: 301–307, 2008.

9.   G. Fincher and B. Stone. Cell Walls and Their Components in Cereal Grain Technology. *Advances in Cereal Science and Technology*, 15:50-65, 1986.

10.   P. Albersheim and A. G. Darvill. Oligosaccharins. *Scientific American*, 253:58-64, 1985.

11.   L. Saulnier and F. Guıllon. Deposition of Cell Wall Polysaccharides in Wheat Endosperm During Grain Development: Fourier Transform-Infrared Microspectroscopy Study. *Journal of Agricultural and Food Chemistry*, 54:2303-2308, 2006.

12.   G. Fincher. Changes in Cell Wall Polysaccharides in Developing Barley (Hordeum Vulgare) Coleoptiles. *Origical Article,* 221:729–738, 2005.

13.   A. C. Darvill and P. Albersheim. Characterization of The Cell-Wall Polysaccharides of *Arabidopsis Thaliana* Leaves. *Plant Physiology*, 107:1129-1138, 1995.

14.   U. Römling. Molecular Biology of Cellulose Production in Bacteria. *Research in Microbiology*, 153:205-212, 2002.

15.   R. M. Brown Jr. The Biosynthesis of Cellulose. *Journal of Macromolecular Science, Part A: Pure and Applied Chemistry*, 33:1345-1373, 1996.

16.   K. Kakar, H. Zhang, B. Scheres and P. Dhonukshe. Clasp Mediated Cortical Microtubule Organization Guides Pın Polarization Axis. *Nature*, 495:529-533, 2013.

17.   G. Guerriero, J. Fugelstad and V. Bulone. What Do We Really Know About Cellulose Biosynthesis in Higher Plants? *Journal of Integrative Plant Biology*, 52:161-175, 2010.

18.   A. N. Fernandes, L. H. Thomas, C. M. Altaner, P. Callow, V. T. Forsyth, D. C. Apperley, C. J. Kennedy and M. C. Jarvis. Nanostructure of Cellulose Microfibrils in Spruce Wood. *Proceedings of the National Academy of Sciences*, 108:1195-203, 2011.

19.   L. Hildén and G. Johansson. Recent Developments on Cellulases and Carbohydrate-Binding Modules with Cellulose Affinity. *Biotechnology Letters*, 26:1683-93, 2004.

20.   T. A. Richmond and C. R. Somerville. The Cellulose Synthase Superfamily. *Plant Physiology*, 124: 495-498, 2000.

21.   S. Robert, G. Mouille and H. Höfte. The Mechanism and Regulation of Cellulose Synthesis in Primary Walls: Lessons from Cellulose-Deficient Arabidopsis Mutants. *Cellulose*, 11:351-364, 2004.

22.   M. Fagard, T. Desnos, T. Desprez, F. Goubet, G. Refregier, G. Mouille, M. Mccann, C. Rayon, S. Vernhettes and H. Höfte. Procuste1 Encodes A Cellulose Synthase Required for Normal Cell Elongation Specifically in Roots and Dark-Grown Hypocotyls of Arabidopsis. *The Plant Cell*, 12: 2409-2423, 2000.

23.   N. G. Taylor, R. M. Howells, A. K. Huttly, K. Vickers and S. R. Turner. Interactions Among Three Distinct Cesa Proteins Essential for Cellulose Synthesis. *Proceedings of the National Academy of Sciences*, 100:1450-1455, 2003.

24.   K. Kudlicka, A. Wardrop, T. Itoh and R. Brown Jr. Further Evidence from Sectioned Material in Support of the Existence of a Linear Terminal Complex in Cellulose Synthesis. *Protoplasma*, 136: 96-103, 1987.

25.   S. Kimura, W. Laosinchai, T. Itoh, X. Cui, C. R. Linder and R. M. Brown. Immunogold Labeling of Rosette Terminal Cellulose-Synthesizing Complexes in the Vascular Plant Vigna Angularis. *The Plant Cell*, 11:2075-2085, 1999.

26.   S. K. Cousins and R. M. Brown. Cellulose I Microfibril Assembly: Computational Molecular Mechanics Energy Analysis Favours Bonding by Van Der Waals Forces as The Initial Step in Crystallization. *Polymer*, 36:3885-3888, 1995.

27.   F. Miart, T. Desprez, E. Biot, H. Morin, K. Belcram, H. Höfte, M. Gonneau and S. Vernhettes, Spatio-Temporal Analysis of Cellulose Synthesis During Cell Plate Formation in Arabidopsis. *The Plant Journal*, 77:71-84, 2014.

28.   G. B. Fincher. Revolutionary Times in Our Understanding of Cell Wall Biosynthesis and Remodeling in the Grasses. *Plant Physiology*, 149:27-37, 2009.

29.   R. A. Burton, S. A. Jobling, A. J. Harvey, N. J. Shirley, D. E. Mather, A. Bacic and G. B. Fincher. The Genetics and Transcriptional Profiles of the Cellulose Synthase-Like Hvcslf Gene Family in Barley. *Plant Physiology*, 146:1821-1833, 2008.

30.   J. C. Cocuron, O. Lerouxel, G. Drakakaki, A. P. Alonso, A. H. Liepman, K. Keegstra, N. Raikhel and C. G. Wilkerson. A Gene from the Cellulose Synthase-Like C Family Encodes a β-(1,4) Glucan Synthase. *Proceedings of the National Academy of Sciences*, 104:8550-8555, 2007.

30.   R. A. Burton, S. M. Wilson, M. Hrmova, A. J. Harvey, N. J. Shirley, A. Medhurst, B. A. Stone and G. Fincher. Cellulose Synthase-Like Cslf Genes Mediate the Synthesis of Cell Wall (1,3;1,4)-Beta-D-Glucans. *Science*, 311:1940-2, 2006.

32.   A. J. Bernal, J. K. Jensen, J. Harholt, S. Sørensen, I. Moller, C. Blaukopf, B. Johansen, R. De Lotto, M. Pauly and H. V. Scheller. Disruption of Atcsld5 Results in Reduced Growth, Reduced Xylan and Homogalacturonan Synthase Activity and Altered Xylan Occurrence in Arabidopsis. *The Plant Journal*, 52:791-802, 2007.

33.   G. B. Fincher. Revolutionary Times in Our Understanding of Cell Wall Biosynthesis and Remodeling in the Grasses. *Plant Physiology*, 149:27-37, 2009.

34.   M. J. Peña, A. G. Darvill, S. Eberhard, W. S. York and M. A. O'neill. Moss and Liverwort Xyloglucans Contain Galacturonic Acid and Are Structurally Distinct from the Xyloglucans Synthesized by Hornworts and Vascular Plants. *Glycobiology*, 18:891-904, 2008.

35.   M. Hoffman, Z. Jia, M. J. Peña, M. Cash, A. Harper, A. R. Blackburn, A. Darvill, And W. S. York. Structural Analysis of Xyloglucans in the Primary Cell Walls of Plants in the Subclass Asteridae. *Carbohydrate Research*, 340:1826-1840, 2005.

36.   L. L. Kiefer, W. S York, A. G. Darvill and P. Albersheim. The Structure of Plant Cell Walls XXVII. Xyloglucan Isolated from Suspension-Cultured Sycamore Cell Walls Is O-Acetylated. *Phytochemistry*, 28:2105–2107, 1989.

37.   T. Hayashi, K. Ogawa and Y. Mitsuishi. Characterization of the Adsorption of Xyloglucan to Cellulose. *Plant and Cell Physiology*, 35:1199-1205, 1994.

38.   M. Lopez, H. Bizot, G. Chambat, M.F. Marais, A. Zykwinska, M.C. Ralet, H. Driguez and A. Buléon. Enthalpic Studies of Xyloglucan-Cellulose Interactions. *Biomacromolecules*, 11:1417-1428, 2010.

39.   D. U. Lima, W. Loh and M. S. Buckeridge. Xyloglucan-Cellulose Interaction Depends on the Sidechains and Molecular Weight of Xyloglucan. *Plant Physiology and Biochemistry*, 42:389-394, 2004.

40.   T. Hayashi. Xyloglucans in the Primary Cell Wall. *Annual Review of Plant Biology*, 40:139-168, 1989.

41.   T. Hayashi, K. Ogawa and Y. Mitsuishi. Characterization of the Adsorption of Xyloglucan to Cellulose. *Plant and Cell Physiology*, 35:1199-1205, 1994.

42.   J. E. Thompson and S. C. Fry. Restructuring of Wall-Bound Xyloglucan by Transglycosylation in Living Plant Cells. *The Plant Journal*, 26:23-34, 2001.

43.   D. J. Cosgrove. Growth of the Plant Cell Wall. *Nature Reviews Molecular Cell Biology*, 6:850-861, 2005.

44.   S. C. Fry, W. S. York, P. Albersheim, A. Darvill, T. Hayashi, J. P. Joseleau, Y. Kato, E. P. Lorences, G. A. Maclachlan and M. Mcneil. An Unambiguous Nomenclature for Xyloglucan-Derived Oligosaccharides. *Physiologia Plantarum*, 89:1-3, 1993.

45.   R. Burton and G. Fincher. Current Challenges in Cell Wall Biology in the Cereals and Grasses. *Frontiers in Plant Science*, 3:130, 2012.

46.   S. T. Tuomivaara, K. Yaoi, A. Malcolm, M. A. O'neill and W. S. York. Generation and Structural Validation of A Library of Diverse Xyloglucan-Derived Oligosaccharides,

Including an Update on Xyloglucan Nomenclature. *Carbohydrate Research*, 402:56–66, 2015.

47.   P. Koehler and H. Wieser. *Chemistry of Cereal Grains*, In *Handbook On Sourdough Biotechnology*. Springer-Verlag New York, Inc., New York, 2013.

48.   D. M. Gibeaut, M. Pauly, A. Bacic and G. B. Fincher. Changes in Cell Wall Polysaccharides in Developing Barley (Hordeum Vulgare) Coleoptiles. *Planta*, 221:729-738, 2005.

49.   S. Gille, A. De Souza, G. Xiong, M. Benz, K. Cheng, A. Schultink, I.-B. Reca and M. Pauly. O-Acetylation of Arabidopsis Hemicellulose Xyloglucan Requires Axy4 or Axy4l, Proteins with a Tbl and Duf231 Domain. *The Plant Cell*, 23:4041-4053, 2011.

50.   Y. S. Hsieh and P. J. Harris. Xyloglucans of Monocotyledons Have Diverse Structures. *Molecular Plant*, 2:943-965, 2009.

51.   K. Keegstra and N. Raikhel. Plant Glycosyltransferases. *Current Opinion in Plant Biology*, 4:219-224, 2001.

52.   D. M. Cavalier, O. Lerouxel, L. Neumetzler, K. Yamauchi, A. Reinecke, G. Freshour, O. A. Zabotina, M. G. Hahn, I. Burgert and M. Pauly. Disrupting Two Arabidopsis Thaliana Xylosyltransferase Genes Results in Plants Deficient in Xyloglucan, A Major Primary Cell Wall Component. *The Plant Cell*, 20:1519-1537, 2008.

53.   R. Burton and G. Fincher. Current Challenges in Cell Wall Biology in the Cereals and Grasses. *Frontiers in Plant Science*, 3:130, 2012.

54.   P. Koehler and H. Wieser. *Chemistry of Cereal Grains*, In *Handbook on Sourdough Biotechnology*. Springer-Verlag New York, Inc., New York, 2013.

55.   N. C. Carpita. *Cell Walls of Higher Plants*. Dietary Fiber: Chemistry, Physiology, and Health Effects, 2012.

56.   S. C. Fry, K. E. Mohler, B. H. Nesselrode and L. Frankova. Mixed-Linkage Beta-Glucan :Xyloglucan Endotransglucosylase, a Novel Wall-Remodelling Enzyme From Equisetum (Horsetails) and Charophytic Algae. *Plant Journal*, 55:240-252, 2008.

57.   S. C. Fry, B. H. Nesselrode, J. G. Miller and B. R. Mewburn. Mixed-Linkage (1→ 3, 1→ 4)-β-D-Glucan Is a Major Hemicellulose of Equisetum (Horsetail) Cell Walls. *New Phytologist*, 179:104-115, 2008.

58.   M. Inouhe and D. J. Nevins. Auxin-Enhanced Glucan Autohydrolysis in Maize Coleoptile Cell Walls. *Plant Physiology*, 96:285-290, 1991.

59.   A. Lazaridou and C. Biliaderis. Cryogelation of Cereal β-Glucans: Structure and Molecular Size Effects. *Food Hydrocolloids*, 18:933-947, 2004.

60.   F. Pettolino, I. Sasaki, A. Turbic, S. M. Wilson, A. Bacic, M. Hrmova and G. B. Fincher, Hyphal Cell Walls from the Plant Pathogen Rhynchosporium Secalis Contain (1, 3/1, 6)-β-D-Glucans, Galacto- and Rhamnomannans, (1,3;1,4)-β-D-Glucans and Chitin. *Febs Journal*, 276:3698-3709, 2009.

61.   N. C. Carpita and M. C. Mccann. The Maize Mixed-Linkage (1→ 3),(1→ 4)-β-D-Glucan Polysaccharide Is Synthesized at the Golgi Membrane. *Plant Physiology*, 153:1362-1371, 2010.

62.   L. Saulnier and A. Rakha. Enzymatic Fingerprinting of Arabinoxylan and β-Glucan in Triticale, Barley and Tritordeum Grains. *Carbohydrate Polymers*, 90:1226–1234, 2012.

63.   J. K. Rose and S.J. Lee. Straying off the Highway: Trafficking of Secreted Plant Proteins and Complexity in the Plant Cell Wall Proteome. *Plant Physiology*, 153:433-436, 2010.

64.   R. Viëtor, S. Angelino and A. Voragen. Structural Features of Arabinoxylans from Barley and Malt Cell Wall Material. *Journal of Cereal Science*, 15:213-222, 1992.

65. E.H. Baydoun and C. Brett. Distribution of Xylosyltransferases and Glucuronyltransferase Within The Golgi Apparatus in Etiolated Pea (Pisum Sativum L.) Epicotyls. *Journal of Experimental Botany*, 48:1209-1214, 1997.

66. A. M. Wu, C. Rihouey, M. Seveno, E. Hörnblad, S. K. Singh, T. Matsunaga, T. Ishii, P. Lerouge and A. Marchant. The Arabidopsis Irx10 and Irx10-Like Glycosyltransferases Are Critical for Glucuronoxylan Biosynthesis During Secondary Cell Wall Formation. *The Plant Journal*, 57:718-731, 2009.

67. M. C. Rodrıguez-Gacio and A. J. Matilla. Softening-Up Mannan-Rich Cell Walls. *Journal of Plant Botany*, 63:3975-3988, 2012.

68. M. G. Handford, T. C. Baldwin, F. Goubet, T. A. Prime, J. Miles and P. Dupree. Localisation and Characterisation of Cell Wall Mannan Polysaccharides in Arabidopsis Thaliana. *Planta*, 218:27–36, 2003.

69. R. Schröder, T. F. Wegrzyn, N. N. Sharma and R. G. Atkinson. Leman4 Endo-B-Mannanase from Ripe Tomato Fruit Can Act as A Mannan Transglycosylase or Hydrolase. *Planta*, 224:1091-1102, 2006.

70. M. A. O'neill, T. Ishii, P. Albersheim and A. G. Darvill. Rhamnogalacturonan Ii: Structure and Function of A Borate Cross-Linked Cell Wall Pectic Polysaccharide. *Annual. Review of Plant Biology*, 55:109-139, 2004.

71. A. Nebenführ and L. A. Staehelin. Mobile Factories: Golgi Dynamics in Plant Cells. *Trends in Plant Science*, 6:160-167, 2001.

72. W. G. Willats, L. Mccartney, W. Mackie and J. P. Knox. *Pectin: Cell Biology And Prospects for Functional Analysis*, in *Plant Cell Walls*. Springer-Verlag New York, Inc., New York, 2001.

73. P. Sriamornsak. Chemistry of Pectin and Its Pharmaceutical Uses : A Review. *Silpakorn University International Journal*, 3:206-228, 2003.

74.	A. Bacic, P. J. Harris and B. A. Stone. *Structure and Function of Plant Cell Walls*. In The Biochemistry Of Plants, Academic Press, New York, 1988.

75.	S. C. Fry. Primary Cell Wall Metabolism: Tracking the Careers of Wall Polymers in Living Plant Cells. *New Phytologist*, 161:641–75, 2004.

76.	E. A. H. Baydoun and S. C. Fry. In Vivo Degradation and Extracellular Polymer-Binding of Xyloglucan Nonasaccharide, a Naturally-Occurring Anti-Auxin. *Journal of Plant Physiology*, 134: 453-459, 1989.

77.	J. M. Eklöf, S. Shojania, M. Okon, L.P. Mcintosh and H. Brumer. Structure-Function Analysis of a Broad Specificity Populus Trichocarpa Endo-β-Glucanase Reveals an Evolutionary Link Between Bacterial Licheninases and Plant XTH Gene Products. *The Journal of Biological Chemistry*, 288: 15786 –15799, 2013.

78.	K. Nishitani and R. Tominaga. Endo-Xyloglucan Transferase, A Novel Class of Glycosyltransferase That Catalyzes Transfer of a Segment Of Xyloglucan Molecule to Another Xyloglucan Molecule. *The Journal of Biological Chemistry*, 267:21058–21064, 1992.

79.	J. Pritchard, P. R. Hetherington, S. C. Fry and A. D. Tomos. Xyloglucan Endotransglycosylase Activity, Microfibril Orientation and the Profiles of Cell Wall Properties Along Growing Regions of Maize Roots. *Journal of Experimental Botany*, 44:1281-1289, 1993.

80.	W. Xu, M. M. Purugganan, D. H. Polisensky, D. M. Antosiewicz, S. C. Fry and J. Braam. Arabidopsis Tch4, Regulated by Hormones and the Environment, Encodes a Xyloglucan Endotransglycosylase. *The Plant Cell*, 7:1555-1567, 1995.

81.	J. K. Rose and A. B. Bennett. Cooperative Disassembly of the Cellulose–Xyloglucan Network of Plant Cell Walls: Parallels Between Cell Expansion and Fruit Ripening. *Trends in Plant Science*, 4: 176-183, 1999.

82.   S. Fry, R. C. Smith, K. F. Renwick, D. J. Martin, S. Hodge and K. J. Matthews. Xyloglucan Endotransglycosylase, a New Wall-Loosening Enzyme Activity from Plants. *Biochemical Journal*, 282:821-828, 1992.

83.   M. Edwards, I. Dea, P. Bulpin And J. Reid. Purification and Properties of a Novel Xyloglucan-Specific Endo-(1,4)-Beta-D-Glucanase from Germinated Nasturtium Seeds (Tropaeolum Majus L.). *Journal of Biological Chemistry*, 261:9489-9494, 1986.

84.   E. J. Mellerowicz, P. Immerzeel and T. Hayashi. Xyloglucan: The Molecular Muscle of Trees. *Annals of Botany*, 102:659-665, 2008.

85.   G. J. Davies, T. M. Gloster and B. Henrissat. Recent Structural Insights into the Expanding World of Carbohydrate-Active Enzymes. *Current Opinion in Structural Biology*, 15:637-645, 2005.

86.   B. Henrissat and A. Bairoch. Updating the Sequence-Based Classification of Glycosyl Hydrolases. *Biochemical Journal*, 316:695, 1996.

87.   G. Michel, L. Chantalat, E. Duee, T. Barbeyron, B. Henrissat, B. Kloareg and O. Dideberg. The K-Carrageenase of P. Carrageenovora Features a Tunnel-Shaped Active Site: a Novel Insight in the Evolution of Clan-B Glycoside Hydrolases. *Structure*, 9:513-525, 2001.

88.   G. Vaaje-Kolstad, V. Farkas, M. Hrmova and G. B. Fincher. Xyloglucan Xyloglucosyl Transferases from Barley (Hordeum Vulgare L.) Bind Oligomeric and Polymeric Xyloglucan Molecules in Their Acceptor Binding Sites. *Biochimica Biophysica Acta*, 1800:674-84, 2010.

89.   G. B. Fincher. Revolutionary Times in Our Understanding of Cell Wall Biosynthesis And Remodeling in the Grasses. *Plant Physiology*, 149:27-37, 2009.

90.   M. Hrmova, V. Farkas, J. Lahnstein and G. B. Fincher. A Barley Xyloglucan Xyloglucosyl Transferase Covalently Links Xyloglucan, Cellulose and (1,3;1,4)-β-D-glucans. *The Journal Of Biological Chemistry*, 282:12951–12962, 2007.

91.   J. K. C. Rose, J. Braam, S. C. Fry and K. Nishitani. The XTH Family of Enzymes Involved in Xyloglucan Endotransglucosylation and Endohydrolysis: Current Perspectives and a New Unifying Nomenclature. *Plant Cell Physiology*, 43:1421–1435, 2002.

92.   Xyloglucan Endotransglucosylation and Endohydrolysis: Current Perspectives and a New Unifying Nomenclature. *Plant Cell Physiology*, 43:1421–1435, 2002.

93.   S. C. Fry, R. C. Smith, K. F. Renwick, D. J. Martin, S. K. Hodge and K. J. Matthew. Xyloglucan Endotransglycosylase, a New Wall-Loosening Enzyme Activity from Plants. *Biochemical Journal*, 282:821–828, 1992.

94.   J. Becnel, M. Natarajan, A. Kipp and J. Braam. Developmental Expression Patterns of Arabidopsis XTH Genes Reported by Transgenes and Genevestigator. *Plant Molecular Biology*, 61:451–467, 2006.

95.   K. Vissenberg, S. C. Fry and J. P. Verbelen. Root Hair Initiation Is Coupled to a Highly Localized Increase of Xyloglucan Endotransglycosylase Action In Arabidopsis Roots. *Plant Physiology*, 127:1125–1135, 2001.

96.   P. M. Sanders, A. Q. Bui, K. Weterings, K. N. Mcıntire, Y. C. Hsu, P. Y. Lee, M. T. Truong, T. P. Beals and R. B. Goldbert. Anther Developmental Defecs in Arabidopis Thaliana Male-Sterile Mutants. *Sexual Plant Reproduction*, 11:297–322, 1999.

97.   R. Yokoyama, J. K. C. Rose and K. Nishitani. A Surprising Diversity and Abundance of Xyloglucan Endotransglucosylase/Hydrolases in Rice. *Plant Physiology*, 134:1088–1099, 2004.

98. F. Divol, F. Vilaine, S. Thibivilliers, J. Amselem, J. C. Palauqui, C. Kusiak and S. Dinant. Systemic Response to Aphid Infestation by *Myzus Persicae* in the Phloem of *Apium Graveolens*. *Plant Molecular Biology*, 57:517–540, 2005.

99. R. G. Atkinson, S. L. Johnston, Y. Yauk, N. N. Sharma and R. Schröder. Analysis of Xyloglucan Endotransglucosylase/Hydrolase (XTH) Gene Families in Kiwifruit and Apple. *Postharvest Biology and Technology*, 51:149–157, 2009.

100. S. Romo, T. Jiménez, E. Labrador and B. Dopico. The Gene for a Xyloglucan Endotransglucosylase/Hydrolase from *Cicer Arietinum* Is Strongly Expressed in Elongating Tissues. *Plant Physiology and Chemistry*, 43:169–176, 2005.

101. V. Bourquin, N. Nishikubo, H. Abe, H. Brumer, S. Denman, M. Eklund, M. Christiernin, T. T. Teeri, B. Sundberg and E. J. Mellerowicz. Xyloglucan Endotransglycosylase Have a Function During the Formation of Secondary Cell Walls of Vascular Tissues. *The Plant Cell*, 14:3073–3088, 2002.

102. M. Rai and H. Padh. Expression Systems for Production of Heterologous Proteins. *Current Science-Bangalore*, 80:1121-1128, 2001.

103. M. Welch, A. Villalobos, C. Gustafsson and J. Minshull. 3 Designing Genes for Successful Protein Expression. *Methods in Enzymology*, 498:43, 2011.

104. S. C. Makrides. Strategies for Achieving High-Level Expression of Genes in Escherichia Coli. *Microbiological Reviews*, 60:512-538, 1996.

105. R. I. Monsalve And G. Lu. Expressions of Recombinant Venom Allergen, Antigen 5 Of Yellowjacket (Vespula Vulgaris) and Paper Wasp (Polistes Annularis), in Bacteria or Yeast. *Protein Expression and Purification*, 16:410-416, 1999.

106. H. Hohenblum, B. Gasser, M. Maurer, N. Borth and D. Mattanovich. Effects of Gene Dosage, Promoters, and Substrates on Unfolded Protein Stress of Recombinant Pichia Pastoris. *Biotechnology and Bioengineering*, 85:367-375, 2004.

107.   R. K. Bretthauer and F. J. Castellino. Glycosylation of Pichia Pastoris-Derived Proteins. *Biotechnology and Applied Biochemistry*, 30:193-200, 1999.

108.   W. Zhang, L. A. Smith, B. A. Plantz, V. L. Schlegel and M. M. Meagher. Design of Methanol Feed Control in Pichia Pastoris Fermentations Based Upon a Growth Model. *Biotechnology Progress*, 18:1392-1399, 2002.

109.   G. P. L. Cereghino, J. L. Cereghino, C. Ilgen and J. M. Cregg. Production of Recombinant Proteins in Fermenter Cultures of the Yeast Pichia Pastoris. *Current Opinion in Biotechnology*, 13:329-332, 2002.

110.   J. M. Cregg and K. R. Madden. Development of the Methylotrophic Yeast, Pichia Pastoris, As a Host System for the Production of Foreign Proteins. *Developments in Industrial Microbiology*, 29:33-41, 1988.

111.   S. M. Patrick, M. L. Fazenda, B. Mcneil and L. M. Harvey. Heterologous Protein Production Using the Pichia Pastoris Expression System. *Yeast*, 22:249-270, 2005.

112.   J. M. Cregg, J. L. Cereghino, J. Shi and D. R. Higgins. Recombinant Protein Expression in Pichia Pastoris. *Molecular Biotechnology*, 16:23-52, 2000.

113.   T. Egli, J. Van Dijken, M. Veenhuis, W. Harder and A. Fiechter. Methanol Metabolism in Yeasts: Regulation of the Synthesis of Catabolic Enzymes. *Archives of Microbiology*, 124:115-121, 1980.

114.   M. Inan and M. M. Meagher. The Effect of Ethanol and Acetate on Protein Expression in Pichia pastoris. *Journal of Bioscience and Bioengineering*, 92:337-341, 2001.

115.   C. White, N. Kempi and E. Komives. Expression of Highly Disulfide Bonded Proteins in Pichia pastoris. *Structure*, 2:1003-1005, 1994.

116. J. L. Cereghino, W. W. Wong, S. Xiong, W. Giang, L. T. Luong, J. Vu, S. D. Johnson and G. P. Lincereghino. Condensed Protocol for Competent Cell Preparation and Transformation of the Methylotrophic Yeast Pichia pastoris. *BioTechniques*, 38:44-48, 2005 .

117. A. L. Goldberg. Protein Degradation and Protection Against Misfolded or Damaged Proteins. *Nature*, 426:18-25, 2003.

118. J. M. Eklöf and H. Brumer. The *XTH* Gene Family. An Update on Enzyme Structure, Function, and Phylogeny in Xyloglucan Remodeling. *Plant Physiololy*, 153:456–466, 2010.